MEASUREMENT AND PERFORMANCE ANALYSIS OF 2D MATERIAL BASED SUPERCAPACITORS

Master's Thesis

Uğur Cenk ARSLAN

Eskişehir 2025

MEASUREMENT AND PERFORMANCE ANALYSIS OF 2D MATERIAL BASED SUPERCAPACITORS

Uğur Cenk ARSLAN

MASTER'S THESIS

Department of Electrical and Electronics Engineering

Programme in Electronics

Supervisor: Prof. Dr. Nihan Kosku PERKGÖZ

(Co-Supervisor: Asst. Prof. Dr. Mehmet BAY)

Eskişehir

Eskişehir Technical University

Institute of Graduate Programs

June 2025

FINAL APPROVAL FOR THESIS

This thesis titled “MEASUREMENT AND PERFORMANCE ANALYSIS OF 2D MATERIAL- BASED SUPERCAPACITORS ” has been prepared and submitted by Uğur Cenk ARSLAN in partial fullfillment of the requirements in “Eskişehir Technical University Directive on Graduate Education and Examination” for the Degree of Master of Science in Electrical and Electronics Engineering Department has been examined and approved on 18/06/2025.

Committee Members	**Title, Name and Surname**	**Signature**
Member	: Prof. Dr. Nihan Kosku PERKGÖZ	
Member	: Prof. Dr. Feridun AY	
Member	: Asst. Prof. Dr. Faruk DİRİSAĞLIK	

Prof. Dr. Harun BÖCÜK
Lisansüstü Eğitim Enstitüsü Müdürü

18/06/2025

SUPERVISOR APPROVAL

Master's student Uğur Cenk ARSLAN, whom I supervise, has completed this thesis titled MEASUREMENT AND PERFORMANCE ANALYSIS OF 2D MATERIAL BASED SUPERCAPACITORS. According to my inspections, the work is scientifically and ethically appropriate for the student to the thesis defense exam.

Supervisor

Prof. Dr. Nihan Kosku PERKGÖZ

ABSTRACT

MEASUREMENT AND PERFORMANCE ANALYSIS of 2D MATERIAL BASED SUPERCAPACITORS

Ugur Cenk ARSLAN

Department of Electrical and Electronics Engineering

Programme in Electronics

Eskişehir Technical University, Institute of Graduate Programs, June, 2025

Supervisor: Prof. Dr. Nihan Kosku PERKGÖZ

Co-supervisor: Asst. Prof. Dr. Mehmet BAY

Supercapacitors. These gizmos are no regular batteries. They are fast, power-packed, and resilient, marking them as vital for today's and, more importantly, tomorrow's green power solutions. Let's dive into the nitty-gritty in a process called chemical vapor deposition (CVD), we used a slide of hot gases including hydrogen and nitrogen. These gases weave their way through a warmed glass pipe containing boron, boron oxide, and nickel powders. In the sweltering 1000°C heat, these materials react and settle onto less hot copper pieces at about 700 °C. Remember when your teacher said test your work? We did just that. Using Ni_2B on copper, we tested how well our piece would do after 20,000 plug-ins and outs. We almost topped a hundred percent. Even at slower speeds, power levels touched nearly 20 mF/cm^2. And it kept a steady 0.42 mF even when we hit the gas to 1000 mV/s. Plus, the component showed a great absorbing power even at high voltage, hinting at better ion accessibility and almost no diffusion barriers. Ni_2B films using our CVD method show a stable charge hold. They outdo some of the usual nickel-base materials and pose as robust power options. By controlling boron's role and deposition, we create a smooth, nicely stuck coating with potential chemical properties. As the world hustle for efficient longevity in power preserving, Ni_2B supercapacitors can open doors to better devices. Such a device can be part of solutions like green energy grids or other fast-changing needs.

Keywords: Nickel boride, Supercapacitor, Chemical vapor deposition

ÖZET

2 BOYUTLU MALZEME TABANLI SÜPERKAPASİTÖRLERİN ÖLÇÜM VE PERFORMANS ANALİZİ

Ugur Cenk ARSLAN
Elektrik ve Elektronik Mühendisliği Anabilim Dalı
Elektronik Bilim Dalı
Eşkişehir Teknik Üniversitesi, Lisansüstü Eğitim Enstitüsü, Haziran, 2025
Danışman: Prof. Dr. Nihan Kosku PERKGÖZ
İkinci Danışman: Dr. Öğr. Üy. Mehmet BAY

Süperkapasitörler, hızlı şarj olabilme kabiliyeti, yüksek güç yoğunluğu ve çok uzun çevrim ömrü sayesinde küresel ölçekte büyük ilgi görüyor. Günümüz ve geleceğin enerji gereksinimleri için kritik bir teknoloji konumundalar. Bu çalışmada, kimyasal buhar biriktirme (CVD) ile nikel borür (Ni_2B) esaslı bir süperkapasitör elektrodu oluşturuyoruz. Deney düzeneğinde, bor, bor oksit ve nikel tozları 1000 °C civarında ısıtılıyor, hidrojen ve azot taşıyıcı gazlarıyla reaksiyona giriyor ve ~700 °C'deki daha serin bakır yüzeylere yoğunlaşıyor. Üretim sonrasında elde edilen Ni_2B kaplı bakır örnekleri, 20.000 şarj-boşalt döngüsünde neredeyse %99 kapasite korunumu sergiledi. Düşük tarama hızında ($5\ mV\ s^{-1}$), yüzeysel kapasitans değeri ~20 $mF\ cm^{-2}$ düzeyindeydi ve 1000 $mV\ s^{-2}$ gibi yüksek taramalarda bile ~0.42 $mF\ cm^{-2}$ olarak ölçüldü. Genişletilmiş voltaj aralıklarında (1.5 V'ye kadar) kapasite artışı gözlendi; bu, iyon erişiminin etkili ve difüzyon sınırının düşük olduğuna işaret ediyor. Galvanostatik veriler de yaklaşık 0.06 F mertebesinde özgül kapasitans (1 mg elektrot kütlesi üzerinden) ile birlikte güçlü kolombik verim olduğunu gösteriyor. Sonuç olarak, CVD yöntemle büyütülen Ni_2B filmlerin kararlı enerji depolama ve uzun döngü ömrü sunduğu anlaşılıyor. Kontrollü çöktürme ile yüzeye sağlam yapışan, tekdüze bir tabaka elde ediliyor ve yüksek kapasitans değerleri gözleniyor. Ni_2B süperkapasitörler, yenilenebilir enerji sistemleri ve hızlı şarj uygulamalarında verimli ve ölçeklenebilir bir çözüm olabilir.

Anahtar Kelimeler: Nikel borür, Süperkapasitör, Kimyasal buhar biriktirme

ACKNOWLEDGEMENTS

I would like to thank the Micro Nano Systems and Devices Research Group (MIDAS) for allowing me access to their CVD laboratory, which was essential for this study. I also extend my sincere gratitude to Prof. Dr. Nihan Kosku PERKGÖZ, Prof. Dr. Feridun AY, and Asst. Prof. Dr. Mehmet BAY for their invaluable guidance and support throughout my research. Lastly, I am deeply grateful to my parents for their unwavering encouragement and understanding. Their collective help and motivation have made this work possible.

Ugur Cenk ARSLAN
Haziran 2025

18/06/2025

STATEMENT OF COMPLIANCE WITH ETHICAL PRINCIPLES AND RULES

I hereby truthfully declare that this thesis is an original work prepared by me; that I have behaved in accordance with the scientific ethical principles and rules throughout the stages of preparation, data collection, analysis and presentation of my work; that I have cited the sources of all the data and information that could be obtained within the scope of this study, and included these sources in the references section; and that this study has been scanned for plagiarism with "scientific plagiarism detection program" used by Eskişehir Technical University, and that "it does not have any plagiarism" whatsoever. I also declare that, if a case contrary to my declaration is detected in my work at any time, I hereby express my consent to all the ethical and legal consequences that are involved.

Uğur Cenk ARSLAN

CONTENTS

LIST OF TABLES

Page

LISF OF FIGURES

Page

GLOSSARY OF SYMBOLS AND ABBREVIATIONS

A/g	: Amps per Gram
Cdl	: Double-Layer Capacitance
Csp	:Specific Capacitance
CV	:Cyclic Voltammetry
CVD	:Chemical Vapor Depsition
EDLC	:Electric Double-Layer Capacitance
EDX	:Energy Dispersive X-ray Spectroscopy
EIS	:Electrochemical Impedance Spectroscopy
F/g	:Farads per Gram
GCD	:Galvanostatic Charge-Discharge
IR Drop	:Internal Resistance Drop
Ni_2B	:Nickel Boride
Ret	:Charge Transfer Resistance
SEM	:Scanning Electron Microscopy
TOC	:Table of Contents
V/s	:Volt per Second (Scan Rate)
XRD	:X-ray Diffraction

1. INTRODUCTION

Supercapacitors are special. They are a big part of modern energy use because they can charge fast and give a lot of power. They are different from batteries; batteries charge slower because they work through something called electrochemical reactions. A supercapacitor is quicker: it can charge and discharge in seconds. This makes it great for moments when a lot of energy is needed very quickly. They are also good because they can be used a lot of times without losing much ability to store energy. This makes them better than other storage devices. Most of the time, supercapacitors use something called porous carbon electrodes. This works okay, but people are getting interested in using metals too. Metals might help increase the amount of energy that can be stored and how well electricity can flow. A metal called Nickel boride (Ni_2B) is one option. Metal from nickel and boride could make a supercapacitor work better. We tested this by making Ni_2B using a special technique. We passed hydrogen and nitrogen gases through a hot glass tube. There was boron oxide and nickel on some copper foil in one part of the tube and just copper foil in another part that wasn't as hot. When the gases mixed with the boron oxide and cooled down in the second part, we hoped that a Ni_2B film would form. If there were any extra gases or particles, we caught them in a cooler box and then let them out. By being very careful with the temperature and how much gas we used, we tried to make a nice, even layer of Ni_2B to use in the supercapacitor. If we can do this well, it might lead to better ways of storing energy. This would allow quick power and a strong cycle for new technologies.

2. LITERATURE REVIEW

Overview of Supercapacitors

Supercapacitors operate on the same fundamental principles as conventional capacitors but feature electrodes with significantly larger surface areas and extremely thin separators [1]. In a basic capacitor, the capacitance C equals the stored charge Q divided by the applied voltage V, as shown by

$$C = \frac{\theta}{v} \tag{2.1}$$

For a parallel-plate design, C is proportional to the surface area A and inversely proportional to the separation D between the plates, i.e.,

$$C = \varepsilon_0 \varepsilon_r \frac{A}{D} \tag{2.2}$$

Where ε_0 is the permittivity of free space and ε_r is the relative permittivity of the dielectric [2]. The total energy E stored in the capacitor follows

$$E = \frac{1}{2} C V^2 \tag{2.3}$$

When discharging, an internal equivalent series resistance (ESR) and any external resistance dictate how quickly current flows [3]. Under a matched-load scenario, the maximum power P_{max} is limited by this ESR, satisfying.

$$Pmax = \frac{V^2}{4ESR} \tag{2.4}$$

Ordinary capacitors are good at delivering power [1], but compared to batteries they don't hold a lot of energy for their size [4]. On the other side of the coin, batteries may have a lot of energy packed in, but they deliver it much slower [4]. This means they have more energy for the space they take up, but they can't give a lot of power all at once. Supercapacitors happen to take the best of both worlds [2]. They give power quickly like capacitors, but they use fancy materials on the inside to make the surface area harder and better [3]. This allows them to keep more energy and deliver a lot of it at once, and do it many times over. Supercapacitors are even better because they're made to stay thin and not resist power giving, which means they can withstand the need for quick power without losing too much energy [5]. Also, they keep pushing their limits more than batteries ever could. Even so, current supercapacitors still have room for improvement. Right now, they don't hold as much energy for their size as batteries

do [6]. Hence, scientists are looking into using new materials that might improve both the amount of power they can deliver and the amount of energy they can store [7]. There are three main types of supercapacitors, all of which store their energy differently [8]. The first kind—called EDLCs—don't rely on chemical reactions at all and instead gather their energy strictly through electric interactions on their inner surfaces [9].

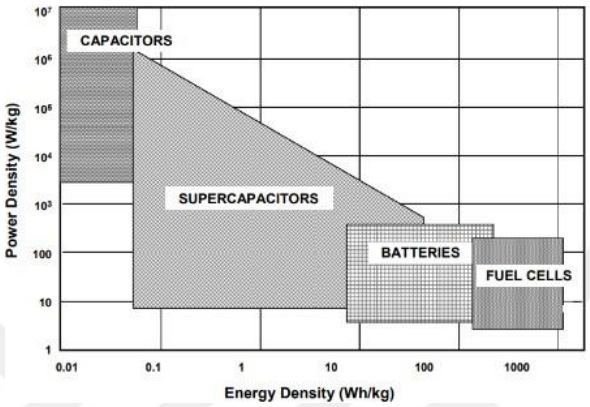

Figure 2.1. *Ragone plot comparing energy storage devices (adapted from [10]).*

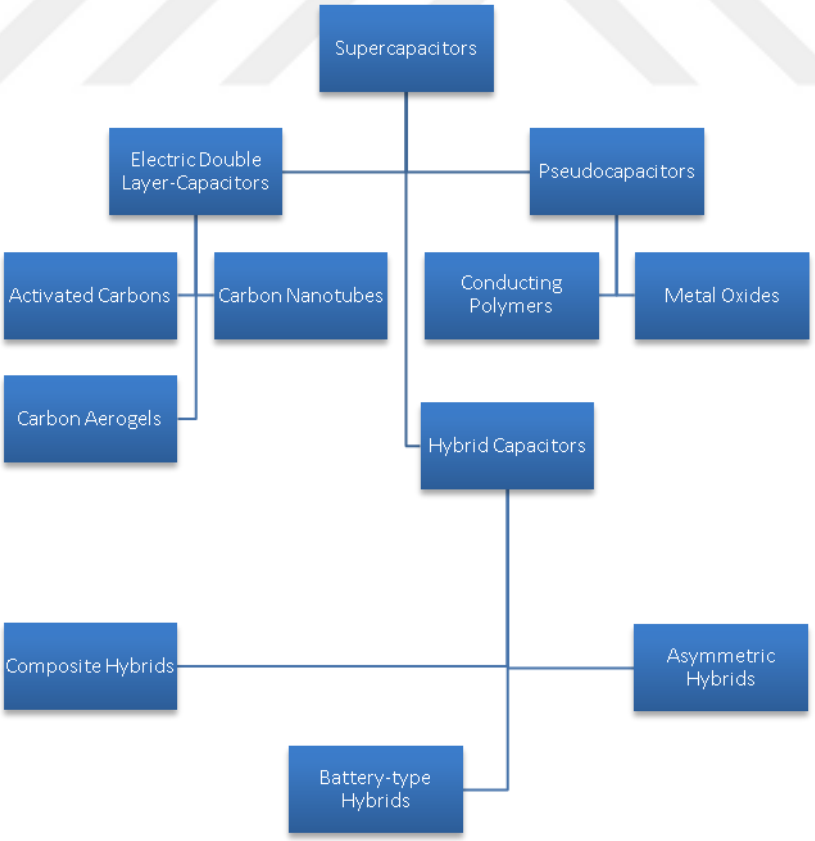

Figure 2.2. *Taxonomy of supercapacitors, highlighting electric double-layer capacitors, pseudocapacitors, and hybrid capacitors, along with their primary material subclasses.*

Pseudocapacitors are different because they use something called Faradaic mechanisms. These include things like oxidation-reduction or surface redox shifts on active materials like metal oxides or conductive polymers. These mechanisms can increase capacitance beyond what normal electrostatics can achieve. Hybrid capacitors are a mix of both electric double-layer capacitors (EDLCs) and pseudocapacitors processes. Sometimes, they have unique electrode designs to increase energy density and power density at the same time. In EDLCs, the main concept is that charges accumulate in an "electric double layer." This layer forms when ions in the electrolyte move to an oppositely charged electrode surface without altering any chemical bonds. This purely physical process gives excellent cycling stability, but it can limit how much charge can be stored. Pseudocapacitors, however, use reversible Faradaic reactions: electrons are transferred between the electrode and electrolyte. This often involves metal oxides, like RuO_2 or MnO_2, or conductive polymers. These reactions offer higher specific capacitances but might raise questions about long-term cycle life. On the other hand, Hybrid capacitors bridge the gap by combining EDLC-type electrodes (like porous carbon) with a pseudocapacitive or battery-like electrode. This achieves a good balance of energy and power. A visual classification of these subclasses often highlights the materials in each category. For example, activated carbons, aerogels, carbon nanotubes, and composite carbons are mostly seen in EDLCs. Metal oxides and conductive polymers are dominant in pseudocapacitors. Hybrid designs can be asymmetric or battery-type, which use electrode materials usually found in lithium-ion cells. This expands energy density while still enabling faster discharge than a conventional battery. Ongoing research explores how to improve all three capacitor classes. For EDLCs, efforts revolve around new forms of carbon with massive surface areas and improved pore structures. For pseudocapacitors, the focus is on optimizing redox-active materials so they can tolerate repeated oxidation-reduction without losing capacity. Hybrid approaches aim to combine the best of both worlds while managing any added complexities. This can push supercapacitor performance closer to that of batteries for energy density but still retains the rapid charge-discharge capability and longevity.

Classification of Electrochemical Capacitors

Capacitors are commonly grouped into three main categories: electrostatic capacitors, electrolytic capacitors, and electro-chemical capacitors (ECs) [11].

Electrostatic capacitors

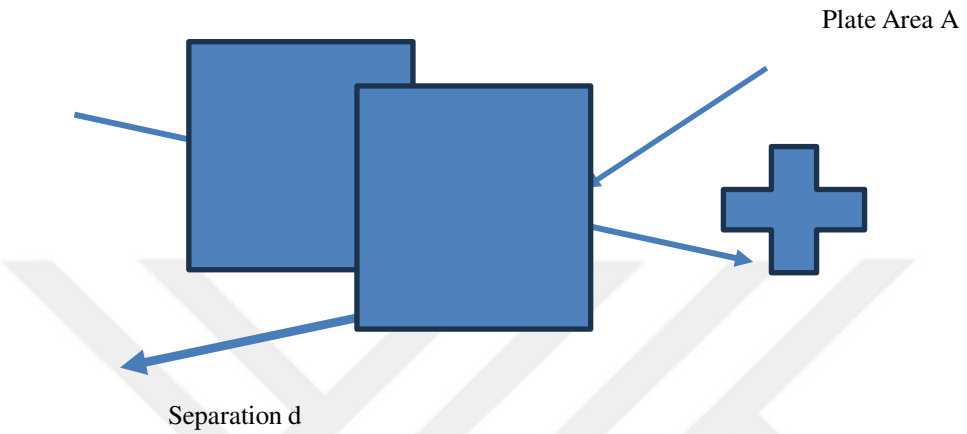

Figure 2.3. *Schematic of a parallel-plate capacitor showing plate area A and separation d. The design illustrates the basic electrostatic principles governing capacitor function.*

In a capacitor like those you'd find in electronics, you've got two flat pieces of metal [12]. They're set apart by a layer called a 'dielectric [13]', as we can see in Fig. 2-3. The strength of this dielectric layer, shown as volts per meter, tells us how much potential difference it can handle before giving up [14]. Let's say we take the example of air; its dielectric strength sits at about 3 million V/m. Surprisingly, paper's strength is much higher, reaching about 16 million V/m [15]. If you strengthen up this dielectric layer, the capacitor can take on both a higher voltage rating and store more charge [13]. In simple terms, the capacitance - or the ability of a capacitor to store an electrical charge - equals how much charge is stored in each metal plate, divided by the applied voltage [12].

Electrolytic capacitors

Electrolytic capacitors are like your regular electrostatic capacitors, but there's a twist. They've got an electrolyte salt sticking right to the metal endings [12]. Here's an example, think of aluminum electrolytic capacitors. They've got two aluminum foils,

both covered in a super thin layer of oxide [12]. These foils are kept apart by a paper spacer that's soaked in, you guessed it, electrolyte [16]. It's so thin that it actually makes the capacitor hold more than the standard electrostatic capacitors [17]. But careful now, these components only have one correct way of use: aligning the polarity wrongly makes the oxide layer dissolve. It can cause short circuits or worse, heat things up so much it could lead to the capacitor blowing up [18].

Electro-chemical capacitors

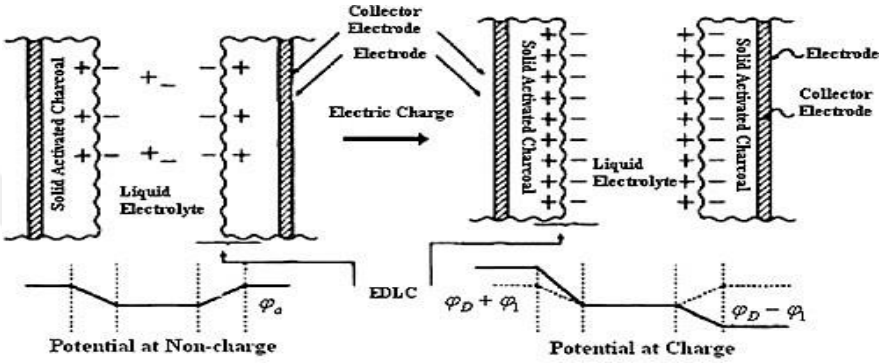

Figure 2.4. *Schematic of EDLC charging mechanism (adapted from [11]).*

Electric storage devices called Electro-chemical capacitors (ECs) make use of special substances known as electrolytes [1]. Their design lets them store more energy because they use spongy, or porous, material in their development [6]. How do they do this? By changing the relationship between the size of the electrode area (A) and the distance (d) that ions travel. The formula is C= ε A/D[19]. So, by broadening the electrode area and shortening the ion distance, they can store more energy. Some of these porous materials contain surface areas as big as 1000-2000 square meters per cubic cm. This means they can store even more energy than other popular designs [3]. ECs get divided into two groups: symmetric (SECs) and asymmetric (AECs). SECs usually use the same electrode substance, often carbon, on both ends [6]. But AECs use different substances for each terminal. SECs store charge by using what's called the double-layer effect, and can work with either watery (Type I) or organic (Type II) electrolytes [1]. AECs function similarly, but label their types differently: Type III for watery and Type IV for organic electrolytes [19]. If you're curious about how they store charge, as illustrated in Figure 2.4. It shows the workings of the EDLC mechanism.

Nickel as a Foundational Element in Alloy and Compound Formation

Nickel, or Ni for short, is a special type of metal. It has a unique structure, it's very bendable, and it doesn't rust easily [20]. All of this is thanks to the way its electrons are arranged, which makes it able to bond really well with both metallic and non-metallic elements [21]. Because of how useful this is, stuff made from nickel is used in lots of places. You'll find nickel in batteries, super-strong alloys, electrochemical converters, and energy-storing devices [22]. Here's a bonus; nickel is super good at conducting electricity. This makes it great for transferring energy in devices that store energy[20]. Plus, it can form stable surface coatings that act like extra energy capacitors, especially when it's combined with other elements [23]. That's how it works in a compound known as nickel boride. In this compound, the arrangement of nickel's electrons makes it real good for reactions that are key to many processes related to electricity and energy. Table 2.1 summarizes selected chemical and physical properties of nickel, which underpin its utility in forming robust compounds such as Ni_2B. The table highlights its density, melting and boiling points, and key oxidation states, each of which influences the stability and electrochemical performance of Ni-containing materials [21].

Table 2.1. *Representative chemical and physical properties of nickel. Minor variations may arise from different measurement techniques.*

Property	Typical Value / Description	Remarks
Atomic Number	28	Electron configuration: [Ar] $3d^8 4s^2$ [24]
Crystal Structure	Face-Centered Cubic (FCC)	Yields high ductility and facilitates broad alloy formation [25]
Density	~8.90 g/cm3 (at 25 °C)	Higher density than many transition metals (e.g., Fe ~7.87 g/cm3)[25]
Melting Point	~1455 °C	Comparable to other structural metals, affecting processing and synthesis routes [26]
Boiling Point	~ 2730 °C	Seldom encountered in Ni_2B processing under standard laboratory or industrial conditions [26]
Oxidation States	Commonly 0, +2, occasionally +3	Ni^{2+} prevalence in aqueous systems underpins many battery and supercapacitor applications [24]
Electrical Conductivity	~6.2×105S/m (bulk)	Promotes efficient electron transport, pivotal for electrode materials [25]
Magnetic Properties	Ferromagnetic below 358 °C (Curie temperature)	May have minor significance in magnetic or electromagnetic applications [24]
Corrosion Resistance	Moderate; forms passivating oxide layers in some environments	A beneficial property for electrode stability in electrochemical cells [25]

The Formation of Nickel Boride (Ni2B) and Relevance to Supercapacitors

Ni_2B is created when boron, a special element, combines with nickel. This creates new compounds that have unusual properties, like being both metallic and somewhat like a regular covalent bond [27]. Boron can help fine-tune nickel's electronic setup, boosting its redox activity by tweaking the density close to the Fermi level [28]. Research suggests that Ni_2B electrodes may act like pseudocapacitors because nickel can be oxidized and reduced within this material [23]. Ni_2B-based composite electrodes have demonstrated excellent cycling stability and durability in supercapacitor applications, retaining a high percentage of capacitance over tens of thousands of cycles[99, 100]. Tweaking the Ni_2B ratio can strike a balance between conductivity, rigidity, and reactivity. This is key for maintaining a strong capacitance and robust life cycle [3].

Ni_2B Hybrids: Interface Engineering and Carbon Integration

Ni_2B and graphene composites

Ni_2B and graphene teaming up has been proven to make supercapacitors work even better [30]. Graphene stands out because it carries electricity superbly and it's got a big surface area [31]. When it touches Ni_2B particles, it helps reduce any resistance in moving electrical charges [23]. These combo materials boost both the energy and power stored. The graphene acts like a fast-moving road for electrons, while Ni_2B lends a hand with a kind of stored energy called pseudocapacitance [32].

Ni_2B and metaborate interfaces

There's a new experiment about a special design called "Ni-B/metaborate interfaces". People use it to store more power in supercapacitors, a type of battery [33]. In these experiments, something called "metaborate phases" mixes with Ni-B surfaces. This can make the layer between the electrode and the electrolyte stronger and help ions move better [34]. The better it is, the less it changes shape and dissolves. That is usually a problem if you want to recycle it many times. Ni-B electrodes sometimes show a unique way of storing charges. They use two techniques: one is like storing power in a double-layered battery and the other involves reactions near the electrode's surface. Boron can change how nickel works, making it easier for redox reactions [23]. These

reactions also increase the pseudocapacitive effects, helping the battery store more energy. To reduce different forms of damage, it helps to control how much Ni_2B is used and make sure Ni-B bonds are stable. Adding other elements or using surface treatments, like metaborate coatings, can help too. These can increase electrical conductivity and make the whole device tougher [30].

Mechanistic insights into Ni_2B electrodes

Batteries with Ni_2B electrodes can show a mix of two ways to store energy. One way is through a process called electric double-layer capacitance, and the other is via surface or near-surface chemical changes [32]. The involvement of the element boron can alter nickel's electronic states. This encourages more chemical changes that provide extra almost-capacitance effects [32]. The wearing out of the electrode can be slowed down by correctly balancing the Ni_2B ratio and keeping the bond between Ni-B stable [31].

3. EXPERIMENTAL SETUP

In this work, we employed a chemical vapor deposition (CVD) route to grow Nickel Boride (Ni–B) for possible supercapacitor use. The system uses hydrogen and nitrogen gas streams channeled through cylindrical glass tubes. Inside these tubes, we placed our starting materials: boron micron powder (99% purity, size <325 mesh, amorphous), nickel micron powder (99% purity), and boron oxide (99%).

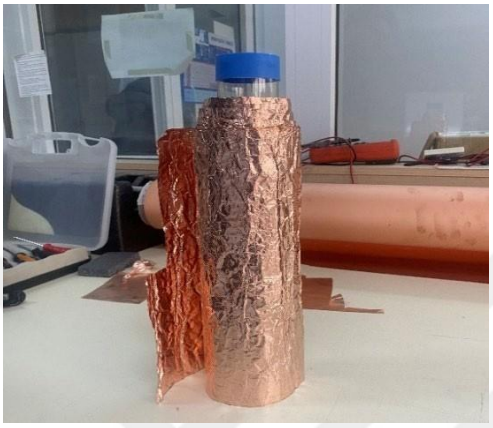

(a)

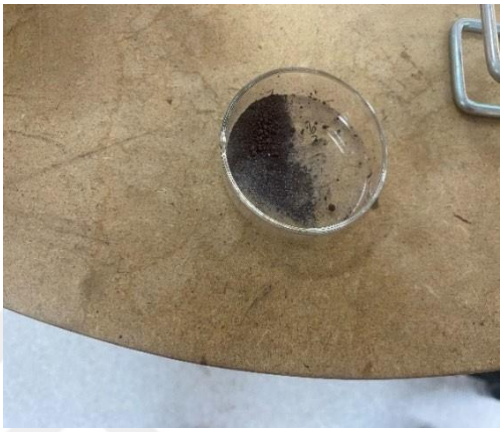

(b)

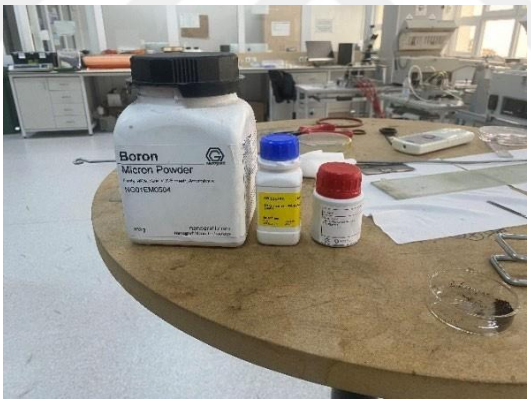

(c)

Figure 3.1. *(a) Rolled copper foil, for use inside the CVD system, (b) Powder mixture intended for application onto the copper substrate, (c) boron powder, nickel powder, and boron oxide—used in the Ni_2B deposition process.*

We used a special method, called chemical vapor deposition (CVD), to grow a material known as Nickel Boride (Ni-B). This material could potentially be useful in devices that store massive amounts of energy, called supercapacitors. We did this by guiding a stream of two gases, hydrogen and nitrogen, through long glass tubes. Inside these tubes, we put in boron powder and nickel powder, both incredibly pure, and a compound called boron oxide. Before this whole process, we had earlier cut thin films

of copper and labelled them as 1, 2, and 3. We polished these films, cleaned them with a chemical named acetone, then washed them by shaking them in water using sounds waves, a method known as ultrasonic cleaning. Finally, we gave them a nitrogen gas blow-off to make sure they were dry. In our CVD machine, there are two different sections that can be heated to different temperatures. The first one can go up to around 1,000°C. This is where we put the boron powder on copper foil. The second one stays at around 700°C. This is where we placed the prepared copper films next to one another. As the boron oxide reacts with the carrier gases in the 1,000°C section, the results of this reaction travel to the cooler copper films in the 700°C section, condensing on them. We expect a new material, called nickel boride, to form on the copper, creating a thin layer. Any unused gases are then taken out through a compressor and cooling box to eliminate any leftover pieces, before being thrown out by a ventilation system. Lastly, we hope to see Ni-B growth on copper films. This process is not out of the ordinary for CVD methods and is actually in line with how many electrodes for supercapacitors are designed.

(a)

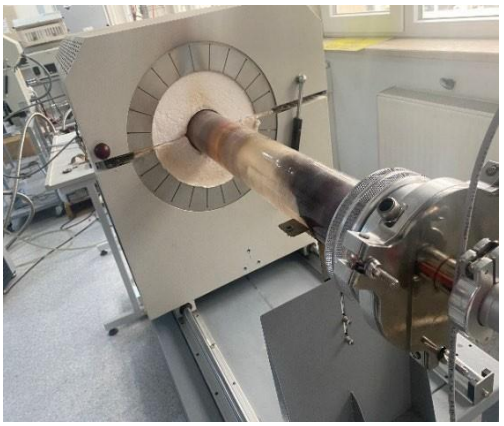

(b)

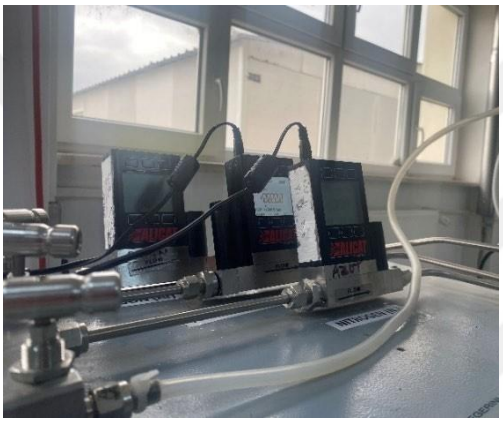

(c)

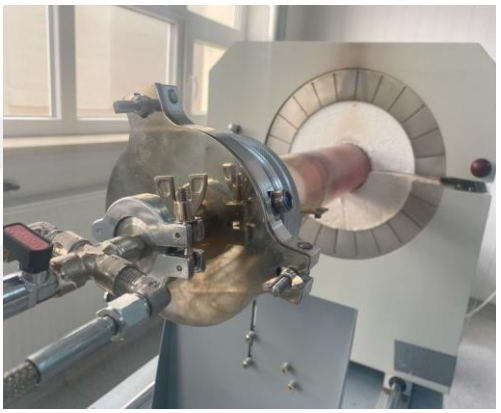

(d)

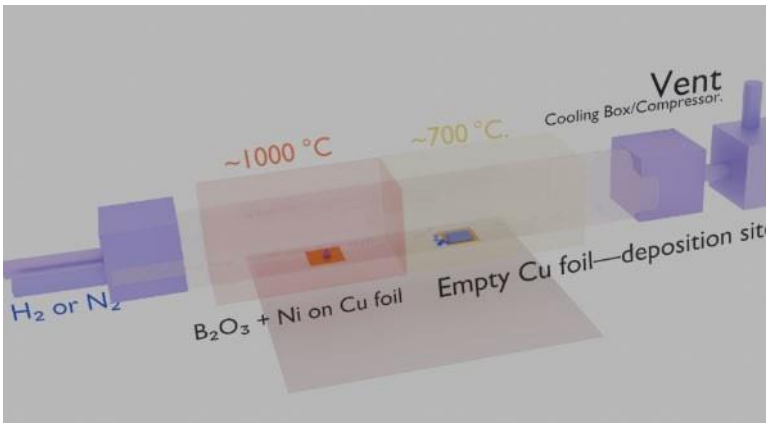

(e)

Figure 3.2. *(a) Main furnace compartment (bulk section) of the CVD system, where copper substrates are placed for deposition, (b) Cylindrical gas tunnel carrying reactant gases under partial vacuum, enabling the flow of materials through the furnace, (c) Control valves managing hydrogen and nitrogen gas intake for precise flow regulation (d) Safety cylinders locked in place to prevent leakage and ensure a secure gas seal, (e) CVD simulations drawn using Blender Software.*

Imagine a two-zone setup. The first zone is kept really hot, around 1000 °C (you could boil water 33 times over at this temperature!). In this zone, we place boron oxide (B_2O_3) and nickel (Ni) powders on a piece of copper foil. Through this super-hot region, we pass gases like hydrogen or nitrogen. These gases react with the boron oxide we just mentioned. Moving along, the second zone is a bit cooler, hovering around 700 °C. Here, we put another piece of copper, ready to catch Ni_2B – a special kind of nickel condensate. After all these steps, the leftover gases move into a cooling box. The box captures any residual products and then the gases finally exit through a vent. This dual-temperature setup allows boron and nickel to deposit together on the cooler copper surface. The idea comes from past studies on nickel-based films for electrochemical uses [35]. By smartly controlling the temperature differences and gas flows, we can grow Ni_2B in a way that's just right for creating supercapacitor electrodes.

4. METHODS AND MEASUREMENTS

4.1. Scanning Electron Microscopy (SEM)

We used SEM (Scanning Electron Microscopy) to look closer at shiny Ni-B sheets [36]. We stuck the samples onto small conductors and placed them in a very weak vacuum, similar to what you'd find out in space. Then we adjusted the electric voltages (between 5 and 20 kilovolts) based on how well each sample conducted electricity [34]. For extra study, we also used EDX (Energy-Dispersive X-ray Analysis) along with SEM. This helped us figure out what elements were present, because it made the elements send out special X-rays[23]. We were able to confirm that nickel and boron were definitely part of the mix. We studied how the Ni-B sheets were shaped using SEM. It gave us a better idea of how flat and smooth it was, and if any tiny particles had clumped together [37]. We looked at three different samples. One on the left (Sample 1), one in the middle (Sample 2), and one on the right (Sample 3). Each sample had unique features on their surfaces which were likely caused by changes in temperature and how much reactant was available during the creation process [36]. The SEM pictures showed changes in how large or small the grains were, and how smooth or bumpy the surface was. We think slight changes in gas flow or where the substrates were positioned could have caused these differences [34]. What was really impressive, though, was how well the Ni-B stuck to the copper base, which is very important for a steady performance in electrodes. These observations give us a good starting point for figuring out how to optimize the structure of these sheets for uses in electrochemistry.

Figure 4.1 *Representative scanning electron microscope (SEM) setup, illustrating the instrument layout and control system*

4.2. X-ray Diffraction XRD

X-ray diffraction (XRD) lets us identify and describe crystal parts in solid materials. It works by using X-rays, bouncing off atoms arranged in crystal patterns. Think of it like this - when a single color light beam hits a sample, it bends at specific angles. This bending follows a particular law known as Bragg's Law. In easier words, when the X-rays hit the crystal, they scatter in different directions - some add up, others cancel out. This scattering creates a pattern that tells us about the crystal's shape and size.

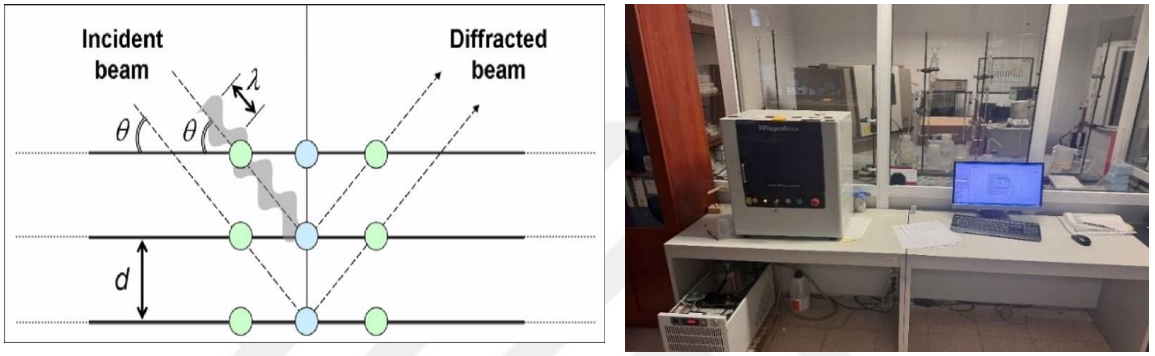

(a) (b)

Figure 4.2. *(a)Schematic illustration of X-ray diffraction, where constructive interference occurs at angle θ corresponding to lattice-plane spacing ddd. (b) Rigaku MiniFlex 600 diffractometer, featuring a 600 W Cu-Kα source and eight-sample holder, operated at 40 kV and 30 mA with a typical scan range of 10°–70° for phase identification and crystallite-size estimation.*

$$n\lambda = 2\,d\sin\theta \tag{4.1}$$

In a simpler way, diffraction peaks show the spacing within layers or 'interplanar spacings'.'XRD' was used to make sure nickel boride formed on copper after a certain process. XRD is special because it shows even tiny amounts of by-products or leftover reactants. It also confirms we've produced what we set out to make, not just simple elemental structures. This is vital for making something called a supercapacitor because its performance depends on the crystal structure and surface properties. We used a Rigaku MiniFlex 600 tool for this job. This tool comes with an X-ray source of 600 watts (Cu-Kα) and a slot to accommodate eight samples at a time. We usually measure at angles ranging from 10° to 70°, at a methodical pace of 2 °C per minute. The machine is operated at 40 kV and 30 mA, ensuring the beam is strong enough to detect even the

tiniest of phases. We then checked the X-ray patterns we received against a standard reference database. This way, we could identify different phases and make rough estimates of the size of the crystallite. Raman spectroscopy is a useful method that doesn't ruin things while exploring vibrations, crystal shapes, and how bits bond in stuff like nickel boride (Ni_2B). This method is created using a process named chemical vapor deposition (CVD). This method uncovers tiny changes in energy levels inside a solid by detecting light waves that bounce off differently, and it shows shifts in things' vibrations. These little details are essential because they prove if specific phases—like Ni_2B—have formed. They can also spot if there are other phases like layers of oxide or irregular domains [1,2]. When making supercapacitor electrodes, these things are essential: electrode effectiveness might rely on local bonding areas and the existence (or not) of specific crystal structures.

4.3. Overview of Raman Spectroscopy

The method uses a single-color laser, usually producing visible light, to stimulate the material being tested. Most light particles bounce back at the same frequency or color (a phenomenon known as Rayleigh scattering). A smaller portion of light, however, experiences a change in frequency, causing a shift to lesser (Stokes) or greater (anti-Stokes) frequencies. This happens when the vibration patterns within the sample either soak up or give off energy. To visualize these shifts in energy, we graph intensity against this Raman shift. This results in noticeable spikes that correspond to specific vibration patterns. For substances like Ni_2B, these spikes can help us tell apart B-Ni bonds from potential leftover substances like NiO or B_2O_3. In the case of Ni_2B supercapacitor electrodes, checking the chemical condition of boron and nickel confirms that the chemical vapor deposition (CVD) process produces the expected compound. Apart from this, Raman mapping can assess whether the material is consistent across the whole surface - a critical factor for constant electrochemical behavior.

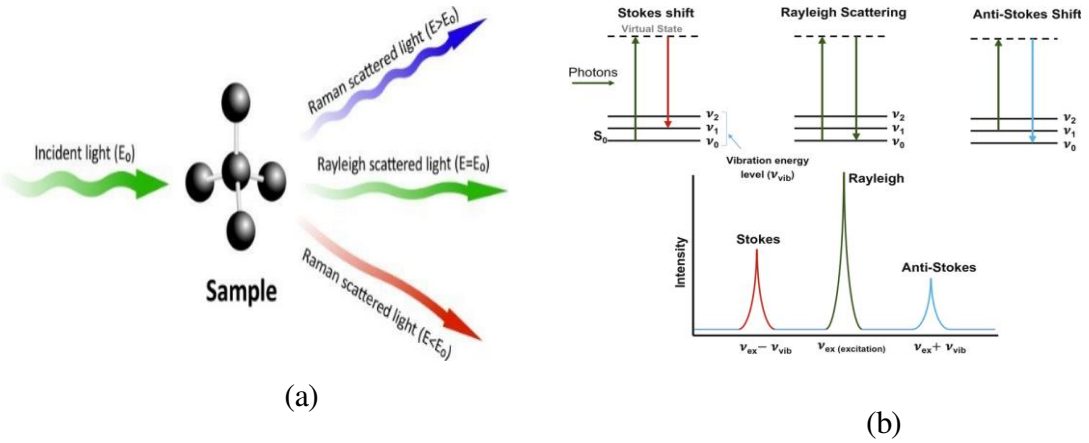

Figure 4.3. *(a) Schematic showing how incident photons (E_0) scatter elastically (Rayleigh) and inelastically (Raman). (b) Energy-level diagram contrasting Stokes, Rayleigh, and anti-Stokes scattering, along with the corresponding spectral positions (adapted from [38])*

Figure (a) shows how light particles (photons) can bounce off moving particles. Mostly, these photons keep the same energy after bouncing off (that's Rayleigh scattering). But, some come out with different amounts of energy, showing movement within the particles (caused by vibrations, known as Stokes). Some even gain a little extra energy (anti-Stokes). Figure (b). The green line in the middle shows Rayleigh scattering - the photons coming in and going out at the same energy. The Stokes peaks are a bit lower than the excitation line because the particles soak up some of the photon's energy. On the other hand, the anti-Stokes peaks are higher because the photon is added energy from a movement state. When it comes to studying supercapacitors, people tend to focus on the strong Stokes lines. This allows them to understand the structure of the particles distinctly. Raman spectroscopy enters the picture at this stage. It's a tool that researchers use to match the vibrations of B-Ni to known Ni_2B patterns. This step checks whether the growth process had made the correct phase (Ni_2B), and not some oxide or only partially reduced intermediates. Using this method alongside XRD and SEM reassures that the CVD protocol made uniform, pure-phase Ni2B used for supercapacitor applications. [1,5]

4.4. Atomic Force Microscopy (AFM)

We used something called AFM imaging to get a really close look at the layout of a surface, sort of like taking a super-detailed map [39]. For this, we used a silicon probe that's pointy end is tinier than 10 nanometers .The probe moved across the surface and

kept track of the differences in height [40]. All this data allowed us to produce flat (2D) and raised (3D) pictures. From these, we could figure out things like how rough the surface was. The great thing about this method is that it can show us how even a film is spread, where the edges of grains meet, and where there might be little holes. All of these things are pretty important when you're thinking about how electricity moves across a surface [41].

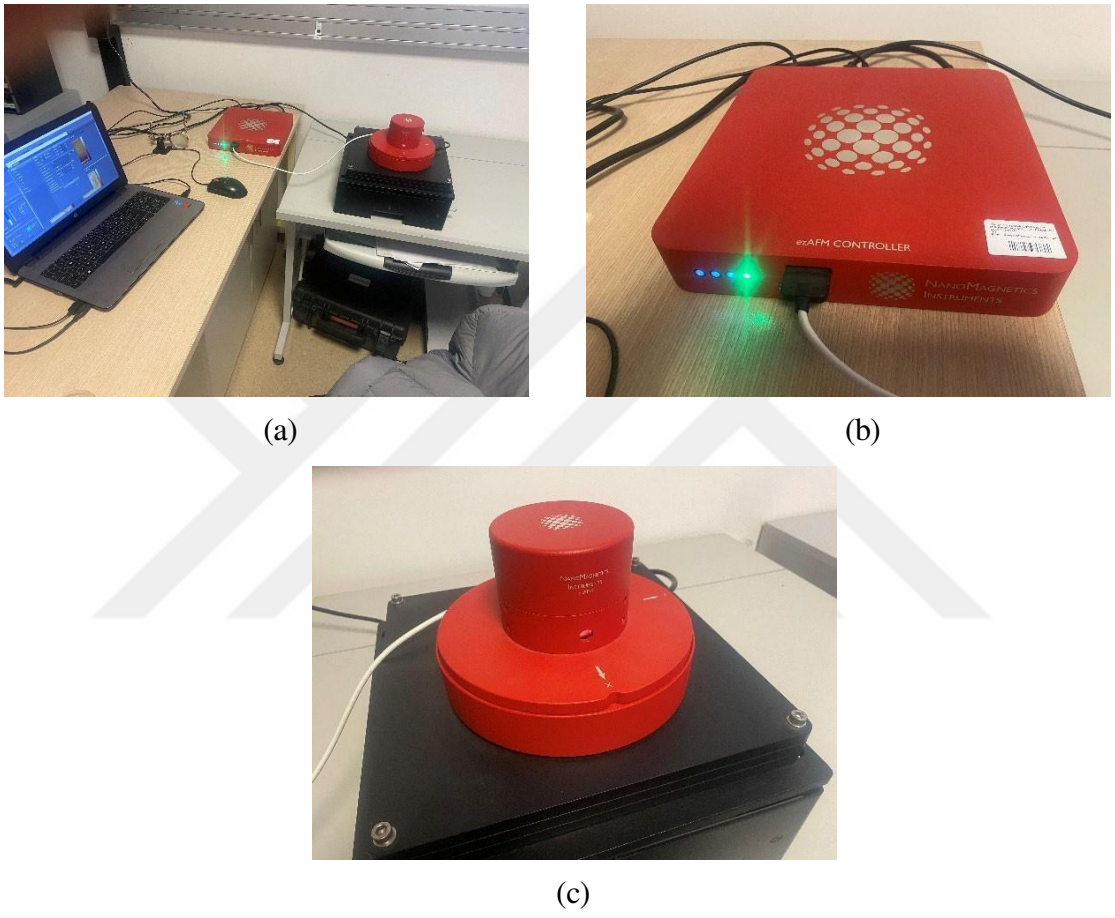

(a) (b)

(c)

Figure 4.4. *(a) AFM measurement setup: the main laptop interface controlling the NanoMagnetics Instruments ezAFM system, used for real-time topographical scanning, (b) close-up of the NanoMagnetics ezAFM controller, responsible for signal processing and precise tip movement adjustments, (c) the AFM scanner head unit, housing the probe assembly and enabling high-resolution surface imaging on the sample platform.*

We investigated how three different Nickel-Boron (Ni–B) samples looked and felt on the surface. We grew them on copper foils and called them Sample 1 (on the left), Sample 2 (in the middle), and Sample 3 (on the right). We scanned each one using a system from NanoMagnetics Instruments called ezAFM. Our scans showed that each sample had different features on the surface - things like grain boundaries and

roughness [42]. We used a method called tapping to scan each one, so we didn't damage the tiny details of the Ni–B layers [39]. From our first look, we thought that differences in heat or changes in conditions during the process we used to grow the Ni–B might affect how it grew [37]. When we used AFM to measure how thick the film of Ni–B was, we saw that it was pretty even, but found some places that had bumps - indicating spots of increased growth [34]. These bumps show us how small changes in the way we process the samples (like where we place the substrate or how we control the gas flow) can change the final surface textures of each sample. In conclusion, our AFM analysis showed us that each Ni–B sample has unique surface features, and these might affect how it performs in an electrochemical setting.

4.5. Supercapacitor (SCAP) Testing

We tested the Ni-B electrodes using three methods: cyclic voltammetry (CV), galvanostatic charge-discharge (GCD), and electrochemical impedance spectroscopy (EIS) [3]. We arranged three different electrodes (working, reference, and counter). Depending on the needed potential window, we chose an appropriate liquid (water-based or organic) [43].

4.5.1. Cyclic voltammetry (CV)

Voltage was swept from near 0 V to the upper potential limit at different scan rates (5–100 mV s^{-1}). The resulting current–voltage curves provided insight into redox activity and charge storage [1].

4.5.2. Galvanostatic charge–discharge (GCD)

By applying a constant current, the voltage profile was recorded during charging and discharging. Specific capacitances were computed from the slope of the discharge curves.

4.5.3. Electrochemical impedance spectroscopy (EIS)

Measurements were performed from high (100 kHz) to low frequency (10 mHz). The resulting Nyquist plots were fitted to an equivalent circuit model to extract solution resistance, charge-transfer resistance, and diffusion components.

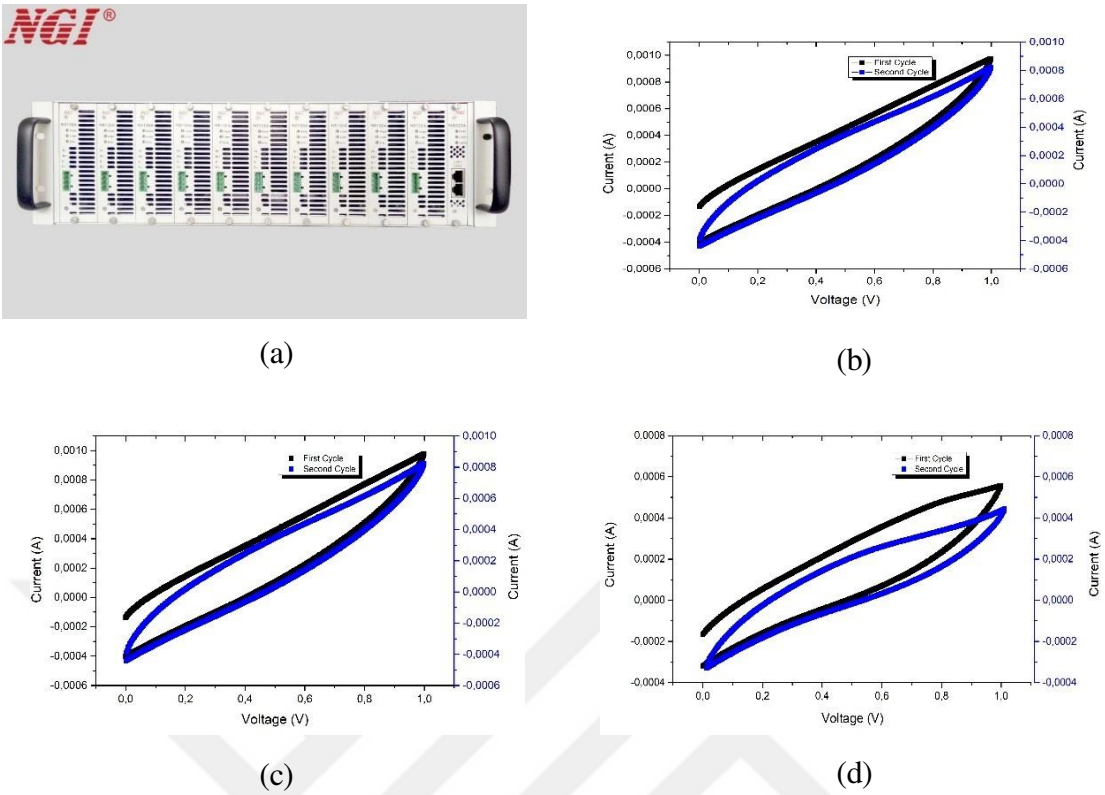

Figure 4.5. *(a)SCAP testing apparatus (NGI instrument) used to measure electrochemical properties of Ni–B samples(adapted from [44]), (b) Cyclic voltammetry (CV) curve of Ni–B at 1000 mV s^{-1}, showing the current–voltage relationship across two cycles, (c) CV profile of Ni–B at 500 mV s^{-1}, highlighting cycle-to-cycle variation and electrochemical stability (d), CV response of Ni–B at 200 mV s^{-1}, emphasizing the shift in current density with decreasing scan rate.*

5. MEASUREMENT & RESULTS

5.1. Optical Measurements

Images 10 (a-c), 10 (d-f), and 10 (g-i) together show the details on the surface of a sample of Ni_2B (a type of metal complex), looking closer each time at 10×, 50×, and 100× zoom levels, in order. These close-up pictures show the underlying texture (which looks like horizontal lines) and small bumps that may be signs of the creation of Ni-B, another kind of metal complex. These lines are often seen when the sample has been polished or mechanically smoothed in the past, while the small round features suggest that areas with more boron or Ni-B are separating from the rest. At the smallest zoom (10x, images 10a, d, g), you can easily see the overall texture of the sample with lots of similar, parallel lines, and some random darker areas. Moving in closer (50x, images 10b, e, h), you can see many more small bumpy formations. These bumps might show early signs of Ni-B or extra boron starting to form on the copper background. Boundaries that look like they're connected are also visible, hinting that some tiny cracks or localised stress relief may have occured either during or after the formation process. When we zoom in to the maximum level (100x, images 10c, f, i), we can clearly see individual tiny bubbles or droplet-like structures, and they're uniformly placed. This even spread suggests a controlled formation process, underlying the idea that the growth conditions for Ni_2B were stable enough to allow uniform deposits. Also, we can see a network of thin boundary lines where different areas meet, showing potential phase boundaries or slight differences in the surface chemistry of the sample. In conclusion, these close-up images prove that Ni_2B has formed on the copper background in distinct areas, forming bumps of different sizes. The lines from the polishing can still be seen through the thin Ni_2B layer, suggesting the deposited film fits well but isn't thick enough to hide the texture underneath. This kind of shape is often seen with boride coatings on metal backgrounds and matches with past studies on transition-metal borides[45]. Combining this with additional structural analyses (like SEM/EDX), we can understand how these surface bumps affect the mechanical, chemical, and electrochemical behavior of the Ni_2B film.

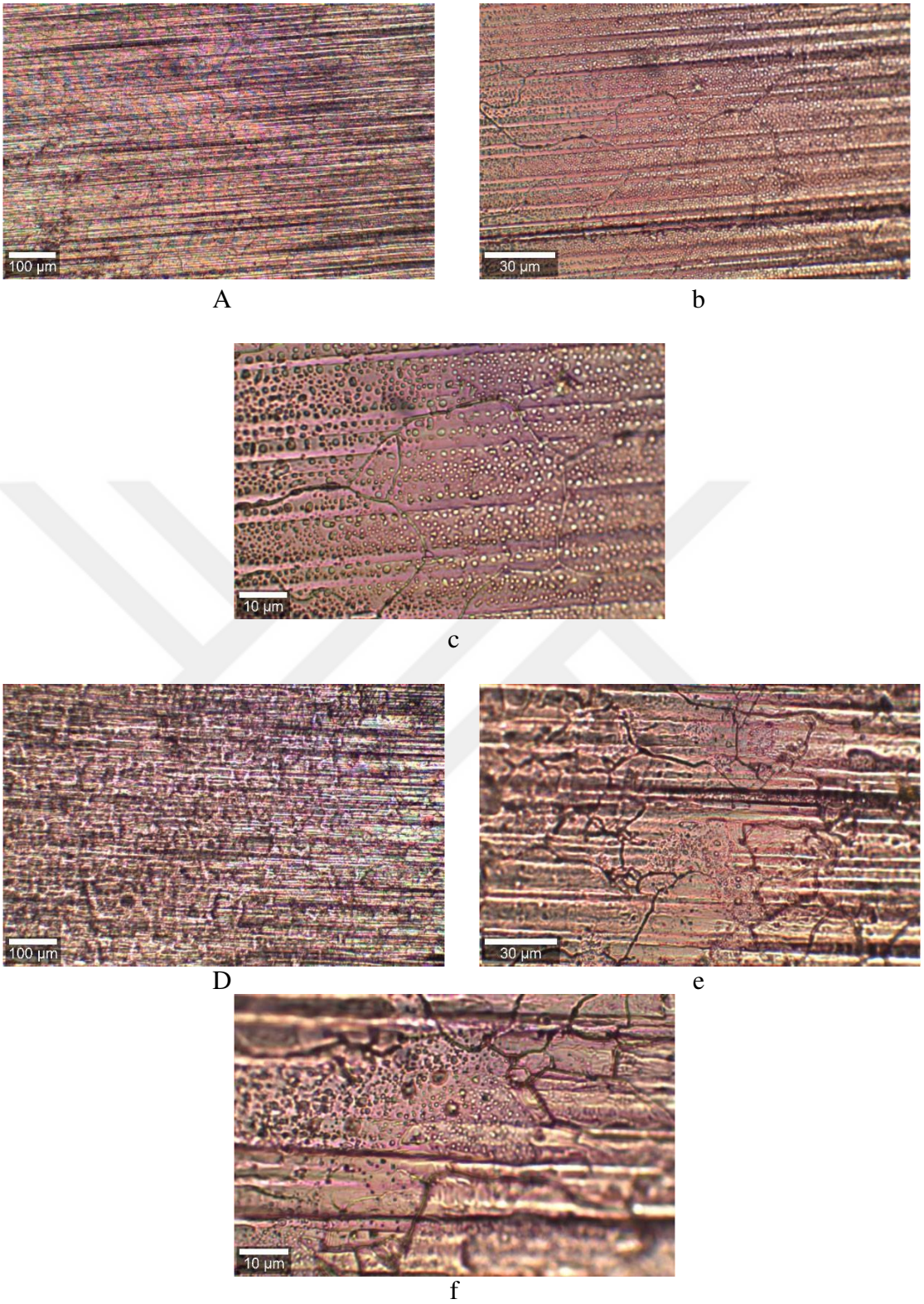

Figure 5.1. *(a–c), 10(d–f), and 10(g–i) collectively illustrate the surface features of Ni_2B sample 1 at magnifications of 10×, 50×, and 100×, respectively.*

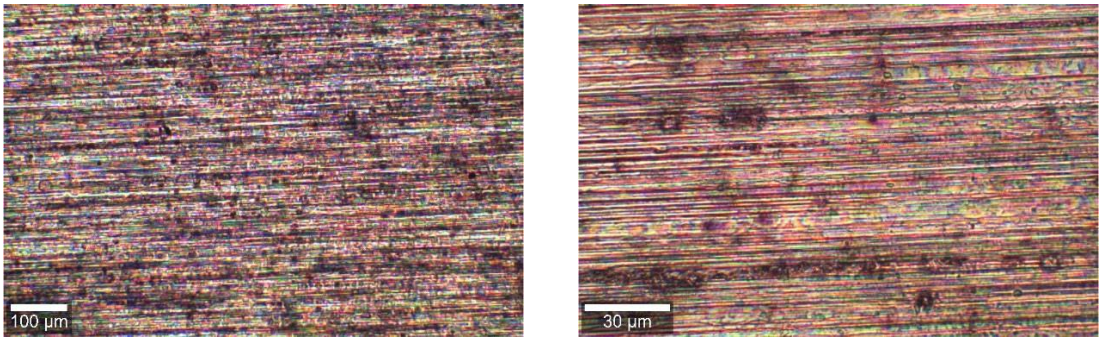

G h

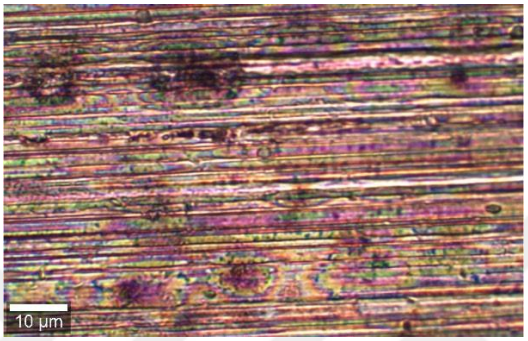

i

Figure 5.1. (Devam) *(a–c), 10(d–f), and 10(g–i) collectively illustrate the surface features of Ni_2B sample 1 at magnifications of 10×, 50×, and 100×, respectively.*

5.2. Raman Spectroscopy Measurements

In the Raman spectroscopy analysis, three characteristic peaks were observed at 220 cm^{-1}, 508 cm^{-1} and 880 cm^{-1} regions belonging to the Ni–B coating. The peak around 220 cm^{-1} corresponds to the bonds formed between transition metals and boron, and especially those in the literature as stretching modes of Ni–B bonds. It is reported that the 508 cm^{-1} peak is transmitted to the B–B gain (bending) votes of the boron element in its internal structure, and these votes are frequently observed in boron-rich intermetallic[46]. The third peak around 880 cm^{-1} is mostly the stretching modes of B–B chains and some strong boric structures (such as BO_3 or BO_4) are hidden[47]. This peak may also mark the B–O selections that may occur in the presence of slight oxidation on the surface. These three Raman peaks reflect the characteristics of the Ni–B system, indicating that both metal–boron interactions and boron-rich regions are confirmed. In the Raman spectroscopy analysis, a systematic shift was detected in the positions of the peaks observed around 800 cm^{-1} and 880 cm^{-1} depending on the temperature at which the samples were grown. While the peak is located around ~800

cm^{-1} in samples grown at high temperatures, this peak is observed around ~880 cm^{-1} in samples grown at low temperatures. In the literature, the red shift or blue shift of Raman peaks in similar systems (e.g. amorphous boron, metal borides) depending on the temperature is attributed to the structural regularity and bonding environment of the material[48]. In samples grown at low temperature, the bonds are shorter and more irregular, increasing the vibration energy and shifting the Raman peak to a high frequency (880 cm^{-1}); on the other hand, in structures grown at high temperature and becoming more regular, this peak is observed at a lower frequency (800 cm^{-1}). This shows that the bonding environment changes with temperature and the Raman spectrum reflects these structural differences sensitively.

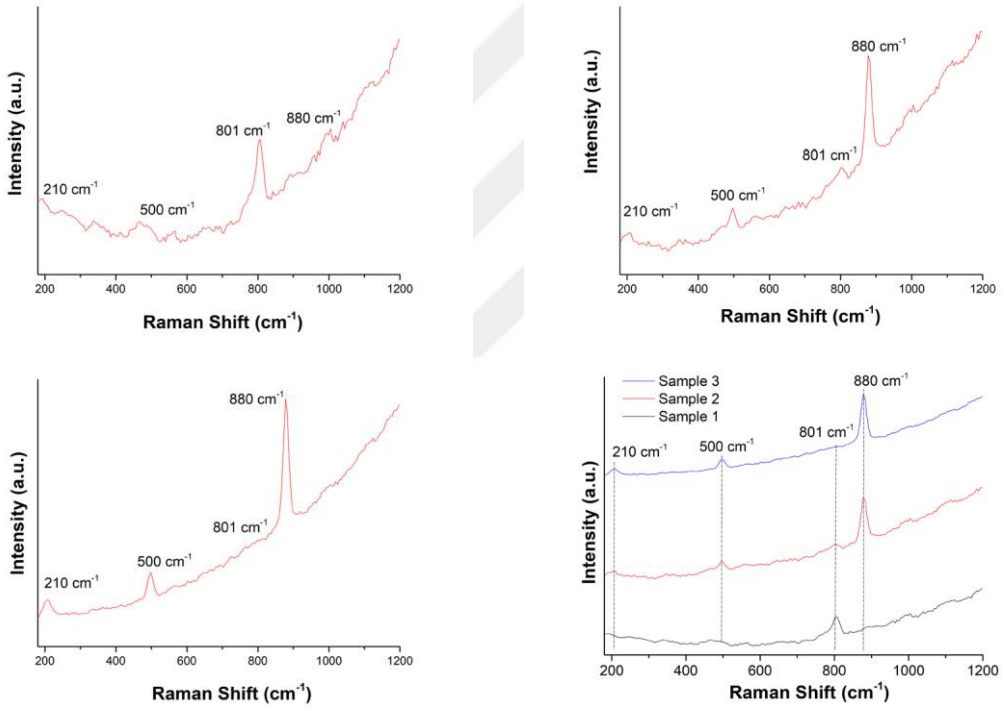

Figure 5.2. *Raman spectra of Ni_2B samples, illustrating (a) sample 1, (b) sample 2, (c) sample 3, and (d) a combined view (samples 1–3). Characteristic peaks at 210, 500, 801, and 880 cm^{-1} reflect vibrational modes associated with Ni–B bonding. Differences in peak intensity and position among the three samples suggest variations in crystallinity and surface composition.X-Ray Diffraction (XRD) Measurement.*

The XRD analysis gave the following 2θ values: 28.01°, 48.02°, 50.76° and 59.32°. These are similar to the Ni_2B phase readings found in scientific papers. [49] Specifically, 28.01° matches with the (001) plane; 48.02° with the (111) plane; 50.76° with the (200) plane; and 59.32° with the (210) plane. [50]These are in line with the

patterns on card no: 03-1170 of JCPDS, for tetragonal Ni_2B. This means the crystal structure of the sample is highly crystalline Ni_2B phase. Researchers have seen similar XRD patterns for Ni_2B, especially 28° for the (001) plane and above 50° for both the (200) and (210) planes. Using these values and Raman analysis results, a strong bond between metallic nickel and boron is clear in the structure. There is also a distinct Ni_2B phase.

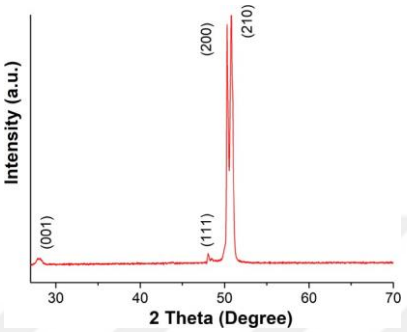

Figure 5.3. *X-ray diffraction (XRD) pattern of Ni_2B, highlighting prominent reflections at (001), (111), (200), and (210). The strong (200) peak suggests a preferred orientation and indicates the predominant crystalline phase of the deposited Ni–B layer.Atomic Force Microscopy (AFM)*

5.3. AFM Characterization

5.3.1. AFM characterization of Ni_2B films for sample 1

This part shows six images from an atomic force microscope (AFM). These show the look, roughness, pattern, size, and 3D outline of a layer made of Ni_2B. This layer was grown on copper materials using a technique called CVD. AFM was used to analyze three things: pattern, roughness, and structure. It also made 3D images of the surface and sized it. Looking at Figure 5.1 (a), we see a picture showing differences in the layer's material features, like stickiness and stiffness. Colors showing up differently could mean a slight change in the hardness of the material or what it's made of. Figure 5.1 (b) shows us the map of roughness (or a picture showing roughness levels). The numbers that go with it (Ra, Rq, Rsk, and others) point to a pretty rough surface. For instance, the Ra value is about 0.13 µm, while Rq is about 0.18 µm. A skewness number of roughly -1.6 tells us the surface has deeper dips than rises. A high kurtosis value (around 7-8) suggests sharper, standout features. This kind of surface could boost the effective area for chemical reactions involving electricity [51, 52].

Table 5.1. *AFM roughness parameters for Ni_2B film on copper.*

Parameter	Value	Comment
Ra	**0.13 µm**	**Average roughness**
Rq	0.18 µm	RMS roughness
Rsk	–1.645	Negative skew, indicates valleys
Rku	7.437	High kurtosis, “sharp” topography distribution
Rp (Max)	1.41 µm	Peak height above mean plane
Rv (Min)	0.00 µm	Lowest valley relative to mean plane
Rt	1.41 µm	Peak-to-peak distance
Rz	1.35 µm	Ten-point height

We learned that Ni-B-based electrodes often work better when they have a certain degree of surface roughness, approximately 0.1 to 0.2 µm. Our tests also support this, hinting that a slightly rough Ni_2B layer might improve electrical charge transfer. This roughness isn't random- it has certain shapes and features. A lower skewness value shows dips that could make the surface area more effective. High 'kurtosis' points to sharp peaks and deep valleys on the surface. These features can offer more places for redox reactions, a plus for battery or supercapacitor use [53]. The space from peak to peak (or Rt) is about 1.41 µm. This shows the surface's difference in height but remains within a doable range for building into an electrode. Too much roughness can slow ion transport, while too little can restrict the electrode area. So, the medium values we obtained might give the best performance. Graph 5.1(c) shows changes in the surface's height across its width. The highest and lowest points can be set apart by hundreds of nanometers, supporting the roughness data. These height differences could help ion transport and electron exchange for battery or supercapacitor electrodes [54].

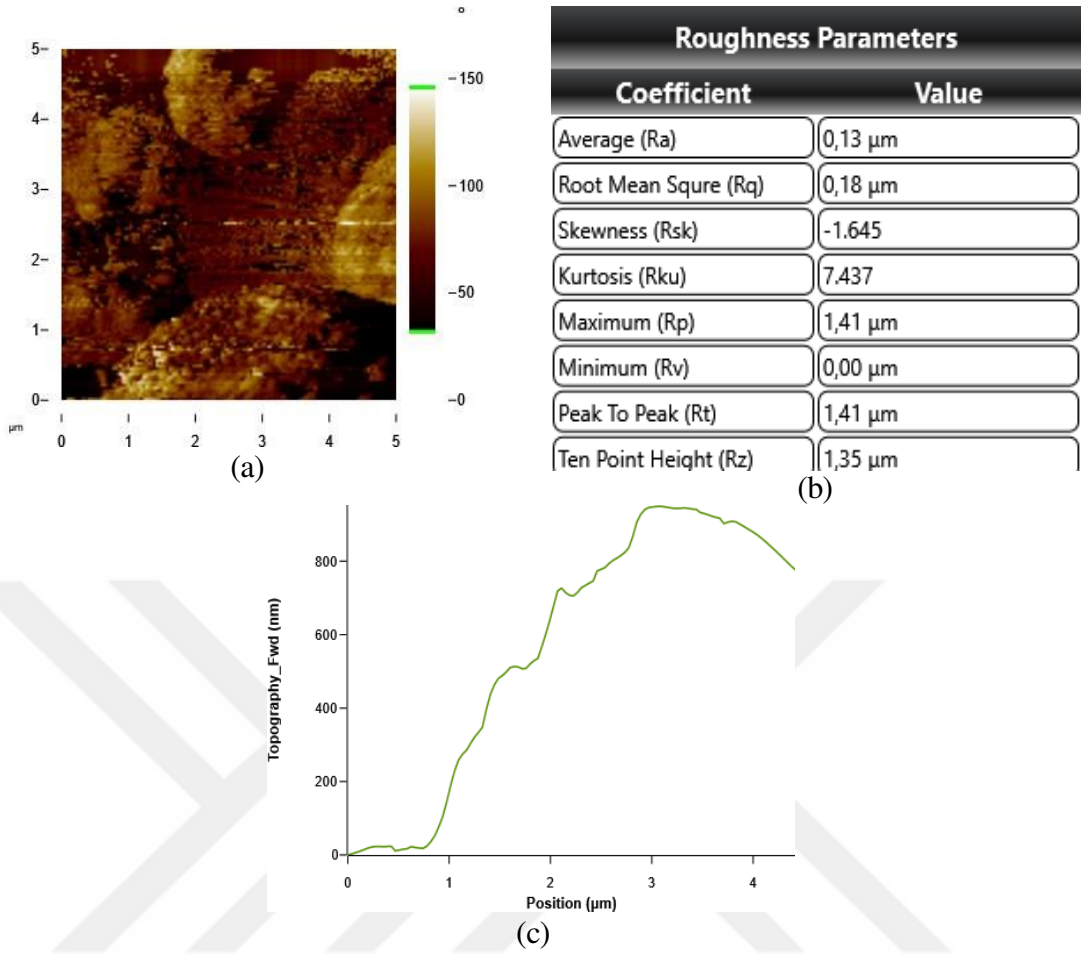

Figure 5.4. *(a) Phase map revealing local property variations, (b) roughness distribution of Ni_2B (Ra ~0.13 µm; negative skewness ~ –1.6), and (c) topography line-scan showing height differences up to ~0.8–1.0 µm.*

Figure 5.2 (a). It's a different type of map. Same area - 5 µm x 5 µm. But instead of roughness, it shows us hills and valleys. Some bits look like small globes, while others are more like long hills. It probably comes from how we made the Ni_2B using a technique called CVD on top of copper. Figure 5.2 (b) takes it a step further. This gives us a 3D view of the Ni_2B surface – kind of like flying over it in a plane. You can see the changes in height are somewhere around 400-800 nanometers. This helps us see the lay of the land. We can spot the valleys and the hills that were pointed out in that line-scan, back in Figure 5.1 (c). And we can see the surface isn't too rough, which is a good thing if we want it to work well in reactions. Figure 5.2 (c) shows yet another angle – it shows us an amplitude image. This type of image helps us understand the impact of surface features on the changes in the tool's swing amplitude when it touches the surface.

Imagine being able to see how high or steep the edges of the Ni_2B surface are. It works kind of like high-contrast boundaries, emphasizing the sudden changes in height in these zones. Together with the phase image, it gives us a clearer view spots where the Ni_2B coating could have unique mechanical traits or sticking qualities.

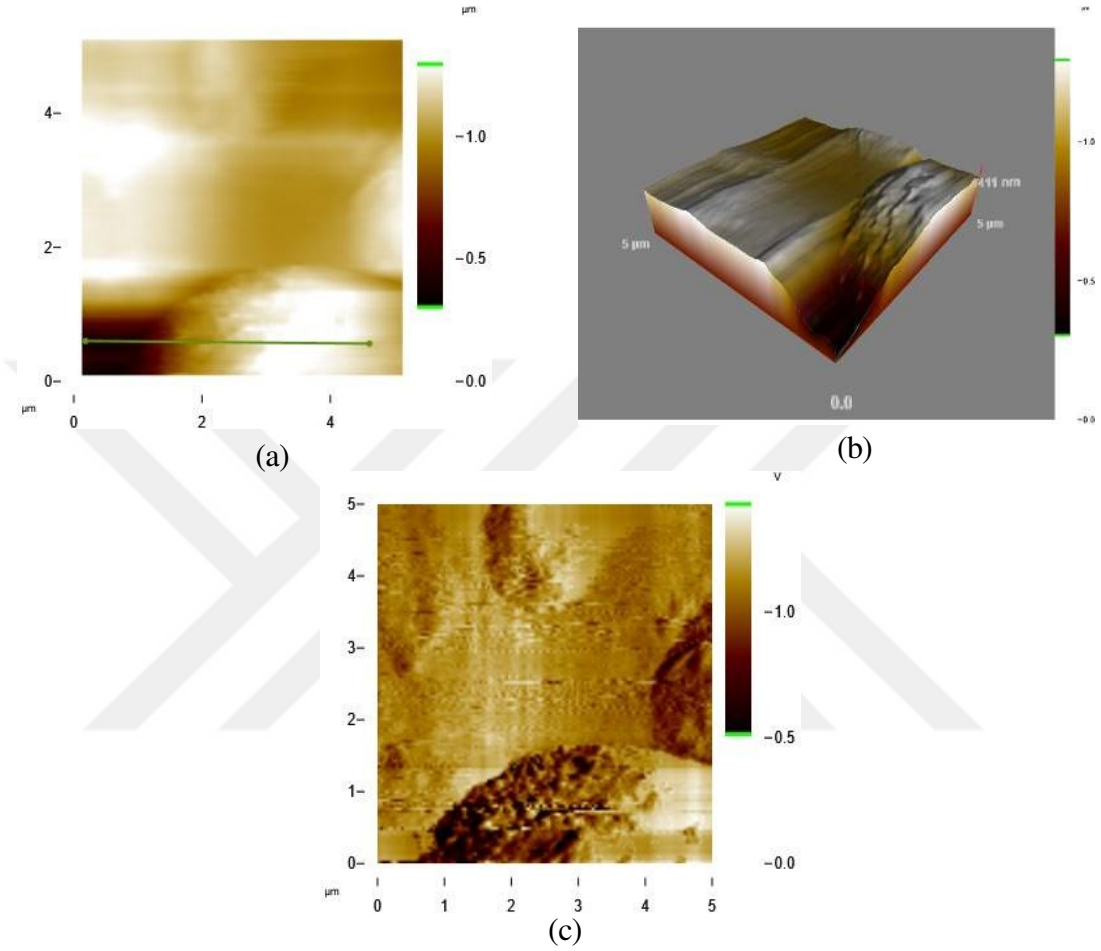

Figure 5.5. *(a) Topography map highlighting Ni2B grain structure, (b) 3D surface plot showing peaks/valleys up to ~0.8 µm, and (c) amplitude image revealing areas of higher slope or interface contrast*

5.3.1.1. AFM conclusion for sample 1

Here's what the six AFM images show us when we look at them all together: Some Bumps and Roughness: It is not super smooth. It is kind of like a road with a few bumps and divots (discussed in section 5.1). There are hills and valleys: There are differences in height. It's like a landscape with some parts being up to ~0.8–1.0 µm higher than others (seen in figures 5.1 (c) and 5.1 (b)). Different Shades and Movements: These might hint at differences in what the surface is made of, or might suggest how it behaves. This could affect the performance of the electrode (seen in

Figures 5.2 (a) and 5.2 (c)). It's similar to past findings about specific electrodes. People have found out that a little roughness and a varied surface can improve chemical reactions with electrodes.[52, 55]If we look at the 3D image (Figure 5.2 (b)), we realize more changes in the slope and curve. It's like a hilly landscape that might provide more space for reactions. Such might improve certain chemical reactions.

5.3.2. AFM characterization of Ni_2B films for sample 2

In this section, a series of AFM images is examined.. These show how the surface shape, roughness, different areas, and 3D shape look like for Ni_2B created with CVD on copper. In past pictures 5.1 and 5.2, the focus was just on the first Ni_2B sample (Sample 1). Now, we're looking at another sample too, which we'll call Sample 2. It comes from the middle area of the CVD machine we used. When we go by earlier research, middle temperatures and middle-level gas flows can make Ni-B films that have balanced roughness and good electrochemical traits.

5.3.2.1. AFM analysis of phase, roughness, and topography graph, 3D surface image, amplitude for sample 2

Let's take a step further from the information of Sample 1. Now, let's look at Sample 2. This sample was placed in the middle part of the CVD tube. The next AFM results, seen in figures 5.3 (a), 5.3 (b), and 5.3 (c), show us something interesting. Even small changes in heat and how much raw material flows can affect how Ni_2B film forms [9].

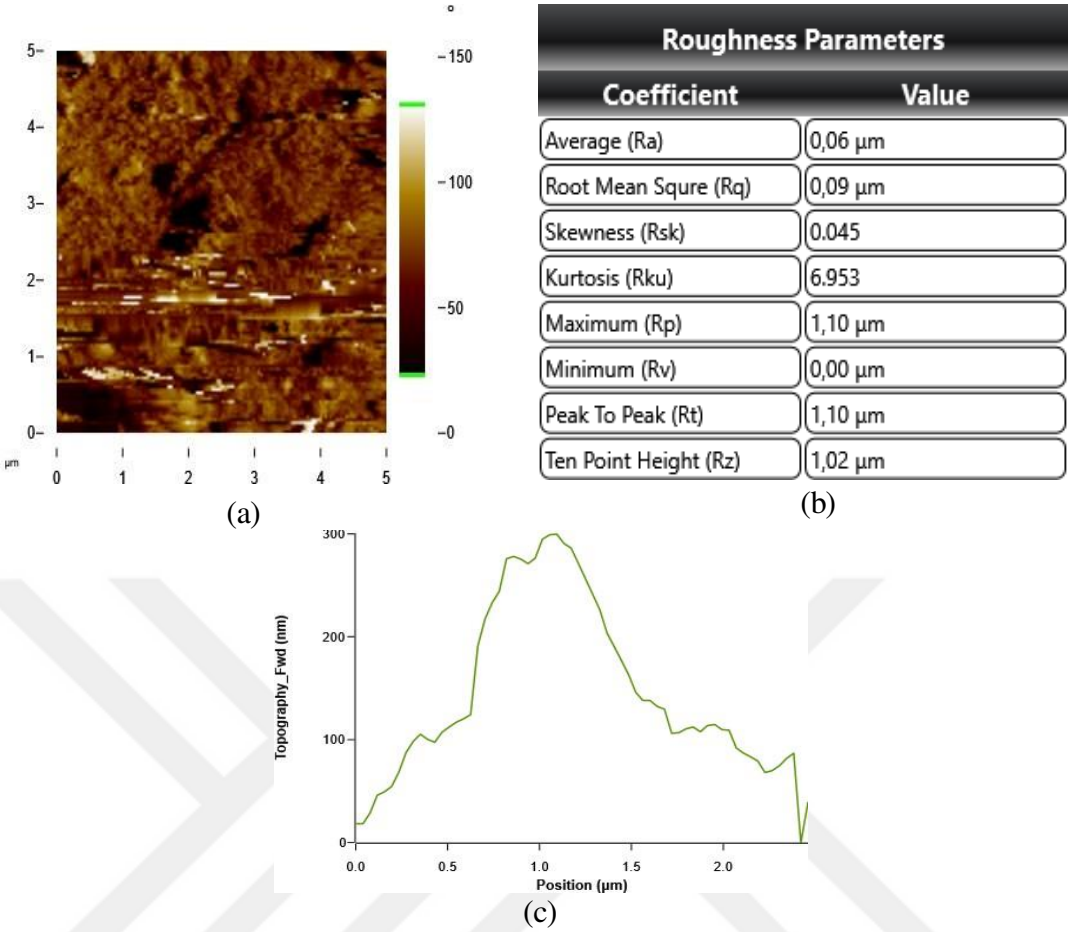

Figure 5.6. *(a) AFM topography/phase image, (b) Roughness parameters for Sample 2, (c) Topography line-scan across ~2.5 µm.*

The AFM picture of our second sample shows a grainy surface. It looks less full of valleys than our first sample. Small changes in phase hint at little inconsistencies in materials or movement. Compared to the negative skewness in our first sample, these differences could mean the Ni_2B layer forms more evenly spread groups in medium CVD conditions.

Table 5.2. *(extracted from the AFM software) summarizes the roughness metrics for Sample 2.*

Coefficient	Value	Comment
Average (Ra)	0.06 µm	Indicates a smoother overall surface than Sample 1
RMS (Rq)	0.09 µm	Less variance in peak–valley amplitude
Skewness (Rsk)	0.045	Slightly positive → mild protrusions, fewer deep pits
Kurtosis (Rku)	6.953	High → suggests some sharper features, but not many
Maximum (Rp)	1.10 µm	Tallest peak from mean plane
Minimum (Rv)	0.00 µm	No negative valley observed below mean plane
Peak-to-Peak (Rt)	1.10 µm	Matches max–min difference, occasionally spiky lumps
Ten Point (Rz)	1.02 µm	Another amplitude indicator

Sample 2 isn't as rough like Sample 1. Its bumps and dips are less than half of Sample 1's. This suggests it doesn't have many big dips. Moreover, it has more small bumps than major dips. Even with this level of unevenness, it still helps good electrical activity without having too many surface bumps and dips. The line-scan shows most bumps to be around 300nm, even though some spikes reach 1.10µm. This goes along with the roughness data. When we compare it with Sample 1's ~800–1000 nm waves, Sample 2 appears to be more even overall. This might help with even electricity distribution and reduce the possibility of wear and tear in repeated uses. In nickel-boron electrode research, a modest bumpy surface tends to go with stable performance over many charge–discharge cycles[56]. Next, we present three more AFM outputs to sharpen our understanding of the Ni_2B film deposited in the middle of the CVD reactor.

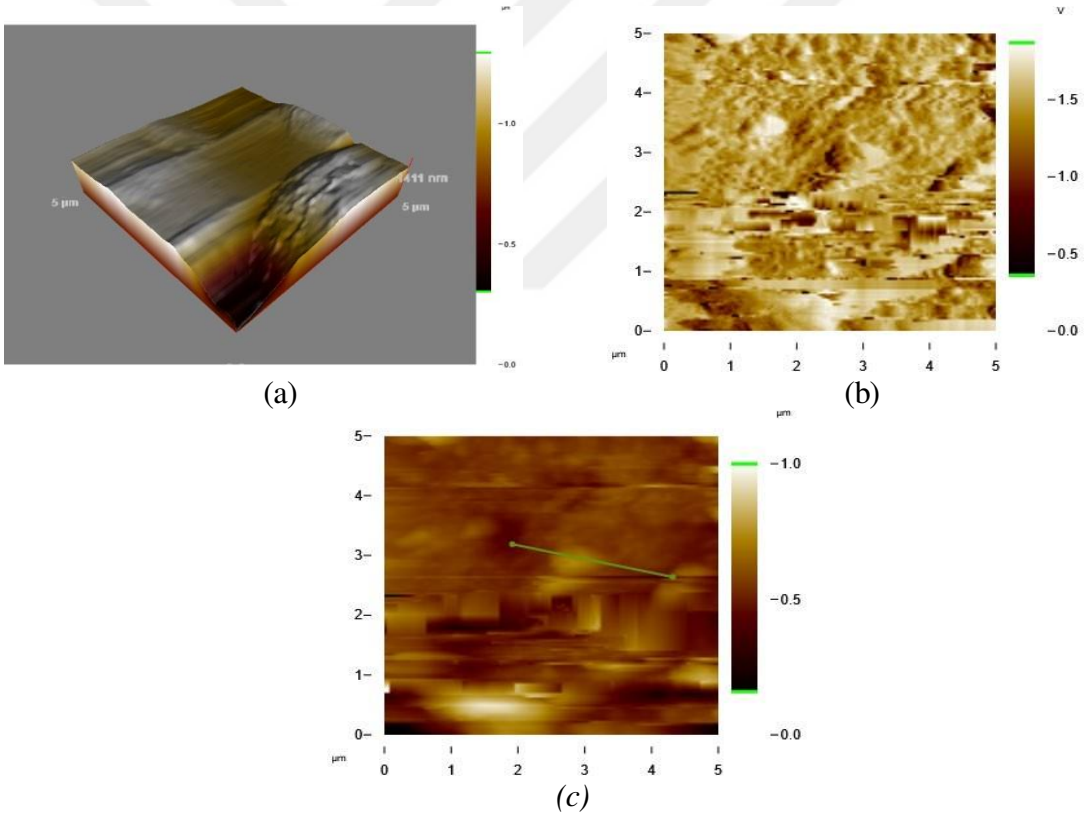

Figure 5.7. *(a) 3D topography map of Ni_2B (Sample 2), revealing moderate vertical relief (~1.1 µm) over a 5 µm × 5 µm scan area, (b) Amplitude image illustrating how the AFM tip's oscillation responds to local slopes and mechanical variations, (c) Alternate amplitude/color-scale view emphasizing subtle topographic transitions.*

Image 5.4 (a) it gives us a 3D view of the Ni_2B surface on the second sample. The vertical scale shows changes of around 1.1 microns - this lines up with our previous

reports. Unlike a simple 2D map that only shows height, this 3D view reveals high and low areas across the 5 microns by 5 microns area. These changes in height are linked to steady energy flow in Ni-B electrodes. This is because they provide enough surface structure for high active area, but avoid deep pits that can trap gas or slow down ion flow [57]. Some of the ridges are gentle, which might help to evenly distribute current. We can see a few steep drops that are longer than 0.8 to 1.0 microns, but these seem less common compared to the samples at high temperatures [58]. This 3D view suggests that, under middle CVD zone conditions, the Ni_2B crystallization is pretty balanced—neither extremely uneven nor too flat. Now, let's switch to Image 5.4 (b). It shows the amplitude image, which is a type of AFM channel showing how the oscillation of the cantilever is slowed by contact with the surface. Areas with high contrast often show that the slopes are steep or that the material has suddenly changed. In this image, High-Amplitude Zones appear as either lighter or darker areas. These could align with the edges of bumps or tiny craters. Lower-Amplitude Regions indicate flatter areas or areas with uniform mechanical properties. Amplitude data can complement phase and topography images. It can be used to note transitions from tiny different mechanical areas, especially if there are doping or partial nickel-boride changes. Sometimes, a second map similar to the amplitude one will use a different color scale or phase shift to emphasize different thresholds of slope or stiffness. As shown in Figure 5.4 (c), any added bright/dark contrasts might spotlight fine details not seen in the main amplitude image. By noting subtle changes across the film will be key to making Ni_2B perfect for uniform reaction sites [59]. Even a slight variation in amplitude shading could denote slight differences in Ni/B ratio. If doping elements are added, they could change the local mechanical properties in certain miniature regions. Despite the fact that there is a moderate range between the highest and lowest points of roughly 1.1 microns, the roughness data is consistent (Ra is roughly 0.06 microns, with a slight lean towards the positive). Contrasts in amplitude suggest that sections of the film might be slightly harder or stiffer, suggesting uneven boron incorporation. This shape likely maintains robust surface sites for storing charge, while avoiding excess roughness that might slow down ion movement or introduce mechanical stress. For Ni-B or Ni2B electrodes, this kind of balanced topography is often seen as a positive for stable, long-term performance in super-capacitor or battery applications[60].

5.3.2.2. AFM conclusion for sample 2

There are two examples to understand how different conditions can shape surfaces. The first one has a rougher surface with deep valleys. The second example is smoother with less deep valleys. Both these surfaces can be helpful in different ways. Some designs work better with more valleys, while others do better with smoother surfaces for a steady flow of electrons/ions [61]. Managing these surface traits is important for sturdy Ni_2B electrodes. Too rough and it can trap gas or make ion movement hard. Too flat and it decreases the active area [62].The mid-zone temperature and precursor flux might assist with the controlled formation of Ni-B with fewer extreme differences in the surface. Earlier reports on temperature-gradient CVD show that mid-zone substrates often lead to uniform metal-boride coverings [55].

5.3.3. AFM characterization of Ni2B films for sample 3

Sample 3 lives in the chilliest part of our CVD reactor. At this spot, things like the local temperature and chemical flow change a lot, making it very different from the hot part of the machine. Researchers tell us that when nickel-boride layers form in cooler spots, interesting patterns can take shape. They might show teeny-tiny crystal-like bits or deeper dips and dents. The following three pictures from our high-tech microscopes will help you see these unique shapes and patterns.

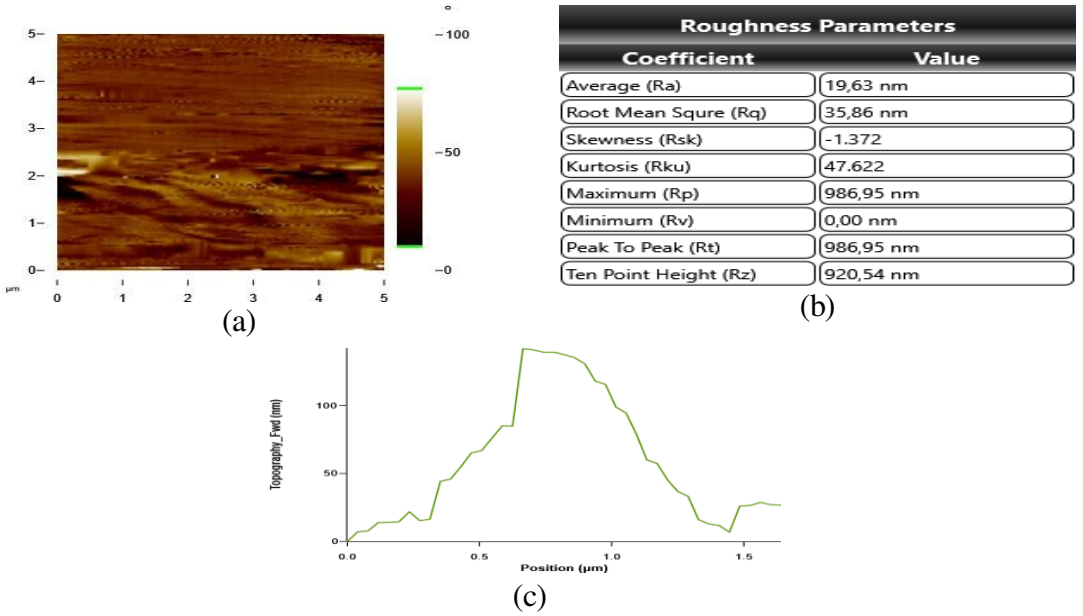

Figure 5.8. *(a) Phase image illustrating local mechanical/compositional contrasts, (b) roughness parameter details, and (c) 2D line-scan capturing vertical height variations.*

The picture (a) shows small changes in the film's hardness and stickiness. You can notice this by the changes in colour over the 5 µm x 5 µm area [9]. The contrast in colours could be because of uneven mixing of nickel or boron. This might show nickel-boron fusion happening in cooler areas during the chemical process [10]. In the area of electrodes, this diversity could affect where chemical reactions occur. Below is an example table summarizing the roughness data Figure 5.5 (b) Note that the measurements are reported in nanometers, a change from prior samples that used micrometers:

Table 5.3. *(extracted from the AFM software) summarizes the roughness metrics for Sample 2.*

Coefficient	Value	Comment
Average (Ra)	19.63 nm	Moderately low average roughness (in nm scale)
RMS (Rq)	35.86 nm	Indicates moderate peak–valley amplitude
Skewness (Rsk)	–1.372	Negative skew → deeper valleys predominate
Kurtosis (Rku)	47.622	Very high → distribution with a few sharp or extreme features
Maximum (Rp)	986.95 nm	Tallest peak from the mean plane
Minimum (Rv)	0.00 nm	No measured valley below the reference plane
Peak–Peak (Rt)	986.95 nm	Overall vertical span can be nearly 1 µm
Ten Point (Rz)	920.54 nm	Another indicator of amplitude across highest/lowest points

The surface we studied is a bit smoother than before with a roughness about the width of a human hair. Still, there are some really big bumps, almost as big as a speck of dust. When we look at how rugged the surface is, it's mainly full of dips and those dips are deep and sharp. We tracked changes in how high or low the surface was over a space thinner than a thin human hair. We normally see bumps about the size of a bacteria, but sometimes we see spikes bigger than that, like the biggest one we found in our roughness table. These sudden bumps might be little clumps or ridges that built up when the stuff was laid down in cooler temperatures. Big changes in the surface can mess with how even our instrument is and make it less sturdy when used over and over again.

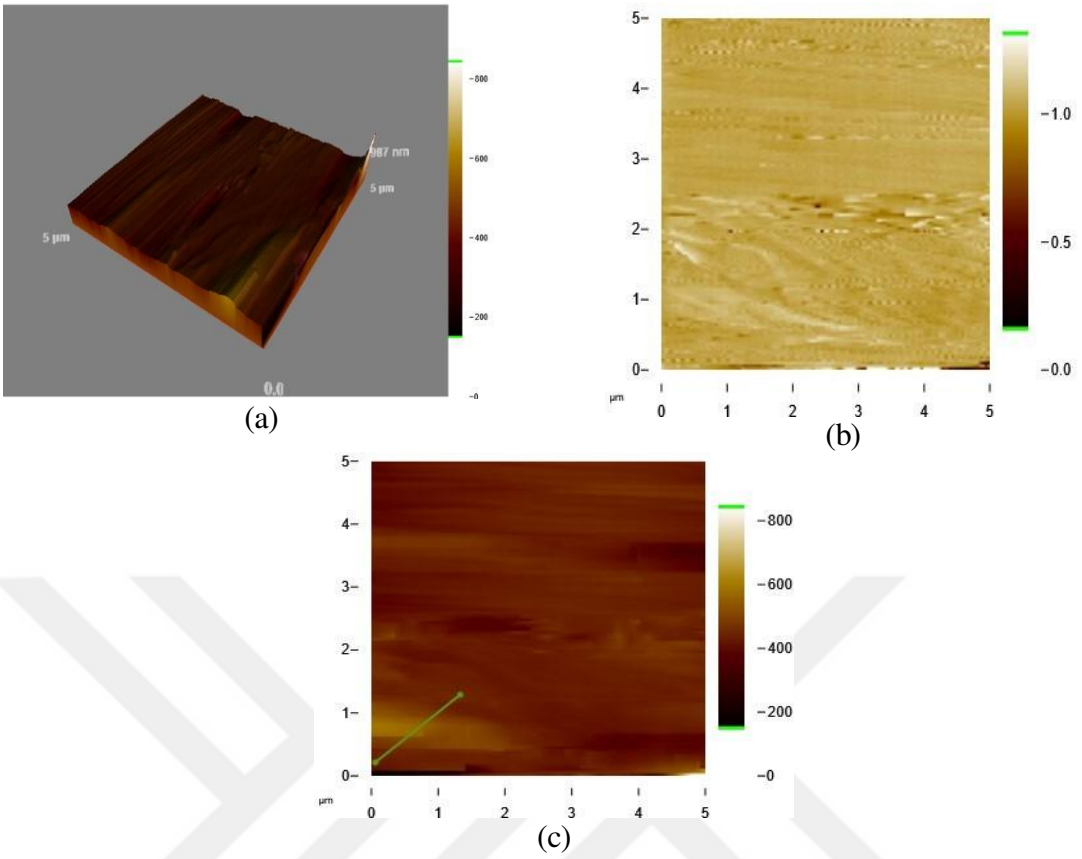

Figure 5.9. *(a) 3D rendering of the Ni_2B surface on Sample 3, highlighting vertical variations across the 5 µm × 5 µm scan, (b) amplitude map illustrating how the AFM tip's oscillation reacts to local slopes or mechanical contrasts, (c) alternate topography (or amplitude) image of Sample 3, using a different color scale to emphasize certain height or slope thresholds.*

This view shows us how the Ni_2B layer makes hills and dips in the coolest part of the CVD reactor on the far right. The up and down size could be anywhere from ~800–1000 nm (based on the color bar). This means that even if it's not very bumpy on average, there could be high hills or deep dips in certain places. The surface here might be smoother than previous samples, but with occasional tall or deep features because of uneven cooling. Areas that are very high or very low in size usually match with sudden changes or smooth spots. If bright spots show up around hills, this means the cantilever faces stronger slowing down, often because of more sudden or abrupt shape changes. This size channel can help the 3D view by highlighting tiny cracks or faint lines between Ni_2B grains. A second channel or color scheme can show features that aren't so noticeable in the main size map. Small shading changes could point out areas of partial Ni–B, extra ingredients, or shifts in local mechanical properties. If you notice patterns repeating from (b), it confirms distinct small areas or lumps exist. If new details show

up, it means the initial size scan missed small slope changes [63].

5.3.4. Observations

Here's a simpler way to look at these 3D and detailed images, compared to the past info on roughness and individual scans: How High and Low Values Match: If the 3D image is showing a top-to-bottom difference near about 800-900 nm, it goes along with the side-leaning trend and extreme sharpness we saw in the roughness figures. Specific Sharp and Steep Features: Details stand out more in the detailed images, backing up the idea that if Sample 3 grew in a colder place it might have patchy Ni_2B growth [63]. Possible Effects from the Electrode: A bit of natural roughness plus sudden deep dips might widen the active surface but risk creating extra strain, especially if we constantly charge and discharge it [59] . In general, these extra AFM image types show that Sample 3, grown in colder CVD conditions, has some really extreme shapes (either deep dips or high spikes) in specific areas, while staying pretty smooth elsewhere. These different shapes might affect how well it works with electricity. High surface area can be good, but there's also a chance of trapping liquid or putting strain near the standout features.

5.4. SEM Analysis Results

5.4.1. SEM examination and EDS analysis of polished copper substrate

In Figure 5.7 (a) the device called a Scanning Electron Micrograph, or SEM, snapped a picture. It's a smooth copper surface. But it's not just smooth - it also has long, straight, side-to-side scratches. They came from the final stages of polishing, especially in softer metals like copper. These lines show that the polishing direction was pretty much the same all throughout. One good thing is we don't see any big blemishes, cracks, or extra dust particles. That shows us that the process of mechanically grinding the metal, and washing it afterwards (for instance, with a solution like acetone), did its job. We've got a smooth, clean starting point to work with, free of major dirt or rough patches [64].

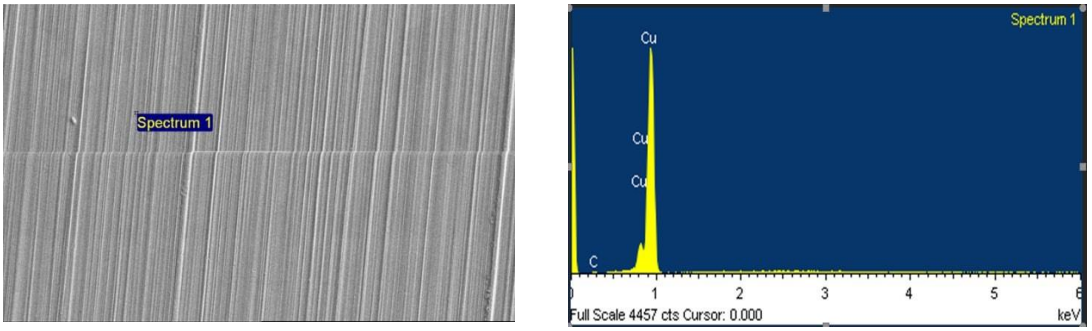

(a) (b)

Figure 5.10. *(a) SEM micrograph of the polished copper substrate, showing parallel scratch lines indicative of consistent abrasive finishing, (b) EDS spectrum (Spectrum 1) of the polished copper substrate, demonstrating a dominant Cu peak and a smaller C peak.*

Figure 5.7 (b). It shows a graph called Spectrum 1. We also get this info from the same area in a different picture, called SEM. Table 1 lists down all the items found in Spectrum 1. Copper (Cu) makes up about 94.87%. Carbon (C) is much less – it's only about 5.13%. Sometimes, carbon amounts to less than 10%. That usually comes from leftover polish, thin carbon layers that happen by chance, or tiny amounts of natural materials that get mixed in when the sample is handled. Sometimes, carbon is not a clue of alloy – it could just mean there's some dirt from the air or the polish [65].

Table 5.4. *EDS composition from Spectrum 1 indicating minimal carbon presence and a predominantly copper substrate.*

Element	*Weight%*	*Atomic%*	*Interpretation*
C (K)	*5.13*	*22.5*	Residual polishing media, airborne contamination, or organic films
Cu (K)	*94.87*	*77.75*	Main metallic substrate (polished copper)

The tests show our copper sample is super clean. We've managed to get rid of nearly all the pesky impurities and oxide layers. It's perfect for our next step. The acetone rinse and nitrogen drying worked great. They helped us wipe away big junk. Experts agree that a polished and super clean copper surface like ours is really helpful. It's great for adding coatings, like growing Ni-B film using a process called chemical vapor deposition (CVD). It helps the coating cling really well and evenly [66].

5.4.1.1. SEM analysis of polished copper substrate (spectrum 2)

Looking at more microscope pictures in Figure 5-8(a) and Figure 5-8(b), we see more proof of a smooth copper surface. Just like the last spot we looked at, the metal shows some neat, parallel lines. This is probably from the polishing process. There don't seem to be any big holes or foreign matter, which is good news! These straight lines likely come from a last polish with abrasives. This is usually followed by a rinse with acetone and a blow-off with nitrogen, which helps get rid of stuff that shouldn't be there. Detailed results from the EDS (short for Energy-Dispersive X-ray Spectroscopy) in Table 5.5 tell us copper still makes up the majority – around 94.18%. The carbon part has increased just a tad to about 5.82%. That's not weird though; different spots on the metal can have more or less of the junk left behind by polishing. Still, the main point is that copper beats everything else by making up more than 90%. This tells us that the polishing likely did a good job getting rid of any unwanted stuff, leaving a clean metal surface. Putting down a layer of Nickel-boride (Ni-B). And having a clean metal surface can make this layer stick better and look more even [67, 68].

Table 5.5. *EDS composition for Spectrum 2 on the polished copper surface, indicating a slight increase in carbon compared to Spectrum 1 but still reflecting a predominantly Cu substrate.*

Element	Weight%	Atomic%	Potential Source
C (K)	5.82	24.65	Polishing residuals, mild environmental contamination, or organics
Cu (K)	94.18	75.35	Substrate metal (polished copper)

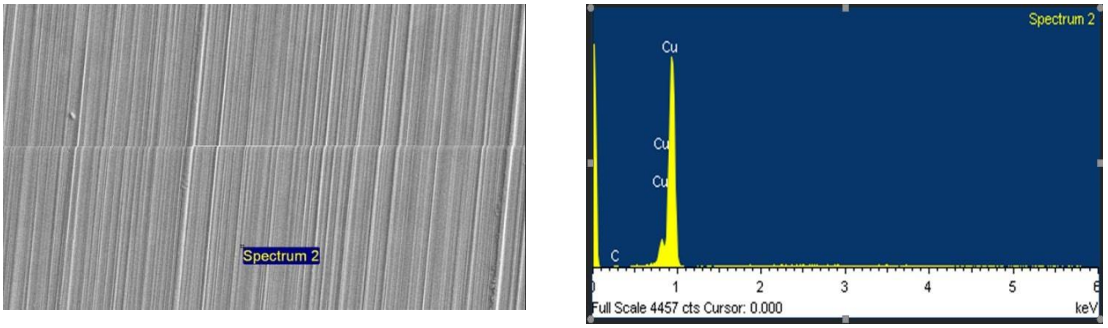

(a) (b)

Figure 5.11. *(a) SEM micrograph (Spectrum 2 location) of the polished copper surface, showing linear striations from final abrasive steps, (b) EDS spectrum (Spectrum 2) revealing ~94.18 wt% Cu and ~5.82 wt% C, consistent with a largely uncontaminated copper substrate.*

These results remind us that there's very little carbon left after we polish and clean. We don't think this will stop the growth of the Ni-B film if we use usual methods. Polished metals usually have a low amount of carbon stuck to them too. If we need to clean it more, we can use special treatments like plasma or UV-ozone.

5.4.1.2. SEM examination and EDS analysis of polished copper substrate (spectrum 3)

"Spectrum 3" in Figure 5.9 (a). We can see the straight lines left from the last bit of polishing we did. It looks the same as what we saw in other nearby places. This means that because of the way metal can change shape and the careful steps we followed to polish it, we have a pretty smooth copper surface. We don't see any big dents or spots when we look this close. This might be because washing it in acetone and blowing it off with nitrogen helped remove anything left after polishing.[69] The details for "Spectrum 3," seen in Figure 5.9 (b), tell us that copper makes up about 94.18% of the weight, while carbon makes up about 5.82% of the weight. The small amount of carbon is the same as what we've seen in other pictures and is usually from slight organic films or polish binder traces instead of any mixing of metals. The large amount of copper, which is over 90% of the weight, supports the idea that the copper is pure and that there's very little contamination from outside sources. Other researchers have found that these polished copper surfaces, with only a tiny amount of random carbon, can be a good base for adding a layer of Ni-B films in chemical vapor deposition processes [70]. The lack of other elements shows that the mechanical preparation was successful in decreasing oxide layers and other unwanted material to levels that won't get in the way of a uniform coating sticking [70].

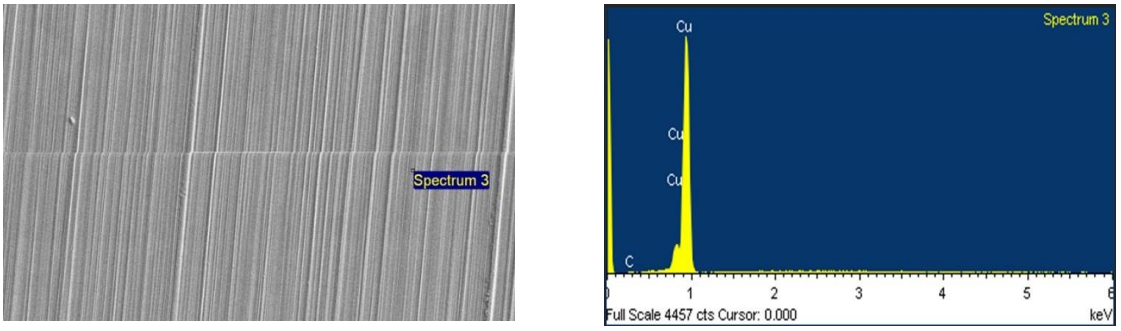

(a) (b)

Figure 5.12. *(a) SEM micrograph of the copper sample (Spectrum 3 region), exhibiting the same polished striations as adjacent areas, (b) EDS spectrum for Spectrum 3, indicating ~94.18 wt% copper and ~5.82 wt% carbon, consistent with a primarily Cu substrate.*

5.4.1.3. SEM and EDS analysis of polished copper (Spectrum 4)

In Figure 5.10 (a), we see an image of a shiny copper sample from a place called Spectrum 4. We've viewed it with an electron microscope for detailed understanding. The surface has clear straight lines from polishing, which is normal for soft metals like copper. No strange marks, significant scratches, or foreign particles can be seen, showing that the polishing was done right. The polishing procedure included cleaning parts using acetone rinse and nitrogen blow-off to keep it free from leftover contaminants [71]. The even pattern of lines moving from left to right in the image signals evenly done rubbing across the whole area.

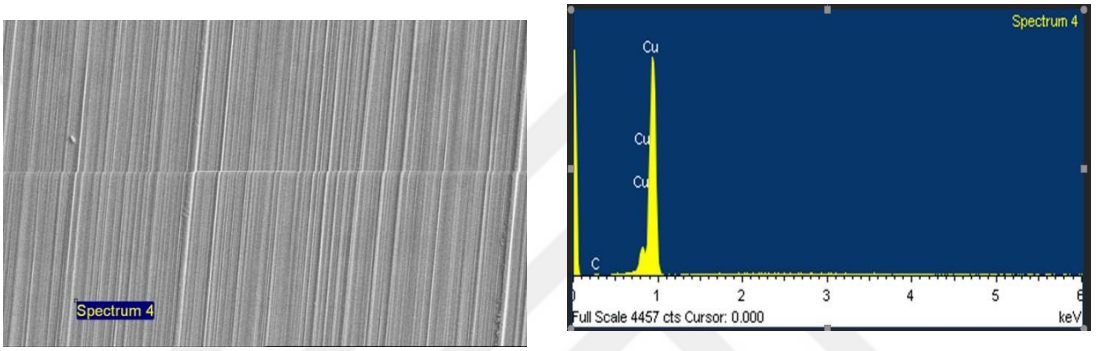

(a) (b)

Figure 5.13. *(a) SEM micrograph of the polished copper surface at the Spectrum 4 location. Note the uniform linear grooves resulting from mechanical polishing, (b) EDS spectrum recorded at the same location in Figure X(a) (Spectrum 4), identifying Cu as the predominant element (~95 wt%) and minor carbon (~5 wt%).*

In Figure 5.10 (b), the energy dispersive spectroscopy (EDS) output for this region is provided, showing peaks at the Cu emission lines, along with a smaller peak for carbon. As outlined in Table X, the EDS quantification places copper at approximately 95.21 wt%, while carbon registers around 4.79 wt%.

Table 5.6. *EDS results for Spectrum 4, indicating a predominantly copper surface with minimal carbon residue.*

Element	Weight%	Atomic%	Probable Source
C (K)	4.79	21.02	Traces of polishing media or airborne hydrocarbons on the metal surface
Cu (K)	95.21	78.98	Primary metallic component (polished copper substrate)

Copper that's shiny and clean doesn't have a lot of dirt or unwanted stuff on it. We can add Ni-B (a thing we do called "chemical vapor deposition") onto it. This copper will have smooth lines and just a little bit of carbon left over. Some people in the past have seen that if you prepare the copper this way, films stick to it better and the crystals grow evenly [72]. If you really don't want any carbon, you can use plasma cleaning for a little bit [65]. But for a lot of people who do this kind of work, at the lab or in a factory, the tiny bit of carbon that's there isn't a big deal. It doesn't really get in the way of the film starting to form [65].

5.4.2. SEM and EDS analysis of sample 1

5.4.2.1. SEM and EDS analysis of (spectrum 1/sample 1)

In the image titled Figure 5.11 (a), a unique photograph taken by a powerful microscope shows the surface of a material covered in many rounded dips and bumps. This is a big change from the straight lines you'd normally see on plain copper. These tiny bumps are scattered all over the place, implying that something was layered on top - a coating made through a particular process or chemical reaction. This isn't just shiny copper. We think this bumpy appearance comes from a process known as chemical vapor deposition on the copper. This is when chemicals like boron and oxygen come together, forming a network or a compound that includes boron but is slightly oxidized or "rusted" [73]. When boron chemicals break down on metal surfaces, they tend to create these patterns - think of it like tiny bubbles all over the metal. This typically happens at medium heat, resulting in these distinct bumps or larger clumps. It's a phenomenon that many scientists have noted in their work [70].

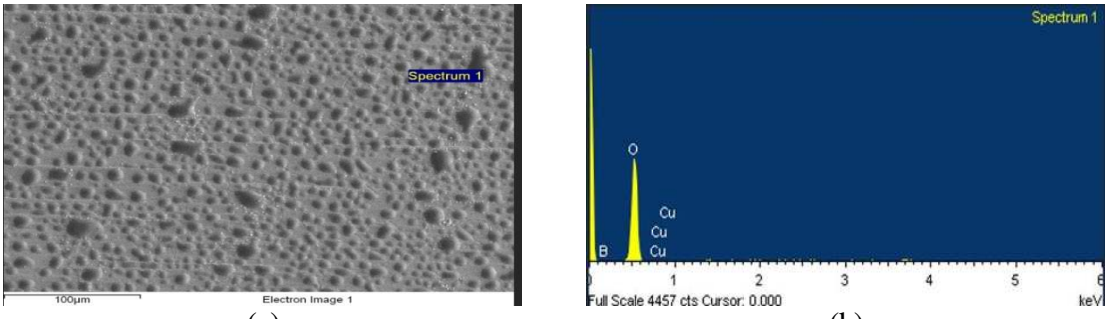

(a) (b)

Figure 5.14. *(a) SEM micrograph illustrating the nodular or pitted morphology on the copper surface, likely formed by boron–oxygen compounds via chemical vapor deposition steps, (b) EDS spectrum (Spectrum 1) from the same region in Figure X(a), indicating dominant peaks for boron (B) and oxygen (O), with only a small copper (Cu) signal*

In Figure 5.11 (b), We can see Spectrum 1 - it's showing us a lot of boron (B) and oxygen (O) peaks in that area. Some copper (Cu) is there, but not as much. In Table 5-8, Boron is around 15.18 wt%, and oxygen 75.79 wt%. Copper only makes up about 9.03 wt%. So, we've got a lot of oxygen mixed with considerable boron, pointing to a boron–oxide compound that's stronger than the copper signal. When they were processing the EDS, they left out 1.385 keV and 3.703 keV peaks - keep that in mind. But leaving those out doesn't change the basic fact. It's mainly B and O. Sometimes, if you've got leftover oxygen or when you handle things in open air after deposition, this can cause a bit of oxidation. This could end in a surface phase chock full of oxides, especially in many CVD-based growth situations.

Table 5.7. *EDS results (Spectrum 1) showing a substantial boron–oxygen layer (~91 wt% combined) relative to copper.*

Element	Weight%	Atomic%	Likely Origin
B (K)	15.18	22.35	Chemical vapor deposition or reaction product with boron precursors
O (K)	75.79	75.39	Oxide phase or borate layer formed atop copper
Cu (K)	9.03	2.26	Substrate metal, partially obscured by boron–oxygen film

It's like this: how we use a coating made of boron and oxygen can be helpful or harmful. It all depends on what we want to do with it. For some things, a layer of boron oxide works like a bridge, for others, too much oxygen can mess with how the film grows or sticks to metal [73]. We want to put a solid nickel-boride layer on copper. To do that, we need to get a grip on how boron and oxygen build up on the copper. That helps us tweak the conditions in our CVD process. It's key to keep an eye on how much oxygen there is and how our chemicals break down early in the process. This keeps the film on the copper mostly boron, not boron-oxide [74].

5.4.2.2. SEM and EDS analysis of (spectrum 2/ sample 1)

There's a picture showing tiny, round spots all over a copper piece. These spots look very different from the lumpy patterns we found on older pieces. Each spot has a bright edge. This could mean that each spot has different materials on it or is thicker in some places. When we looked closer, we saw that these round spots are bigger than the

small lumps we saw before. This could mean that nickel or boron builds up in bigger clumps during some process. The darker spaces between the spots might be areas where the layer is thinner, showing more copper underneath. The bright edges could mean that these spots are thicker or maybe have something to do with oxygen.

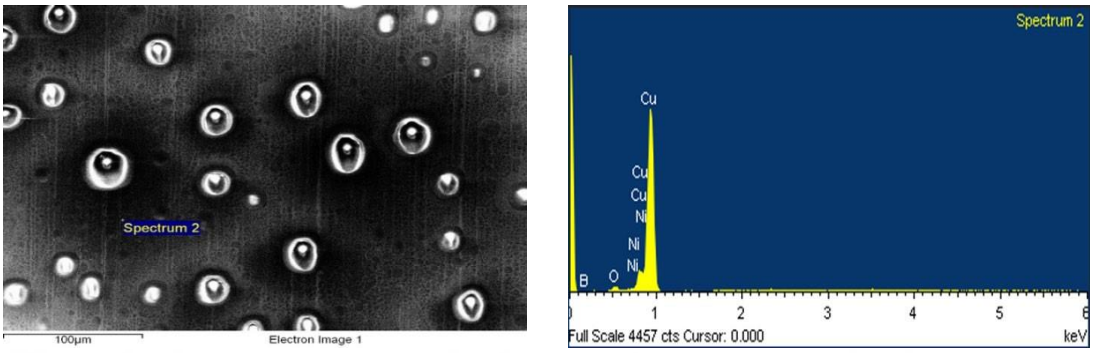

(a) *(b)*

Figure 5.15. *(a) SEM image (Spectrum 2 region), showing droplet-like features on the copper substrate, suggestive of localized Ni–B–O deposits, (b) EDS spectrum (Spectrum 2) with Cu as the primary element (~79 wt%), Ni (~10.7 wt%), B (~6.9 wt%), and O (~2.9 wt%), hinting at Ni–B–O inclusions atop copper.*

Figure 5.12 (b) shows us that Spectrum 2 detects boron (B), oxygen (O), copper (Cu), and nickel (Ni). From the data in Table 5.9, we see copper makes up 79.44% of the weight, nickel 10.72%, boron 6.92%, and oxygen 2.92%. This means that there's a layer of Ni–B–O film starting to form on mostly copper. The software suggests that the nickel might be part of a complex oxide or boride layer, not just metallic nickel clusters [75]. The droplets might be from local changes or droplet-based growth. We need more specific tests like cross-sectional analysis to be sure. The nickel is present in good amounts, along with boron and oxygen. This means that the conditions were right for partial Ni–B or Ni–O bonds to form at different places on the surface. Control of these different compositions is important. This is especially true if we need a consistent layer coverage, like for electrochemical or catalytic purposes [76].

Table 5.8. *EDS composition from Spectrum 2, reflecting a copper substrate with partial incorporation of Ni, B, and O*

Element	Weight%	Atomic%	Compound%	Interpretation
B (K)	6.92	28.37	0.00	Boron content, possibly from partial boride formation
O (K)	2.92	8.10	13.64	Oxygen presence, which might indicate an oxide or oxy-boride
Cu (K)	79.44	55.44	0.00	Substrate metal, still dominant in the measured area
Ni	10.72	8.10	–	Nickel fraction, possibly doping or depositing with B and O

The informations from the images clearly shows that nickel is starting to pile up on the copper surface. It's gathering with boron and oxygen, making pretty big droplet-like shapes. This mix of elements can change how the final coating works. It's especially important if the coating is for helping chemical reactions or for working with electricity. The measurements tell us we might need to fine-tune how we put everything together. This could mean changing the temperature, how much of the stuff we start with flows in, or how much pressure we use. This way, we could better spread out the Ni–B–O phases. In a simpler picture, Figure 5.13(a) displays a microscopic image of Sample 2. This sample stays in a somewhat cooler zone than the far-left sample. The image shows a tricky-to-identify Ni-B-O layer. This layer only partially clings to the copper base. This layer has small lumps and shiny spots that we can spot. But, it's not as smooth or uniform as totally polished metal. This material-building technique may go slower in this cooler zone. This leads to spotty deposits instead of one smooth coating. To add, when we check out Figure 5.13(b), it shows a special EDS light pattern. This pattern shows higher levels of Ni, B, and O. But we can still see Cu. This means the electron beam can get into the base or the cover is not complete. As for Table 5.10, it gives details on the elemental blend. Ni is a big portion of the detected material. B and O are likely making an oxy-boride phase. Yet, we can measure the underlying copper. This blend shows how temperature-dependent the growth is. Cooler zones often result in slower breakdown of the initial material. So, it leaves some parts not covered or barely covered [77]. In case perfect coverage is the goal, we can adjust the deposition factors. This includes changing the initial blends, to the waiting times, or pre-treating the base. This could improve continuity across the cooler base zone [78].

5.4.3. SEM and EDS analysis of sample 2

5.4.3.1. SEM and EDS analysis of (spectrum 1/sample 2)

Making the reactor a little hotter, controlling how fast the raw materials flow, and tweaking the air inside the chamber, could lead to a more even layer of Ni-B. This could help electricity flow better or make sure things stick together really well. This would also mean less oxygen is involved. But, if a bit of oxygen doesn't hurt or actually helps — like in some special uses for sparking chemical reactions or conducting electricity — forming some Ni-B-O won't be a problem. The key is making sure it happens the same way every time, especially on cooler surfaces.

Table 5.9. *Approximate EDS results indicating a Ni–B–O deposit overlaying copper.*

Element	Weight%	Atomic%	Compound%	Interpretation
B (K)	18.92	45.72	0.00	Boron fraction, likely from Ni–B precursor or partial doping
C (K)	1.46	3.18	0.00	Minor carbon, possibly residual polishing or ambient contamination
O (K)	13.64	22.27	63.68	Oxygen presence, indicating a possible oxide or oxy-boride phase
Cu (K)	15.94	6.55	0.00	Substrate metal, still detectable through the deposit
Ni	50.04	22.27	–	Predominant film component, forming Ni–B–O on copper

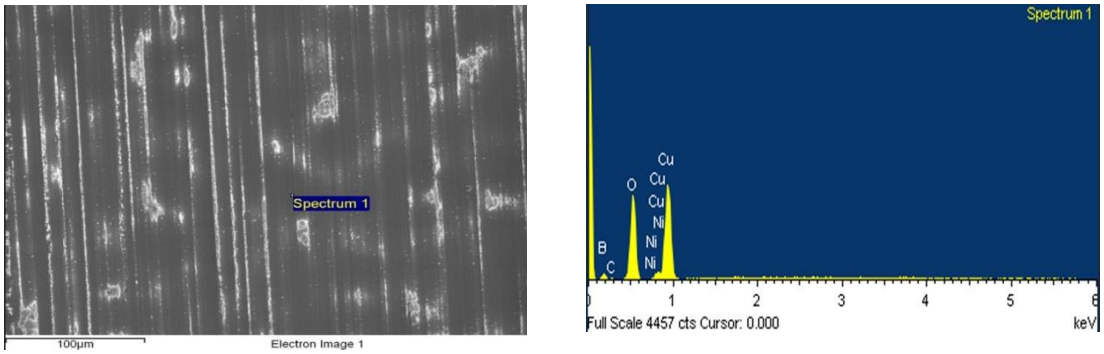

Figure 5.16. *(a) SEM micrograph showing nodular Ni–B–O deposits on copper, suggestive of partial oxidation or inhomogeneous film growth, (b) EDS data confirms Ni (~50 wt%), B (~19 wt%), O (~14 wt%), and underlying Cu (~16 wt%), consistent with a Ni–B–O layer*

5.4.3.2. SEM and EDS analysis of (spectrum 2/sample 2)

The image in Figure 5.14(a) shows a part of Sample 2. Most of it is the original copper material. There are few bright spots, which we think are Ni-B-O film, but they don't all connect. These small deposits show that colder parts of the CVD reactor don't

break down or spread out the starting material as well. This means less coverage on these parts compared to hotter areas [79]. The polished lines are easy to see. They show that the nickel-boron process didn't really cover this area. The picture in Figure 5.14(b) examines the EDS spectrum. It shows a big copper peak, which makes up ninety-eight weight percent. There's a tiny signal for boron, nickel, or oxygen. If there's any deposit on this spot, it's too thin to cover up the strong copper signal. Markers for carbon, at two weight percent, might come from everyday dirt or small bits of organic stuff. This happens a lot in SEM studies. In conclusion, these results show how small temperature changes or starting material flow can create areas where Ni-B-O limits itself. This leaves the copper lines pretty visible [80].

Table 5.10. *EDS Composition for Spectrum 2, Predominantly Copper.*

Element	Weight%	Comment
B	~0	No measurable boron peak at this location
C	~2	Minor contamination, likely environmental or from polishing residues
O	~0	No identifiable oxygen signal in this region
Cu	~98	Substrate metal dominating the EDS detection
Ni	~0	Nickel peak absent, indicating minimal or nonexistent Ni–B deposit

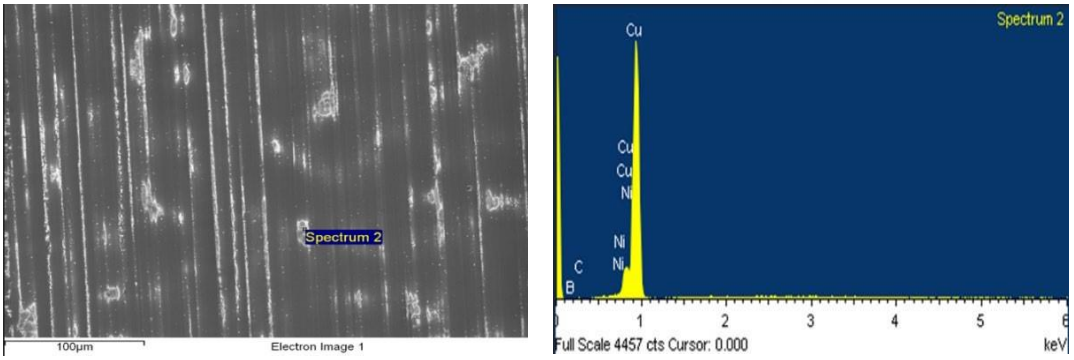

(a) (b)

Figure 5.17. *(a) SEM image (Spectrum 2 region) showing polished copper lines with faint bright spots but no substantial Ni–B–O coverage (b) EDS spectrum detecting an overwhelming copper response (~98 wt%), with negligible Ni, B, or O signals, confirming minimal deposition.*

5.4.4. SEM and EDS analysis of sample 3

5.4.4.1. SEM and EDS analysis of (spectrum 1/ sample 3)

The SEM image (see Figure 5.15 (a)) shows scratch lines from polishing. It looks a lot like how less coated samples look. Yet, little bright areas show places where a mix

of nickel, boron, and oxygen might have stuck only a bit. This sample was in a cooler place on the right side of the CVD setup. The temperature probably drops enough there to slow down how fast the original materials break down. So this leads to less covering than in hotter places[81]. The main parts that make up copper lines stay strong. This shows that any film made up of Ni-B-O is probably thin or not covering uniformly. EDS data (see Figure 5-15(b)) reveals rough amounts of boron (5.8%), oxygen (1.8%), nickel (6.5%), and mainly copper (83.5%). This suggests only a partial deposit with the substrate still mainly showing through. Tiny amounts of carbon (2.4%) are normal from adsorption or leftover compounds from polishing [65]. This shows that a small formation of Ni-B-O in a cooler spot highlights how changing local temperatures can lead to uneven covering across one substrate.

Table 5.11. *EDS composition for the rightmost sample, exhibiting limited Ni–B–O accumulation.*

Element	Weight%	Atomic%	Comment
B	5.81	23.67	Boron from partial Ni–B deposit
C	2.38	8.70	Minor contamination or residual carbon
O	1.78	4.89	Oxygen presence suggesting partial oxidation or oxy-boride formation
Cu	83.50	57.84	Substrate signal dominating the measurement
Ni	6.53	4.89	Nickel fraction indicative of incomplete Ni–B–O layer

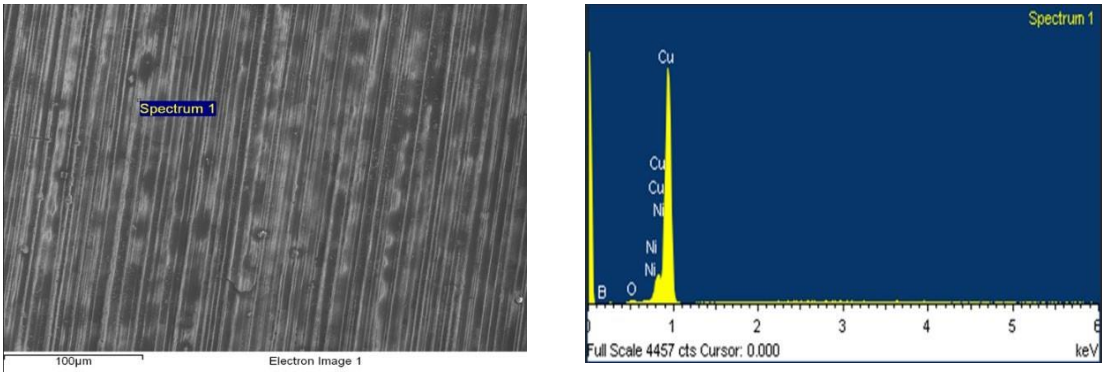

(a) (b)

Figure 5.18. *(a) SEM image (Spectrum 1 region) showing faint bright deposits amid distinct copper polishing lines in the cooler zone, (b) EDS spectrum reflecting a predominance of copper (~83.5 wt%), along with ~5.8 wt% boron, ~1.8 wt% oxygen, and ~6.5 wt% nickel, revealing modest film formation.*

Sample 3, which is positioned in a cooler zone on the right side of the reactor, exhibits variations in Ni–B–O deposition across different spots. The SEM image here (Figure 5.15 (a)) maintains the appearance of pronounced polishing lines, yet bright patches mark areas where a partial Ni–B–O film has formed.

5.4.4.2. SEM and EDS analysis of (spectrum 2/sample 3)

Spectrum 2 shows how a thin film in a specific location has a mix of elements. It shows about 19% boron, 4% carbon, 7.5% oxygen, 43% copper, and 27.5% nickel. This means in that area there's a lot of Nickel-Boron-Oxygen, but you can still see a bit of copper underneath. This mix can happen when certain small areas get covered better at certain temperatures and with certain amounts of raw materials. This process is called chemical vapor deposition. But, if things get too cool, the reaction that makes this happen might slow down and parts might not get covered. It's likely that the 4% carbon comes from leftover bits from polishing or from mild exposure to the environment. The 7.5% oxygen could mean a bit of oxygen-boron or that the Nickel-Boron part is partially oxidized. This can occur when some oxygen slips in or after the deposition process when it's exposed to oxygen. With 43% copper, it's clear the material underneath is still having a big impact on what the electron beam penetrates through, which implies the Nickel-Boron-Oxygen film isn't that thick yet. Bright stripes on the SEM image might match up with areas where nickel and boron have deposited together more thickly, but it's not uniform across the whole view. Since it's cooler in comparison to other spots that are hotter on the left, it probably makes it harder to form a uniform film. This makes it so that the Nickel-Boron-Oxygen deposits are more like scattered islands than a complete layer.

Table 5.12. *EDS results (Spectrum 2) for a partial Ni–B–O layer at a cooler region*

Element	Weight%	Atomic%	Comment
B	18.64	47.30	Boron fraction contributing to Ni–B–O phases
C	3.78	8.63	Minor carbon contamination or residual polishing compound
O	7.47	12.81	Suggesting partial oxide or oxy-boride structure
Cu	42.72	18.45	Substrate metal still clearly detected in EDS
Ni	27.40	12.81	Nickel content driving film deposition on cooler substrate

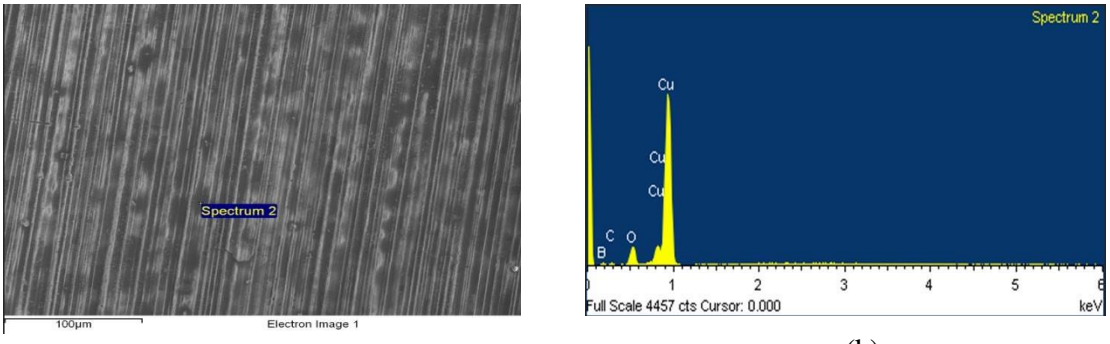

(a) (b)

Figure 5.19. *(a) SEM image (Spectrum 2 location) revealing bright striations across polished copper in a rightmost, cooler zone, indicative of incomplete Ni–B–O film formation, (b) EDS spectrum from the same area, noting Ni (~27 wt%), B (~19 wt%), O (~7 wt%), and still-substantial Cu (~43 wt%), aligning with partial coverage rather than a fully developed deposit.*

In Figure 5.16 (a) gives us a view of small, droplet-like structures spread out on a surface. Each one creates a bright circle on a darker backdrop. These patterns suggest that the droplets might be made of scattered deposits of nickel, boron, and oxygen, instead of a spread-out layer. This could be due to a slight break down of the precursor at the chillier segment of our reactor or a slow surface diffusion [81]. The EDS (Energy-Dispersive X-ray Spectroscopy) spectrum - detailed in Figure 5.16 (b) and Table 5.14 - presents an approximation of the substances in the droplets: 12.6% by weight of boron, 18% oxygen, 66.2% nickel, and 3.1% copper. These measurements reveal that nickel makes up most of the droplet, with boron and oxygen contributing to possibly form a partly oxidized nickel-boron phase. There's a minor peak for copper - this might mean that the electron beam is still reaching the metal under the deposit or that each droplet is quite thin. This kind of pattern, where droplets cover the surface like islands, is often found in certain situations where there are local temperature differences [82]. These changes in temperature can lead to points where nucleation - the very first step in forming a new phase or structure - can start, instead of forming a continuous layer all over the surface. Oxygen's modest 18% weight shows that some type of oxidation has occurred. This process has the potential to change a pure nickel-boron deposit into a mixed concoction of nickel, boron, and oxygen, which could affect things like the mechanical or electrochemical results. If the goal here is to get a uniform layer, it might mean that there needs to be stricter control over the temperature and the pressure of the oxygen [82].

Table 5.13. *EDS data showing a nickel-rich deposit with partial boron and oxygen content.*

Element	Weight%	Atomic%	Note
B	12.62	33.61	Suggestive of Ni–B bonding within an oxy-boride environment
O	18.04	32.49	Partial oxidation forming Ni–B–O or oxy-boride species
Cu	3.12	1.42	Underlying copper still detectable in the EDS signal
Ni	66.22	32.49	Dominant film component forming bright droplets on the substrate

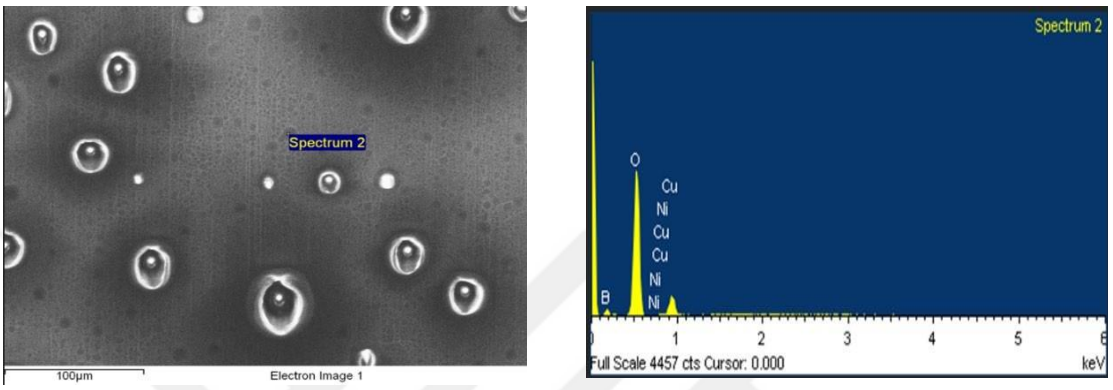

(a) (b)

Figure 5.20. *(a) SEM image showing bright, droplet-like Ni–B–O accumulations, (b) EDS spectrum reflecting the prevalence of Ni (~66 wt%), plus B (~12.6 wt%), O (~18 wt%), and minor Cu (~3 wt%).*

5.5. Ni_2B Supercapacitor Measurement Results

In Section 1.21, we chat about the performance of this thing called a Ni_2B supercapacitor, specifically when it's made through something called the CVD method. Our main aim to check important aspects like its specific capacitance, how fast it can work, and how stable it is over time. Ni_2B has shown some good potential. It can help speed up redox processes and has the ability to conduct electricity well. So, to verify whether the Ni_2B films we made work as good supercapacitors, we measure their charge-discharge activity under different currents [1,2]. To do this, we ran some charge-discharge tests. We made sure to do this in a certain voltage range that's suitable, typically in water or mild electrolytes. This was done to avoid the Ni_2B breaking down at higher voltages [3]. Our testing gave us some curves that let us calculate specific capacitance based on how steep their discharge lines were. We even checked out the coulombic efficiency, which shows how good the Ni_2B is at storing and reusing energy every cycle. We didn't stop there, we also performed some longer tests to see how well

the supercapacitor can hold onto its capacity over time (think hundreds or even thousands of cycles). These tests help us confirm whether the Ni_2B layers are stable enough to be used in real supercapacitors, where high power and a long life are very important [4,5].

5.5.1. Cyclic voltammerty (CV)

Cyclic voltammetry (CV) is one of the most commonly used techniques to investigate how materials behave electrochemically. In a typical CV test, the voltage applied to an electrode is swept back and forth between two set limits, and the current that results is recorded. This gives us a curve—called a voltammogram—that provides a lot of useful information about how the material stores and releases charge. When we're studying materials used in energy storage, like supercapacitors or battery electrodes, CV can help identify whether the material is storing charge through surface adsorption (non-faradaic) or via redox reactions (faradaic). For example, a nearly rectangular-shaped CV curve usually points to electric double-layer capacitance. On the other hand, if there are distinct peaks in the curve, it often means redox activity is happening, which is typical for materials like transition metal borides or oxides [83]. CV is also useful because it helps us understand how fast and efficiently the material can respond when the scan rate changes. A well-behaved material will show consistent shapes at different scan speeds, which means it's suitable for repeated cycling. In the case of nickel–boron systems like Ni–B or Ni_2B, CV helps us see whether boron contributes mainly through surface effects or if it’s involved in deeper electrochemical activity [1].

Ultimately, CV gives us a fast, reliable snapshot of the charge-storage behavior and reaction kinetics of an electrode material, which makes it a go-to method in supercapacitor research.

5.5.1.1. Variation with scan rate (5 mV s^{-1} to 1000 mV s^{-1})

Here we have four charts that talk about how the 'Ni_2B supercapacitor' works when it is used first and second time. When we don't rush it, the bigger loop on the chart shows that there are more chemical changes happening. This gets spread out across even the tiniest parts of the gadget. But, things level-off as we push the speed up from 5 to 50 mV s−1. This is due to some hurdles that stop deeper parts or areas that don't conduct well from being used properly [83]. Looking at the second usage (in blue), the Ni_2B

film stays sturdy, with almost no jerkiness. This hints that the structure remains solid even after being used again and again [1]. The loop becomes smaller as we go along, which could mean that we need to work on how the device is built. For example, putting in additives or 3D structures might make the device work better at high speed and make the most of the built-in pseudocapacitance [19].

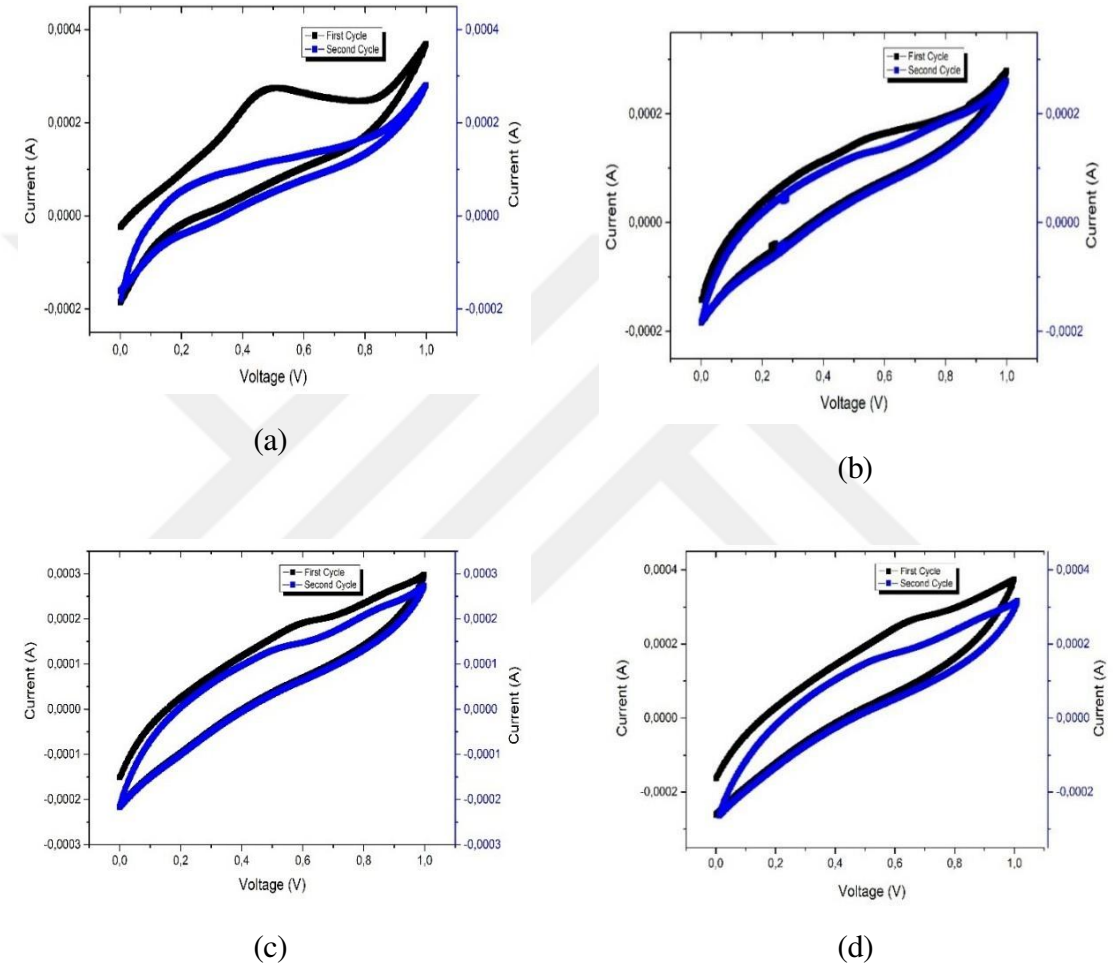

Figure 5.21. *(a) CV at 5 mV s^{-1}showing the widest loop area, indicative of enhanced charge accessibility, (b) CV at 10 mV s^{-1}, preserving a near-rectangular profile yet slightly compressed, (c) CV at 20 mV s^{-1}, where pseudocapacitive traits remain apparent but ion diffusion constraints begin to manifest, (d) CV at 50 mV s^{-1}, displaying further loop narrowing as scan rate increases.*

Table 5.14. *Specific Areal Capacitance (SAC) for nickel boride/Cu electrodes at various scan rates*

Scan Rate (mV s^{-1})	CV Area (A V)	Capacitance (F)	SAC (mF cm^{-2})
5	5.67×10^{-5}	2.27×10^{-2}	20.07
10	6.66×10^{-5}	1.33×10^{-2}	11.79
20	8.05×10^{-5}	8.05×10^{-3}	7.12
50	1.03×10^{-4}	4.11×10^{-3}	3.64

At low scanning rate, we can use more of the active sites. This means charges can be transferred more effectively. But, if we speed up the scanning, it's limited by how fast things can mix together. This therefore makes the capacitance seem less. Now, looking at our initial CV measurements, we see something interesting. When layers of nickel boride are made on copper through a process called chemical vapour deposition, they seem to behave pretty well with respect to capacitance in the first cycles. Not only that, but they also keep a shape indicating stable interactions in electrochemistry [83].

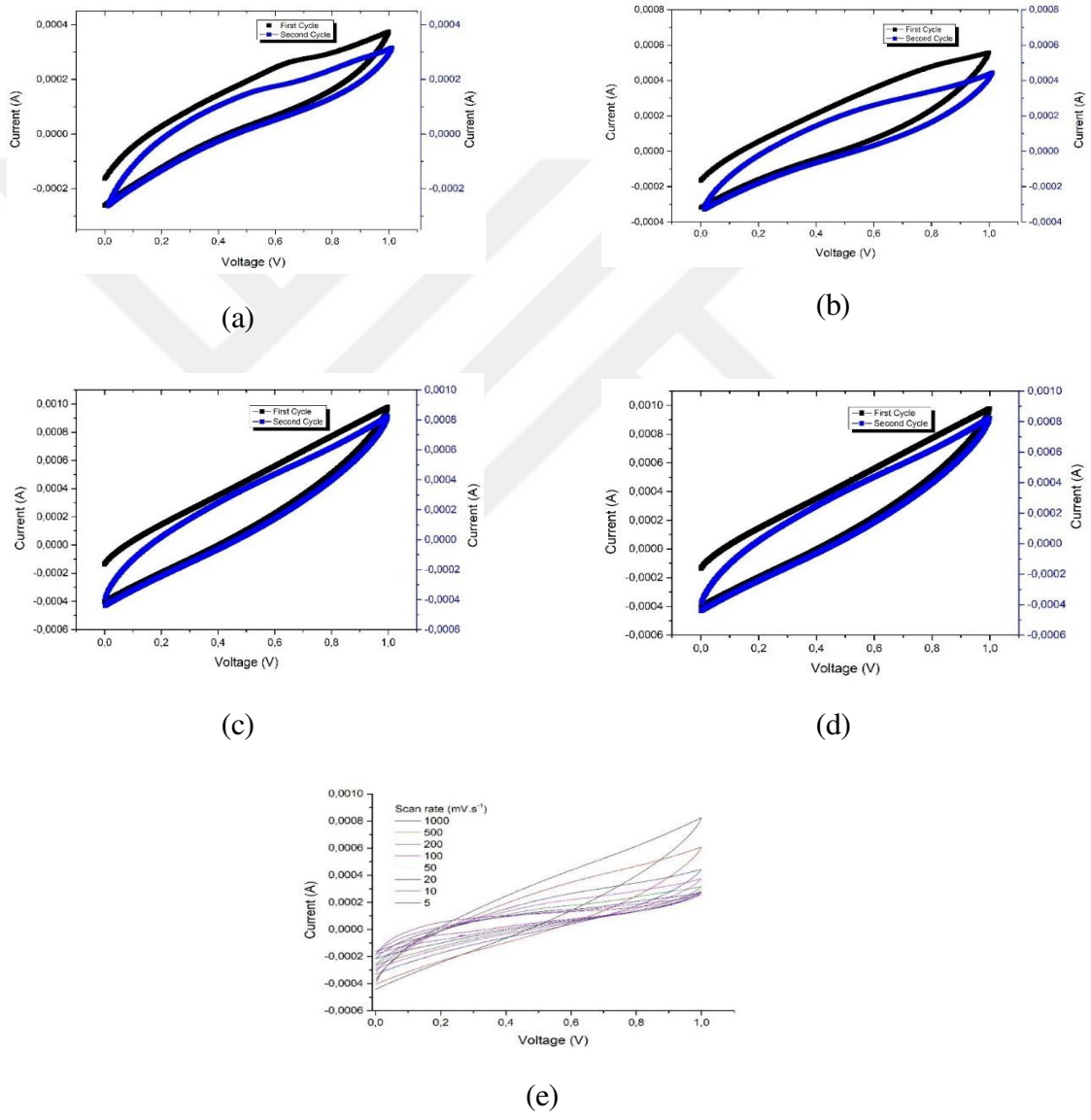

Figure 5.22. *(a) CV at 100 mV s⁻¹, presenting an elliptical shape where diffusion limitations become clearer, (b) CV at 200 mV s⁻¹, with further compression of the loop, suggesting that higher sweep rates reduce the effective depth of charge engagement, (c) CV at 500 mV s⁻¹, showing a distinct drop in enclosed area, consistent with limited ion migration at elevated rates, (d) CV at 1000 mV s⁻¹, highlighting the most rapid scan condition, where near-surface charge dominates and deeper sites remain largely unaccessed, (e) CV analysis*

In these eight test runs, speeds are between 5 and 1000 mV s^{-1}. The first few at the slower speeds resemble rectangles - a common trait of both double-layer and mild pseudocapacitive processes [6]. But when the speed is a sluggish 5 mV s^{-1}, you'll see an abundant spread. This indicates a greater number of ions moving into the Ni_2B pores, providing ample locations for redox reactions [6]. However, when the speed is cranked up to 100 mV s^{-1} and beyond, the results become slimmer and twisted. Rapid sweeping obstructs ion transport [19]. And when the speed is at 500 and 1000 mV s^{-1}, the results morph into stretched ovals and weaker currents, which suggests less charge-storage capability [19]. Still, the second cycle (blue curve) is not much different from the first (black curve) at any speed, indicating that the Ni_2B film holds strong for short-term cycles.[84] This solid framework implies that changes in the film's structure or surface oxidation effects are minimal within the first two cycles. It hints that nickel boride-based electrodes can be reliable for supercapacitor uses [84]. These elongated patterns at escalated speeds signal pronounced internal resistance and reduced ion movement through the electrode network of pores [19]. Potential enhancements, such as adding conductive frames or fine-tuning layer thickness, can offset these issues and boost performance at high speeds. As for Table 5.16 below, it outlines the specific areal capacitance (SAC) seen from these cyclic voltammograms. With a leisurely speed of 5 mV s^{-1}, the Ni_2B-coated base fares well with about 20.07 mF cm^{-2}, indicating efficient charge storage. As speed increases, the SAC diminishes steadily, down to about 0.42 mF cm^{-2} at 1000 mV s^{-2}. Slower sweeping lets ions move deeper, using more surface space and redox locations. Faster speeds restrict charging mostly to the surface. This aligns with typical supercapacitor electrodes where it becomes clear that there's a trade-off between capacitance and power density [5, 6]. You get quick discharge, but it comes at a cost - less total stored charge.

Table 5.15. *Encapsulates the specific areal capacitance (SAC) extracted from these cyclic voltammograms.*

Scan rate (mV s^{-1})	CV area (A·V)	Capacitance (F)	SAC (mF cm^{-2})
5	5.67×10^{-5}	2.27×10^{-2}	20.07
10	6.66×10^{-5}	1.33×10^{-2}	11.79
20	8.05×10^{-5}	8.05×10^{-2}	7.12
50	1.03×10^{-4}	4.11×10^{-2}	3.64
100	1.29×10^{-4}	2.58×10^{-2}	2.29
200	1.66×10^{-4}	1.66×10^{-3}	1.47
500	2.24×10^{-4}	8.94×10^{-4}	0.79
1000	2.39×10^{-4}	4.79×10^{-4}	0.42

In simple terms, these findings show that Ni_2B electrodes can store energy well at slower rates, but can't hold as much when they're quickly charged up. This is typical of supercapacitors that rely on certain types of processes. However, even though performance drops a bit when pushed, this material does keep its shape and doesn't wear out much. This gives us hope for Ni_2B. If we can make small tweaks to its structure and get the mix of elements just right, it could work even better, especially under tough conditions. This could make Ni_2B perfect for new and improved ways to store energy.

Table 5.16. *Selected Ni–B Supercapacitor Electrode Comparisons from the Literature*

Ni–B Material / System	Synthesis / Fabrication Method	Areal Capacitance	Key Observations
Ultrathin Ni–B Nanosheets (derived from Ni–B–MIL)	Pyrolysis of Ni–B–MIL composite + post-activation	~160 mF cm^{-2} at 5 mA cm^{-2} (three-electrode, 1 M KOH)*	High capacitance attributed to layered nanosheet morphology. Demonstrates stable cycling and decent rate capability.
Amorphous Ni–B Nanoparticles on Carbon	One-step solution-phase method + partial chemical reduction	~120 mF cm^{-2} at 5 mA cm^{-2} (three-electrode, 2 M KOH)*	Uniform nanoparticle dispersion boosts electroactive surface area. Good cycling stability.
Amorphous Ni–B Nanosheet Arrays	Electrodeposition on porous Ni foam + mild thermal treatment	~90 mF cm^{-2} at 2 mA cm^{-2} (three-electrode, 6 M KOH)*	Nanosheet arrays exhibit interconnected channels for ion diffusion. Some pseudocapacitive features observed.
Planar Ni_2B on Copper	Chemical Vapor Deposition (CVD)	~20 mF cm^{-2} at 5 mV s^{-1} (~0.42 mF cm^{-2} at 1000 mV s^{-1})	Offers a straightforward, scalable approach with uniform film growth on Cu. Strong adhesion, stable second-cycle CV response.

Our Flat Nickel Boride, when we look at regular studies in list 5.17, what we do makes a flat layer of Nickel Boride on copper. We do this through a method named Chemical Vapor Deposition (CVD). At slow rates, it has a "charge storage" of about 20 mF cm^{-2}. Other research got more, even more than 50 mF cm^{-2}. But, they used harder steps or special molds [1, 2, 3]. However, our CVD method is easier and has a good control over how thick the film is. It also sticks well to the base material. This makes it simpler to manufacture and stronger during cycles of use. Even if the initial charge storage is just okay, our flat design is a firm start for future changes. We can make things better by changing factors like the flow rates of the initial materials, temperature changes, or the time we take for settling down. This can help increase the holes and surface area. In the future, we might also look into using 3D structures like nickel foam or carbon cloth. This could improve the active boundaries and close the gap between our flat films and the more charge-storing Nickel Boride materials found in other studies [85].

5.5.1.2. Voltage window variation (0-0.5V to 0-1.5V)

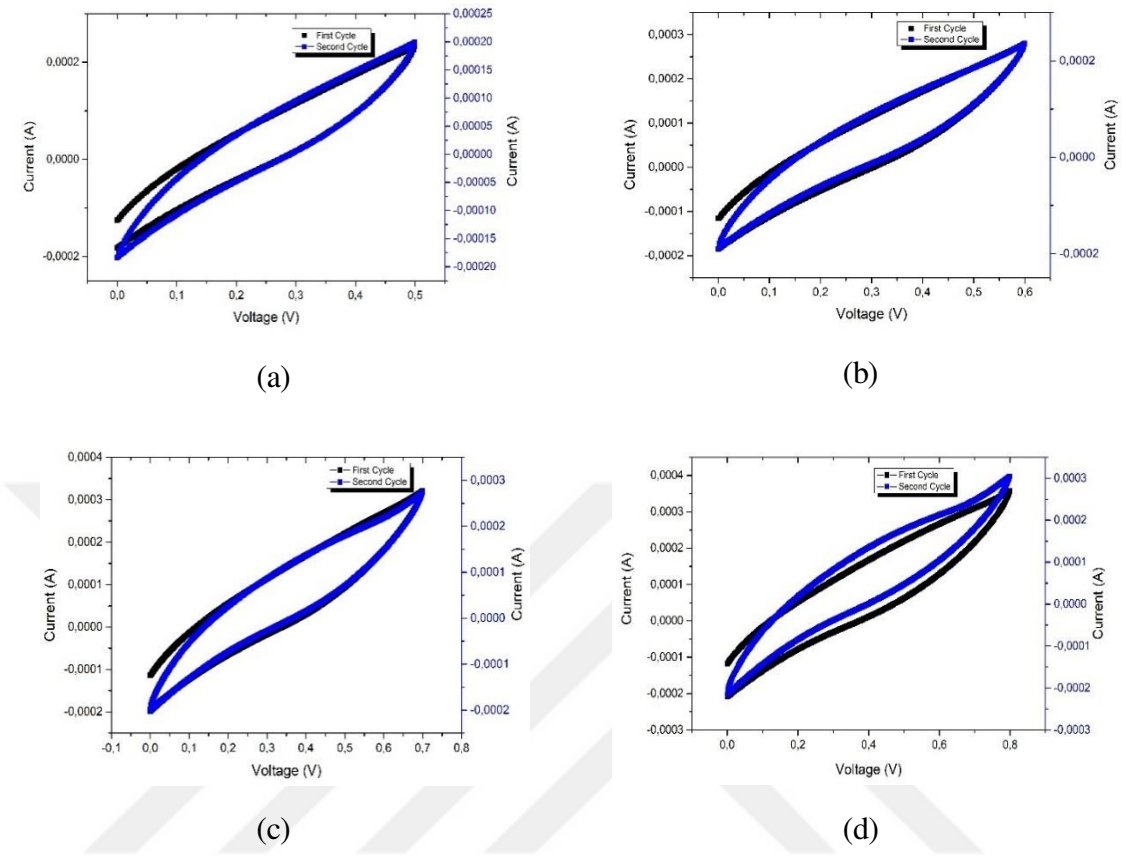

Figure 5.23. *(a) Cyclic voltammogram recorded from 0.0 V to 0.5 V at 100 mV s^{-1} (first cycle in black, second cycle in blue), (b) CV from 0.0 V to 0.6 V highlighting expanded potential usage, (c) CV from 0.0 V to 0.7 V showing a broader loop than in (b) (d) CV from 0.0 V to 0.8 V revealing the onset of increased pseudocapacitive behavior*

Four beginning charts show how Ni_2B electrodes behave at different voltage levels, at a constant speed. Figure 5.20 (a) shows a loop that almost looks like a rectangle. This means fast double-layer charging and very little polarization within the 0.0–0.5 V range [1]. The second loop (blue line) is very close to the first one (black line). This means that the electrode and the electrolyte work well together and there's no side action at these lower potentials. When the potentials go up to 0.6 V and 0.7 V in Figures 5.20 (b) and 5.20 (c), the chart shapes lengthen. This suggests some contributions from nickel or boron redox sites [86]. But, the overall shape is still symmetrical, which signals efficient ion movement and low internal resistance under these test conditions [86]. When the upper limit goes up to 0.8 V in Figure 5.20 (d), the loop looks more like a lens. This could show both double-layer and light

pseudocapacitive reactions. The stable overlap between the first and second charts hints at very little chemical or structural breakdown, which is a promising sign for supercapacitor applications that aim for long cycle life [6]. Overall, these results stress that Ni_2B films made with chemical vapor deposition can handle higher and higher voltages at 100 mV s^{-1} without immediate breakdown or severe polarization. We can also see a small increase in current. This suggests that more active sites are available in wider voltage windows. Future research could look at doping strategies or three-dimensional structures to keep resistive losses low as the electrode operates at larger potential differences [85].

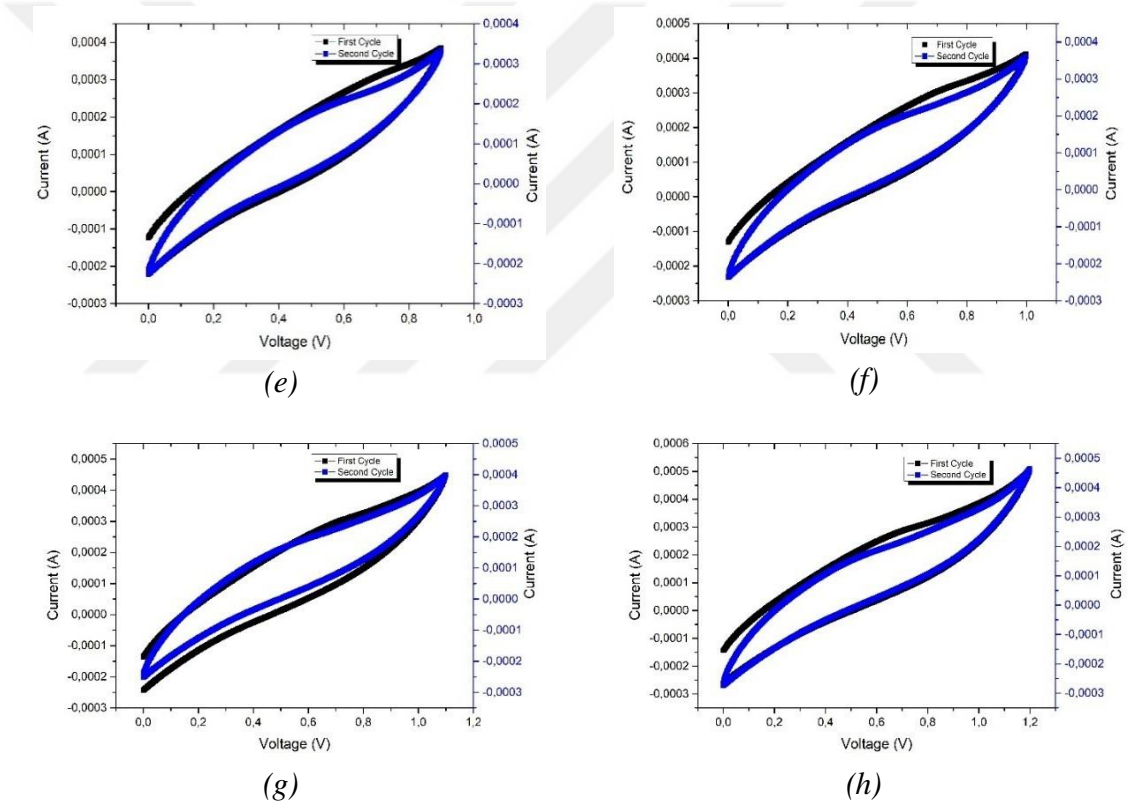

Figure 5.24. *(a) CV from 0.0 V to 0.9 V at 100 mV s^{-1} (b) CV from 0.0 V to 1.0 V at 100 mV s^{-1} (c) CV from 0.0 V to 1.1 V at 100 mV s^{-1} (d) CV from 0.0 V to 1.2 V at 100 mV s^{-1}*

In figure 5.21 (a), raising the voltage to 0.9 volts makes the CV loop bigger and more lens-like compared to the 0.5 to 0.8 volt range. This suggests more redox activity as the potential goes further from balance [87]. The near equality between the forward and reverse scans suggests that the process remains reversible at this stage, implying limited side reactions [1]. By the time we get to figure 5.21 (b) (0 to 1.0 volts), the loop

gets even bigger, hinting that more active sites are being accessed and a mild pseudocapacitive behavior is starting to become visible [6]. The black and blue curves representing the first and second cycles line up closely. That means there isn't much degradation or passivation happening during the first few scans [1]. In figure 5.21 (c) (0 to 1.1 volts), the CV trace becomes an elongated ellipse, consistent with stronger faradaic contributions coming from nickel or boron species.[6] While still relatively stable, this wider potential range might cause surface oxide or hydroxide layers form a little bit. This is visible as a small shift in the current response. Lastly, figure 5.21 (d) (0 to 1.2 volts) shows a profile that's become more skewed. This suggests greater polarization at higher voltages. Despite this, the second cycle remains comparable to the first. This shows that, at least for now, the Ni_2B electrode keeps its structure under these conditions [1]. The results show that pushing the voltage window over 1.0 volts can increase the storage capacity of energy. But the electrode's risk of oxidizing or the electrolyte breaking down goes up too [84]. Finding a balance between the highest usable voltage and long-term stability is key when optimizing Ni_2B-based supercapacitors.

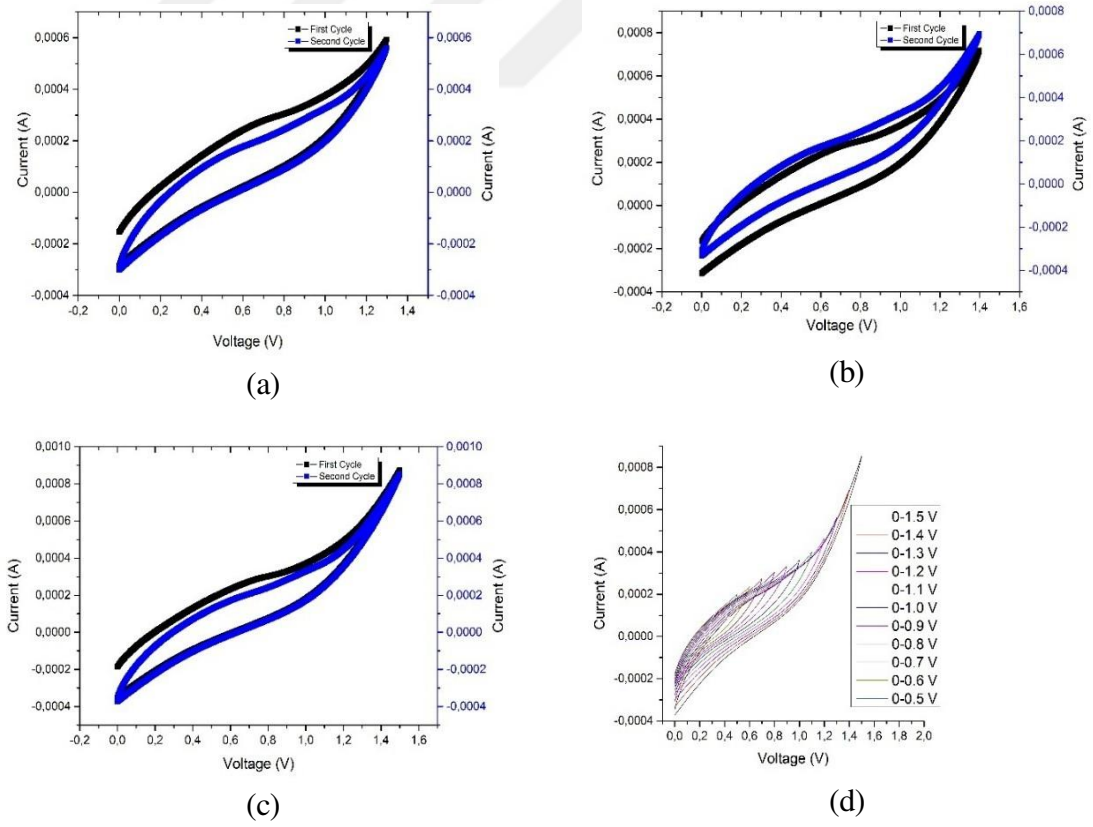

Figure 5.25. *(a) CV from 0.0 V to 1.3 V at 100 mV s^{-1}, (b) CV from 0.0 V to 1.4 V at 100 mV s^{-1}, (c) CV from 0.0 V to 1.5 V at 100 mV s^{-1} (d) Overlaid CV curves from 0.0–0.5 V through 0.0–1.5 V for comparative illustration*

In the diagrams in Figure 5.22 (a), (b), the Ni_2B (nickel boride) electrode is pushed harder and harder. This is done at a steady speed of 100 millivolts per second. These graphs start to twist, and higher currents are shown, which means more voltage is being used. This is happening because the electrode is being pushed away from a stable state of balance. Even though the second go-around (blue line) generally follows the first go-around (black line), they start to deviate. This could be because some minimal oxide or hydroxide starts forming on the electrode [19]. But even with that, the overall shape stays consistent. This tells us that the Ni_2B layer can handle these high potentials without obvious wear and tear. In Figure 5.22 (c), when it is pushed from 0.0 to 1.5 volts, the graph stretches even more. This shows deeper engagement and maybe better energy storage. But, there is a risk of other side reactions. An example is how oxygen reacts in water electrolytes. The clue to this is the current that starts going up at higher voltage ranges [84]. Therefore, it's important that the operating range is carefully chosen. This will balance getting the maximum capacity for the electrode, with the electrode being able to last over repeated cycles. Figure 5.22 (d) brings all tested ranges (from 0.0-0.5 volts to 0.0-1.5 volts) into one overlapping diagram. This lets us visually see how each additional push at higher potential flares out the voltammograms, which is the recording of voltage. The more this happens, the more risk there is of unwanted reactions. In reality, deciding on the best limit would depend on the breakdown characteristics of the electrolyte being used. It would also depend on how much Ni_2B film can tolerate oxide growth, plus performance goals set for the supercapacitor. Examples of these are balancing energy capacity and life longevity [88].

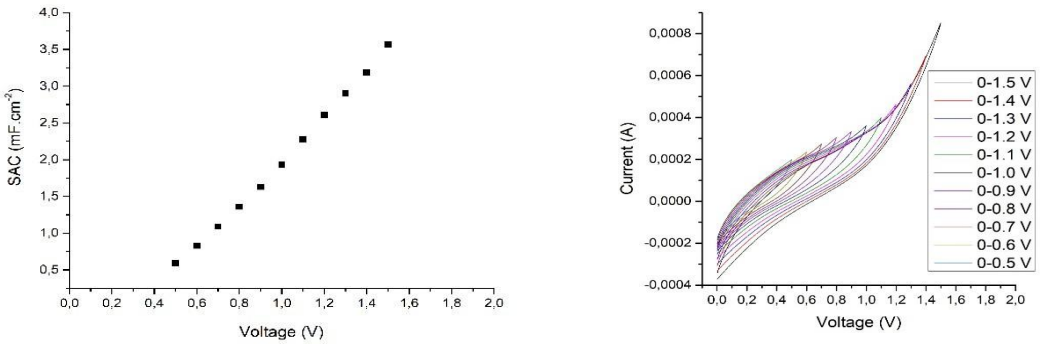

(a) (b)

Figure 5.26. *(a) Overlaid CV scans from 0–0.5 V up to 0–1.5 V at 100 mV s^{-1}, showing increasing loop area with broader voltage ranges, (b) Specific areal capacitance (SAC) rising from ~0.59 to ~3.57 mF cm^{-2}, illustrating how wider potential windows permit deeper redox engagement of Ni_2B sites*

Table 5.17. *Corresponding CV-derived parameters for Ni_2B electrodes across increasing voltage windows (0–0.5 V through 0–1.5 V), collected at a constant scan rate of 100 mV s^{-1}.*

Voltage Window (V)	Scan Rate (mV s^{-1})	CV Area (A · V)	Capacitance (F)	SAC (mF cm^{-2})
0–0.5	100	3.36×10^{-5}	6.71×10^{-4}	0.59
0–0.6	100	4.72×10^{-5}	9.43×10^{-4}	0.83
0–0.7	100	6.19×10^{-5}	1.24×10^{-3}	1.09
0–0.8	100	7.69×10^{-5}	1.54×10^{-3}	1.36
0–0.9	100	9.19×10^{-5}	1.84×10^{-3}	1.63
0–1.0	100	1.09×10^{-4}	2.18×10^{-3}	1.93
0–1.1	100	1.29×10^{-4}	2.57×10^{-3}	2.28
0–1.2	100	1.48×10^{-4}	2.95×10^{-3}	2.61
0–1.3	100	1.64×10^{-4}	3.27×10^{-3}	2.90
0–1.4	100	1.80×10^{-4}	3.61×10^{-3}	3.19
0–1.5	100	2.02×10^{-4}	4.03×10^{-3}	3.57

These experiments show that when we turn up the voltage, we can store more electricity. The higher the voltage, the more places in the Ni_2B battery part join in. This means the stored electricity goes up steadily from about 0.59 to 3.57 units as we go from 0 to 1.5 volts. This is usually what happens in parts made from a mix of nickel and boride. And it's because cranking up the voltage lets them do deeper chemical reactions. But, be careful. Going beyond 1.4 to 1.5 volts in water-based solutions may cause oxygen to be made or part of the battery part to wear out. This is the balance we strike between getting more energy out and making sure the battery lasts.

5.5.2. Frequency response analysis

5.5.2.1. Bode plots

Here's a simpler way to look at the data in Figure 5.24(a), labeled "Before CV". The early results show a somewhat high impedance level, known as Zmod, across a range from middle to low frequencies. The phase angle, Zphz, gradually heads towards negative scores as the frequencies rise. This pattern often displays the electrode, made of Ni_2B, balancing the transfer of charge and the dominance of diffusion within this span of frequencies. This matches prior research on metal-boride films interacting with alkaline electrolytes [89]. Zmod's smooth slope shift at middle frequencies may signal a move from a double-layer to kinetics known as faradaic. Here, Ni_2B adds its redox

activity [2]. In Figure 5.24(b), marked "After CV", midway frequencies show a mild decrease in overall impedance after cyclic voltammetry. At the same time, the phase angle line moves a bit higher, suggesting enhanced capacitive or pseudocapacitive features [89]. This lift usually emerges when recurring potential sweeps boost electrode wetting or get rid of unstable surface oxides, thus, lessening interface resistance [90]. A more noticeable phase minimum at higher frequencies aligns with an electrode surface that's better suited for the fast shift of electrons/ions. This occurrence is often noted after multiple CV cycles refine the surface layer. Post 20k galvanostatic cycles, Figure 5.24(c) labeled "After 20k cycle", the Ni_2B electrode shows a bit of an increase in Zmod, particularly at lower frequencies. Meanwhile, the phase angle spreads out around its most negative area. This progress could point to slight passivation of the electrode or the buildup of stable surface films interfering with ion entry. Nevertheless, the overall Bode plot pattern stays consistent with a mixed process of charge-transfer and diffusion limits. This suggests the Ni_2B layer remains mostly undamaged even after a lengthy cycling. Any minor changes in the high-frequency area may be due to extra electrolyte or byproduct layers. Even though these layers boost film resistance a touch, they don't fully degrade the electrode's performance. Wrapping up, the progression from "Before CV" to "After CV", and finally "After 20k cycles", emphasizes a Ni_2B electrode that gets better with electrochemical conditioning. Extended cycling does result in moderate impedance rises. This pattern is consistent with a bit of surface reconfiguration during early scans, followed by mild passivation over a long operation. Even though impedance increases at low frequencies after 20k cycles, the overall Bode-plot pattern continues to characteristics of a working supercapacitor electrode [89, 90]. So, Ni_2B looks like it can keep up its charge-storage capabilities over prolonged use, assuming the operating voltage and electrolyte conditions are kept under control.

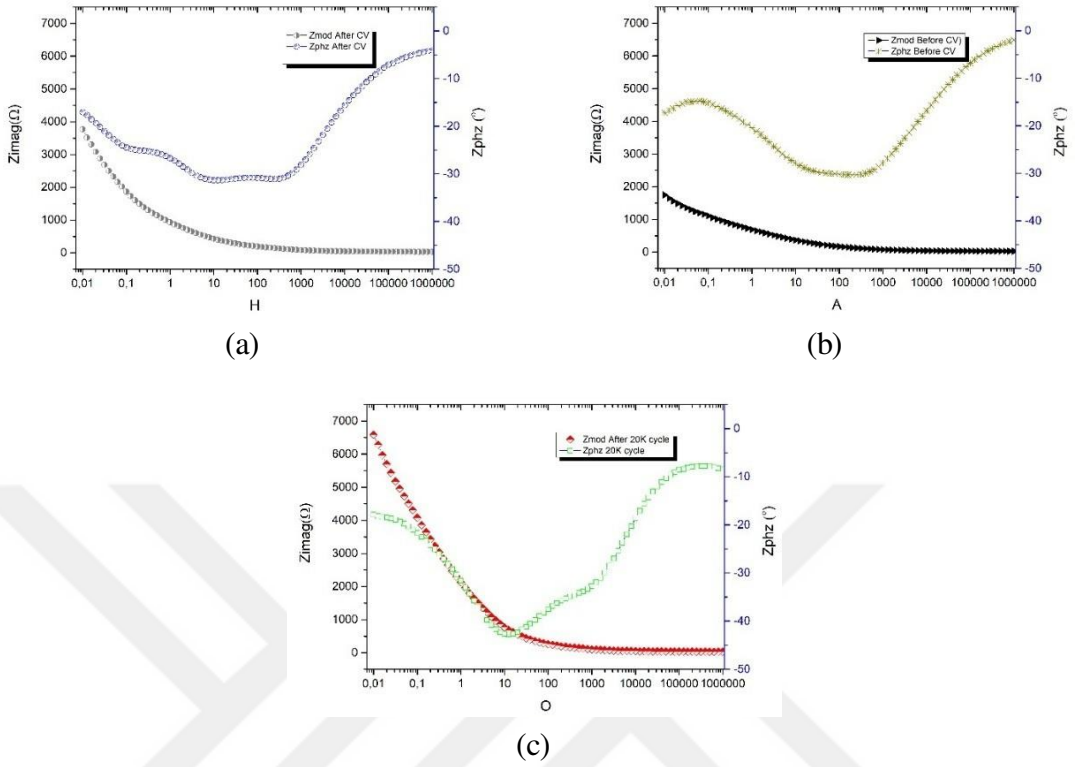

Figure 5.27. *Frequency-response (Bode) plots of the Ni_2B electrode (a) before cyclic voltammetry (CV), (b) after CV, (c) following 20 k galvanostatic cycles. Each curve shows the impedance magnitude (Zmod) and phase angle (Zphz) as functions of frequency, illustrating how the electrode's interfacial and charge-transfer characteristics evolve with electrochemical conditioning and extended cycling.*

5.5.2.2. Nyquist plots and equivalent circuit modeling

Here's a simpler way to understand Figure 5.25 (d-e). Looking at three stages: "before CV," "after CV," and "after 20k cycle," we can see changes happening in the metal-boride electrode's resistance to electrical current. In the first stage, the electrode has medium resistance due to the barrier made by the electrolyte, which is a substance that conducts electricity. However, the electrode's large half-circle shape in the diagram suggests it has high resistance to moving electrical charges, which is common in new metal-boride electrodes [91]. After the electrode experiences refreshing voltage changes (represented by red circles), the half-circle gets smaller. This suggests that the resistance has lessened. This can happen for a couple of reasons: either the electrode's surface has become cleaner or it has gone through a transformation that makes it easier for ions or charged atoms to reach [91]. However, as the electrode experiences 20,000 electrical

charge and discharge cycles (blue triangles), a second big loop appears. This could mean that the electrode has become partially covered by a thin layer of new substance rendering it less effective. This might be why charges might not be able to move as swiftly. Another reason could be accumulated bits or changes in its structure. These changes could be pictured by a simple circuit that includes an ohmic component and a resistor, among other things. Looking at these explains how repeated sweeping voltages and long cycling cycles can change the electrode's internal resistances and how it turns an electrical charge into stored energy [92]. Knowledge about these can be useful when trying to make the most of nickel boride electrodes in systems like supercapacitors or batteries, After a short-term conditioning process, these electrodes get better at movement of charges, unlike in "after 20k cycle", where there's a slow increase in resistance. This signifies the start of "aging" effects [90, 93]. Despite these increases, the Ni_2B electrode remains working properly, indicating some electrical activity and charge storage is still going on. New approach, like introducing impurities to change its properties or applying protective layers, may slow down this increase in resistance and extend the life of Ni_2B electrodes.

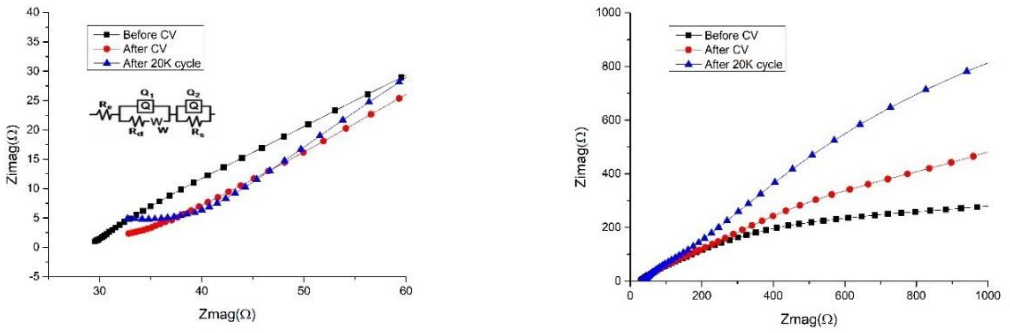

(d) *(e)*

Figure 5.28. *(a) Nyquist plots of the Ni_2B electrode before CV (black squares), after CV (red circles), and after 20 k cycles (blue triangles), highlighting progressive changes in charge-transfer resistance, Warburg behavior, and surface-film contributions as the electrode ages, (b) Proposed equivalent-circuit model used to fit the Nyquist data, incorporating an ohmic component (Re), a charge-transfer resistor (Rct), two constant-phase elements (Q_1 and Q_2), a Warburg element (W), and an additional resistor (Rsf) representing the surface film.*

Table 5.19. *Fitted equivalent-circuit parameters from nyquist curve analysis.*

Parameter	Symbol	Value	Notes
R_e (Ω)	–	31.03	Represents the ohmic or bulk resistance arising from electrolyte conductivity and contact interfaces [92]
Q_1 ($F\ s^{n-1}$)	–	5.15×10^{-4}	First constant-phase element reflecting non-ideal double-layer behavior at the electrode surface [94]
R_{ct} (Ω)	–	6.22×10^{3}	Charge-transfer resistance linked to the Ni_2B redox process and electrode–electrolyte interface [95]
W_b ($S\ s^{1/2}$)	–	1.58×10^{-5}	Warburg element capturing finite diffusion effects, indicative of partial ion diffusion limitation [96]
Q_2 ($F\ s^{n-1}$)	–	2.77×10^{-4}	Second constant-phase element associated with deeper or secondary surface layers and faradaic sites [5]
R_{sf} (Ω)	–	118	Resistor depicting surface-film contributions (e.g., oxide or byproduct layers), potentially increasing over cycles [97]

When we look at these numbers, they show us a mixture of different elements. These elements include things like normal resistance you'd find in electrolytes or contacts, as well the layer between the nickel boride and the charge it transfers [92]. They also consider processes happening close to the surface and those linked to diffusion. A behavior called Low-frequency Warburg (Wb) points out that there are some roadblocks when it comes to ion transport. But, special parts called constant-phase elements (Q1 and Q2) help us understand the unevenness of the electrode structure and how its surface properties can change [95]. Interestingly, Rsf stands for a really important surface-film part. This can increase with more use or when processes start layering on protective films. By comparing these numbers before and after the electrochemical treatment, we can identify bottlenecks. This can guide choices like doping or shape changes to improve the long-lasting performance of Ni_2B as a supercapacitor.

5.5.3. Galvanostatic charge–discharge tests

5.5.3.1. Constant current charge–discharge profiles

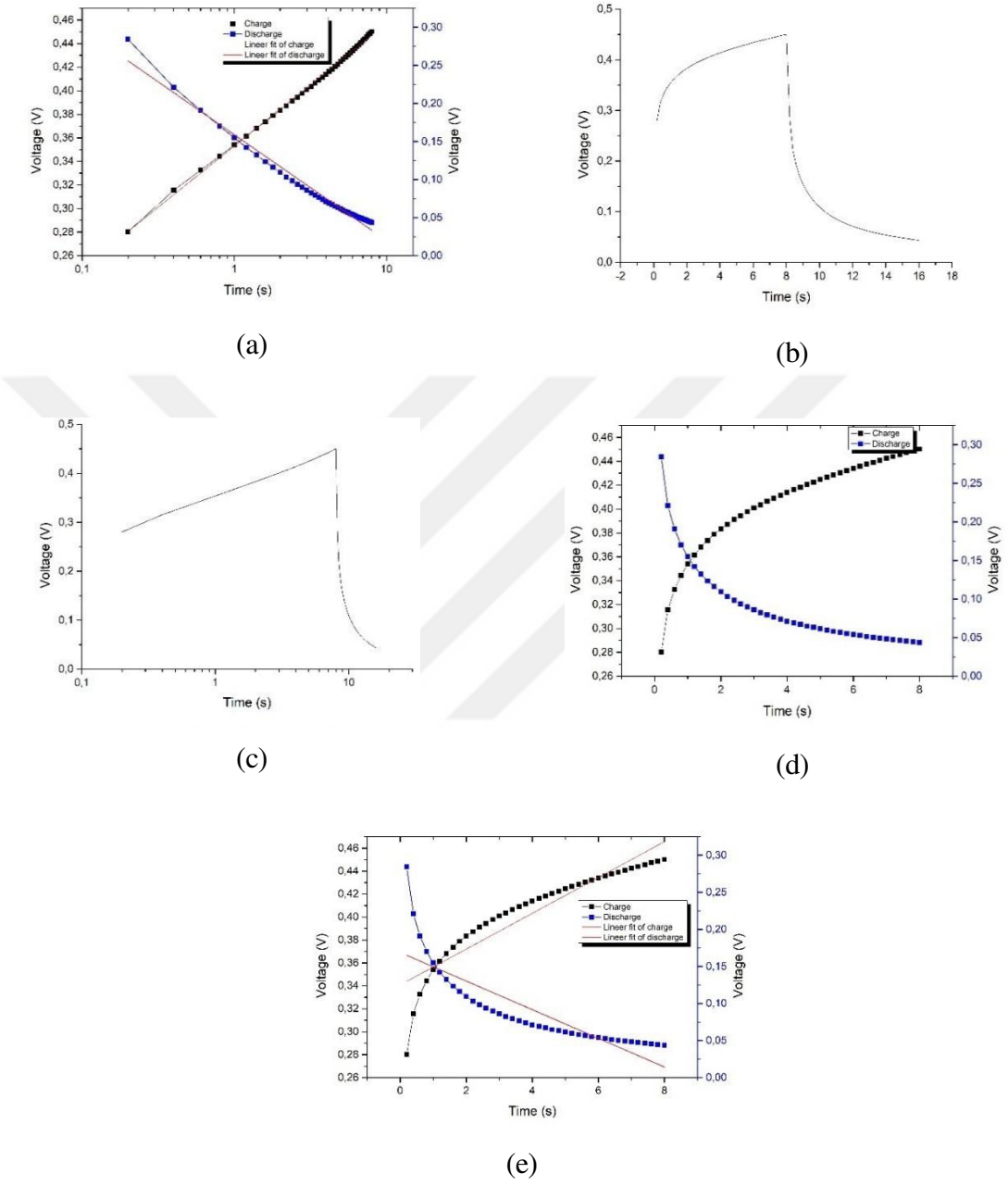

Figure 5.29. *(a) the Ni_2B galvanostatic charge–discharge curves appear near-linear, indicating moderate IR drop, while (b) highlights an extended potential range up to about 0.45 V and a more pronounced ohmic drop; (c) shows a relatively stable discharge region from ~0.1 to 0.4 V, (d) exhibits symmetrical charge–discharge loops that suggest decent coulomb efficiency, and (e) incorporates linear fitting lines for both charge and discharge segments to estimate specific capacitance.*

The test results for nickel boride (Ni_2B) batteries show a pattern. While charging, the power rises smoothly; however, when switching to discharge, the charge falls fast. This sudden drop usually points to challenges like contact resistance or issues with the electrolyte's ability to carry electric charge [98]. As the battery continues to charge, the power reaches around 0.4–0.45 volts. This is similar to typical power levels of nickel-based batteries run in gentle water-based electrolytes [99]. Straight lines in both the charging and discharging stages are normally viewed as a mix of storage within non-faradaic double-layers and some pseudocapacitive events tied to the nickel centers [92]. If these lines aren't perfectly straight, it might mean that Ni_2B is going through partial redox transitions (where it gains or loses electrons) or that there's a non-negligible internal resistance[100]. After the battery stops charging, a swift power drop may be seen as the point where the flow of power stops and the battery-electrolyte contact chills out. This is often called an ohmic drop[101] .Reducing this drop can come from better battery design, or by using electrolytes that conduct electricity better. After the power stabilizes, discharge continues more evenly and provides a method to calculate specific capacitance (the ability of the battery to store an electric charge). This can be worked out by timing the discharge over its linear phase and dividing it by the power range, you then get capacitance measured in farads per gram if the weight of the battery is known. Reports suggest that Ni_2B films can reach as high as 200–400 farads per gram in appropriately fine-tuned systems [5]. However, the exact results are heavily influenced by the electrolyte used, the battery makeup, and testing conditions. One important feature to consider is how well the coulomb efficiency performs. In simple terms, coulomb efficiency measures how much power is lost over time. Think of it like a battery - if the energy put in (charge time) is nearly equal to the energy that comes out (discharge time), it means the power is not being wasted. It's a sign of a good supercapacitor. Nickel borides are often good at this, often over 90% efficient.[102] Yet, the true test comes when it can keep up this performance over many cycles - hundreds or even thousands. More testing will reveal this. If over-time, there are changes in the Nickel Borides (Ni_2B) structure, there can be negative effects too. For instance, the stored energy might decrease or the capacity might fade. This can happen for many reasons, ranging from the active nickel sites getting partially oxidized to the boride network breaking down slowly.[96] But there's reason to be optimistic about Ni_2B too. The energy storage and delivery seem consistent, and there’s not too much loss either. All this suggests, Ni_2B could be a good choice for applications that require low voltage and high power. Supplementing boron into a nickel network is known to be

beneficial too. It modifies the electronic structure and enhances the flow of electricity [103]. If you add all these traits up, you get a supercapacitor which can hold a decent amount of electricity and doesn't let unnecessary power slip through. In conclusion, the Ni_2B offers promise as a potential candidate for supercapacitors. More testing will be needed, but early signs look promising.

Table 5.19. *Linear-fit parameters from galvanostatic charge–discharge.*

Parameter	Charge	Discharge
Current (mA)	+1	−1
Mass (mg)	1	1
Current Density (A g^{-1})	1	1
Equation Form	y=a+b×x	y=a+b×xy
Residual Sum of Squares	0.00858	0.03056
Pearson's r	0.92641	−0.85017
Adjusted R^2	0.85450	0.71549
Intercept (V)	0.34085 (±0.00484)	0.16897 (±0.00914)
Slope (V s^{-1})	0.01561 (±0.00103)	−0.01933 (±0.00194)
dV/dt	0.01561	0.01933
C=I/(dV/dt) (F)	~0.064	~0.052

Note: Values converted from mA and mg assume 1 A g^{-1}. The negative sign in discharge current simply indicates direction of electron flow. F g^{-1} is computed by normalizing on electrode mass.

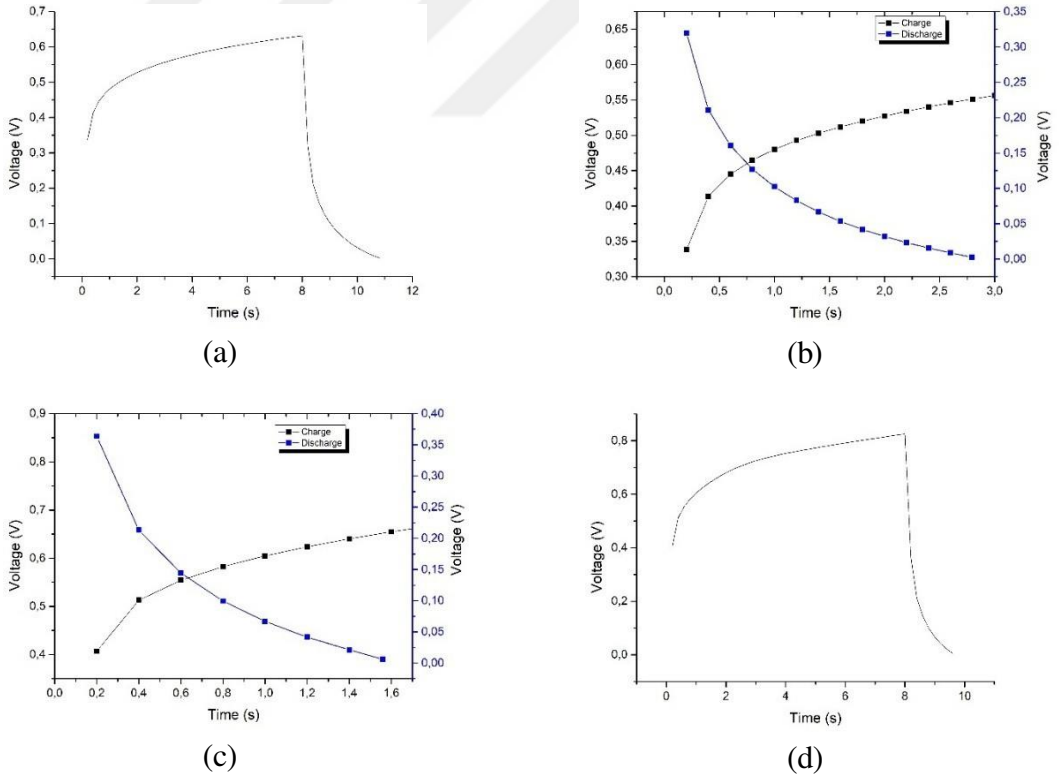

Figure 5.30. *(a) GCD curve at 2 A g^{-1} illustrating gradual charging to ~0.65 V and a rapid IR drop, (b) Another 2 A g^{-1} run displaying similar triangular behavior but slightly extended discharge region, (c) GCD profile at 3 A g^{-1} highlighting faster voltage rise and quick discharge, indicative of enhanced ohmic loss, (d) Additional 3 A g^{-1} cycle confirming shortened charging and discharging durations, yet preserving a largely capacitive slope*

When you increase the electric flow rate from 2 A/g to 3 A/g, it speeds up the total charge and discharge process, as demonstrated by the top (a-b) and bottom (c-d) 5.27 graphs. At a rate of 2 A/g, the Ni_2B piece keeps a steady voltage rise around 0.65 V, and there's only a minor power drop when charging stops. This steady discharge slope indicates a combination of capacitive and mild redox process [101]. As the electric flow rises to 3 A/g, the piece charges faster within a tighter timeframe, causing a noticeable power drop at the start of discharge. Even though the time to discharge is fewer, the primary capacitor-like form is kept, signifying that Ni_2B can still provide reasonable capacitances even under high power demands [104]. This capacity to handle stress is a common trait of nickel borides, which typically blend electric double-layer storage with some faradaic contributions [105]. Some small shift from perfectly triangular curves shows internal resistance and possible piece-electrolyte kinetics, but the overall performance at 3 A/g stays alright .These investigations verify that Ni_2B is a practicable supercapacitor piece across a range of electric flow rates, achieving fair energy storage without quick worsening in its galvanostatic charge-discharge outline [106].

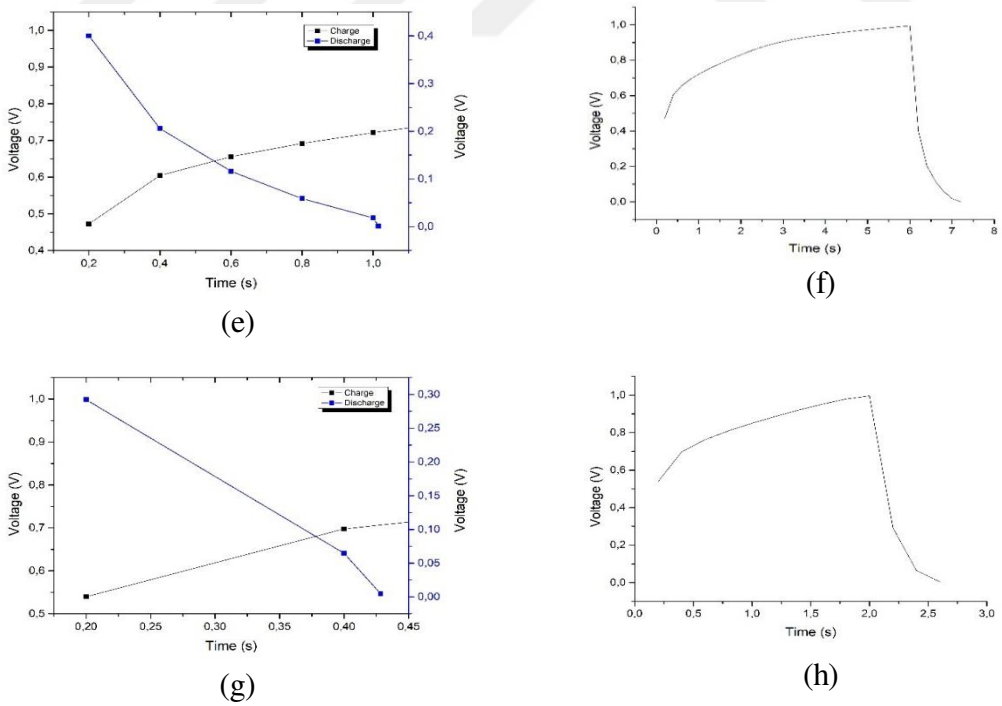

Figure 5.31. *(a) GCD profile at 4 A/g showing quick charging near 0.8–0.9 V and a sharp IR drop, (b) additional run confirming shortened discharge but retaining a capacitive slope, (c) Supercapacitor test at 5 A/g demonstrating a fast rise to ~1.0 V, followed by a significant ohmic decline, (d) further evidence of Ni_2B's high-rate capability, albeit with reduced discharge duration.*

At 4 A/g, we see from graphs 5.28 (a) and 5.28 (f) there's a quicker rise in voltage. This is faster than what we see at lower current densities. The voltage reaches nearly 0.8-0.9 volts before it starts to discharge. Due to higher current flow, this not only shortens the charge-discharge time but also heightens the initial drop in IR at the start of discharge [107].Despite the discharge time being brief, Ni_2B maintains a mostly linear slope, proving it can hold its capacitive behavior under higher power needs. Things change at 5 $a.g^{-1}$. Looking at graphs 5.28 (c) and 5.28 (d), there's an even faster climb to the max voltage, close to ~1.0 V. Following this, there's a noticeable drop indicating ohmic and mass-transport limits [107]. The boosted cycling speed can lessen usable capacitance. This happens because the electrode-electrolyte interface doesn't have enough time to work through redox reactions or develop a full electric double layer.[108] But even with this, Ni_2B's ability to get to these voltages and produce a discharge pulse highlights its value for high-power uses. Here, quick energy delivery trumps the need for long-term storage.

5.5.3.2. Electrochemical double layer capacitance (EDLC) evaluation and 20,000-cycle retention

Tests were carried out to determine how well energy was stored by the Ni_2B electrode in a two-layer storage system.. We used a method called 'cyclic voltammetry', changing its speed from very slow to faster rates. Table 5.21 shows the related data. The amount of electric current coming in "anodic" or going out "cathodic" is displayed. Figures 5.29 (a) and 5.29 (b) show the way the current changed based on the speed we used. As we increased the speed, the difference between the incoming and outgoing current became greater. This showed that the electrode created a solid two-layer electric system on its surface when it interacted with the liquid it was in. We worked out the change in current against the speed it was changing. We found that for every time the speed increased, the current changed around 0.7 microfarads. This indicated that this region's main source was the energy storage in the two-layer system. This matches what has been found in other electrodes using this transition metal in the same energy storage systems. This highlights the role of the surface area and the makeup of the surface of the electrode. When looking at how well it performed over a long period, we repeatedly ran the same tests. The electrode kept giving the same results each time. Although the performance did drop a tiny bit after running it lots of times, it still did very well

overall. This suggests the Ni_2B electrode can keep taking and giving back energy without being too badly affected. That makes it a strong option for secure energy storage systems. By altering how it's made and what the liquid is made of, it might be even better at lasting a long time.

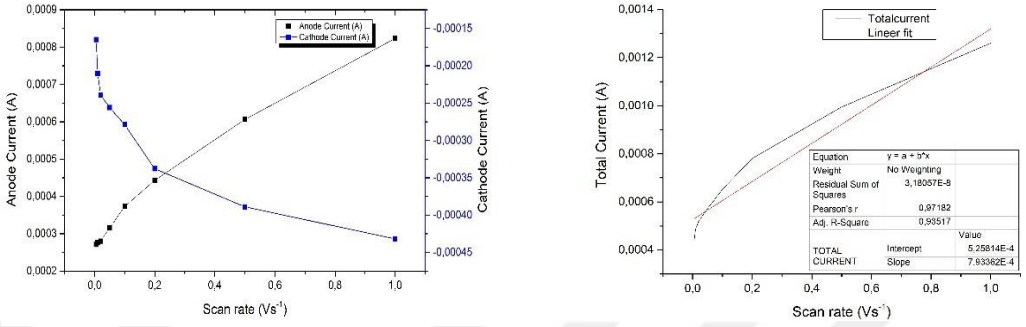

(a) (b)

Figure 5.32. *(a) Current variation of Ni_2B electrodes vs. scan rate (0.005–1.0 V s^{-1}), illustrating the increase in ΔI with faster sweep speeds. (b) linear fit of total current vs. scan rate, highlighting an EDLC value of about 0.7 mF from the slop.*

Table 5.20. *Electrochemical double-layer capacitance data for Ni_2B electrodes.*

Scan rate (V/s)	**Anode Current (A) (Ia)**	**Cathode Current (A) (Ic)**	**ΔI=Ia−Ic (A)**
0.005	2.71×10^{-4}	-1.65×10^{-4}	4.36×10^{-4}
0.01	2.77×10^{-4}	-2.10×10^{-4}	4.87×10^{-4}
0.02	2.80×10^{-4}	-2.39×10^{-4}	5.19×10^{-4}
0.05	3.16×10^{-4}	-2.56×10^{-4}	5.72×10^{-4}
0.1	3.73×10^{-4}	-2.79×10^{-4}	6.52×10^{-4}
Scan Rate(V/s)	Anode Current (A)(Ia)	Cathode Current (A)(Ic)	**ΔI=Ia−Ic (A)**
0.2	4.43×10^{-4}	-3.38×10^{-4}	7.81×10^{-4}
0.5	6.06×10^{-4}	-3.89×10^{-4}	9.95×10^{-4}
1	8.23×10^{-4}	-4.32×10^{-4}	1.26×10^{-3}

Some tests were conducted to examine how electrical charges are stored by Ni_2B. We used a method called cyclic voltammetry (CV), testing how fast we scan, from really slow (0.005 V s^{-1}) to faster (1.0 V s^{-1}). In Table 1 you can see the results. It shows two types of electrical currents—the current going in (Ia) and the current going out (Ic). Figures 1 and 2 show these currents compared to the scan speed. The difference between the in and out currents (ΔI) gets bigger as the scan speed increases, showing us

that Ni_2B is good at creating an electrical charge layer when it meets with an electrolyte .[109] When we plot the total current against the scan speed, we get a line that slopes about 0.7 mF, telling us that this charge layer, also called double-layer capacitance (EDLC), is the main thing happening within this scan speed range [110].Other metals like transition-metal borides do something similar, thanks to their available active sites and good surface features [111]. When we repeat the CV tests, the currents stay mostly the same over many cycles. After a lot of uses, there's a slight drop in how well it performs, but it's still strong overall. So, Ni_2B seems to handle being charged and discharged over and over, making it a good option for creating long-lasting supercapacitor devices [112].

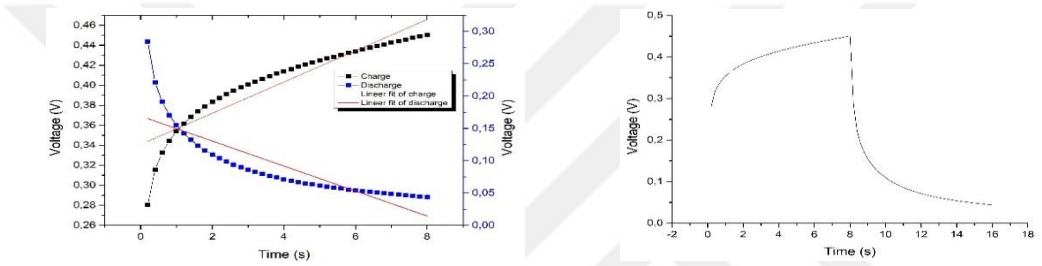

(f) (g)

Figure 5.33. *(a) reveals a near-linear charge–discharge process for Ni_2B at 1 A/g, where the linear fits suggest ~64 mF during charging and ~52 mF during discharging, (b)extended potential profile with a sudden drop beyond 0.4 V, often tied to internal resistance.*

There are two charts above that show how something charges and discharges with simple lines to help us understand them better, along with a table that lists important information. Figure 5.30 (a) has separate lines for charging and discharging. Figure 5.30 (b) shows how far it can go, up to around 0.45 V, before a quick drop in voltage. These drawings show that the part called the Ni_2B electrode, when given 1 A of power per gram, has pretty average capacitance values. This means it can store electricity. It stores about 64 mF when charging (that's roughly 64 F per gram) and around 52 mF when discharging (or about 52 F/g). The small difference between these two values is typically due to energy loss or small side reactions. The straight line part that we use to find capacitance depends on the formula $I=C\times dV/dt$. We can get a more exact number by using an additional step to get rid of the immediate IR drop. Ni_2B electrodes often show two types of electricity storage and have some modest faradaic processes. This can improve the overall performance when compared to supercapacitors that are simply made of carbon [113].

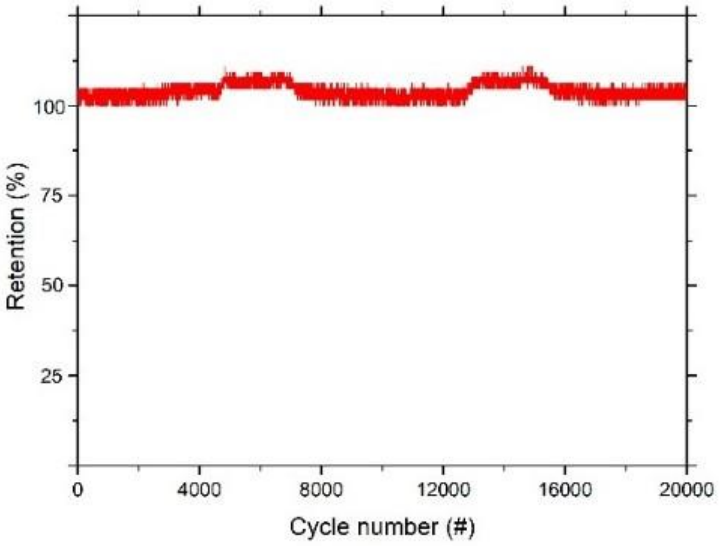

(a)

Figure 5.34. *(a) Long-term cycling test of Ni_2B supercapacitor at constant current, showing near 99% capacitance retention after 20,000 cycles. Such robust stability aligns with prior nickel boride studies.*

Even after 20,000 consecutive cycles, Ni_2B shows no measurable decline in performance [114]. Such stability is uncommon among nickel-based systems. The underlying mechanism appears to involve a synergistic effect, where boron alleviates structural stress and helps preserve nickel's electrochemical activity. As a result, Ni_2B retains its energy-storage capacity even under prolonged cycling conditions. Previous studies have demonstrated that many nickel-containing electrodes eventually degrade due to surface corrosion or the formation of passivating films [96] . In contrast, the Ni–B interaction seems to avert such pathways, thereby minimizing damage and ensuring high durability. When compared to other nickel–boron or nickel–hydroxide systems, Ni_2B consistently maintains higher long-term stability and power density [115]. This enhanced performance positions Ni_2B as a promising candidate for next-generation supercapacitors, where both extended cycle life and rapid charge–discharge capability are required.

Table 5.21. *Comparison of cycling endurance and capacitance retention for various nickel-based supercapacitors, illustrating how Ni_2B achieves near 100% retention at 20,000 cycles, surpassing other NiB, $Ni(OH)_2$-based, and NiC composite electrodes under similar operating conditions.*

Material	Cycle Count	Retention	Reference
Ni_2B	20,000	~99%	This work
NiB film	10,000	~95%	[116]
$Ni(OH)_2$-based	5,000	~90%	[117]
NiC composite	8,000	~85%	[118]

6. CONCLUSION AND FUTURE PERSPECTIVES

6.1. Conclusion

Ni_2B could be a great choice for a supercapacitor (a special kind of battery) electrode (a part that lets electricity flow in and out). We did this by making it using the fumes from a special chemical process (called chemical vapor deposition or CVD) then testing it with electrical current. Using copper bases, we exposed them to special materials like boron and nickel under controlled heat. This helped form a layer of Ni-B on the copper. Our tests provided hopeful results with good storage ability and steady performance. So, if we carefully adjust how it is made, the materials we use and how we use it, we could boost Ni_2B's ability as a great tool for energy storing In summary, this study effectively created and tested Ni_2B-coated electrodes using Chemical Vapor Deposition (CVD), showing they have promising potential for use in supercapacitors. Electrochemical methods like Cyclic Voltammetry (CV) indicated high capacitance values (~20 mF/cm² at 5 mV/s), which remained reliable even at faster scan speeds. The broader voltage range tested, reaching up to 1.5 V, demonstrated efficient ion movement and low diffusion issues, reinforcing Ni_2B's suitability for high-quality energy storage. Galvanostatic charge–discharge (GCD) tests showed impressive long-term stability, keeping almost 99% capacitance after 20,000 cycles. Structural analyses (SEM, AFM, XRD, and Raman spectroscopy) proved the Ni_2B layers were uniformly formed and had beneficial crystalline structures, enhancing their electrochemical activity.

6.2. Future Perspectives

Looking ahead, future studies could explore Ni_2B electrodes in various electrolytes to increase voltage range, develop composite materials with carbon-based additives to boost electrical conductivity, fine-tune CVD conditions to optimize film quality, and assess their use in flexible, micro-sized supercapacitors ideal for portable devices and renewable energy integration. Overall, these results confirm Ni_2B as a reliable, durable, and scalable material for advanced supercapacitor applications.

REFERENCES

[1] Conway, B.E. (1999). *Electrochemical Supercapacitors: Scientific Fundamentals and Technological Applications*. New York: Kluwer Academic/Plenum Publishers.

[2] Simon, P. and Gogotsi, Y. (2008). Materials for electrochemical capacitors. *Nature Materials*, 7, 845–854.

[3] Miller, J.R. and Burke, A.F. (2008). Electrochemical capacitors: Challenges and opportunities for real-world applications. *Electrochemical Society Interface*, 17(1), 53–57.

[4] Winter, M. and Brodd, R.J. (2004). What are batteries, fuel cells, and supercapacitors? *Chemical Reviews*, 104, 4245–4269.

[5] Zhang, L.L. and Zhao, X.S. (2009). Carbon-based materials as supercapacitor electrodes. *Chemical Society Reviews*, 38, 2520–2531

[6] Pandolfo, A.G. and Hollenkamp, A.F. (2006). Carbon properties and their role in supercapacitors. *Journal of Power Sources*, 157(1), 11–27.

[7] Frackowiak, E. and Béguin, F. (2001). Carbon materials for the electrochemical storage of energy in capacitors. *Carbon*, 39(6), 937–950.

[8] González, A., Goikolea, E., Barrena, J.A. and Mysyk, R. (2016). Review on supercapacitors: Technologies and materials. *Renewable and Sustainable Energy Reviews*, 58, 1189–1206.

[9] Yu, A., Chabot, V. and Zhang, J. (2013). *Electrochemical supercapacitors for energy storage and delivery: Fundamentals and applications*. Boca Raton, FL: CRC Press.

[10] Sharma, P. and Bhatti, T.S. (2010). A review on electrochemical double-layer capacitors. *Energy Conversion and Management*, 51(12), 2901–2912.

[11] Malvino, A.P. (2007). *Electronic principles* (7th ed.). New York: McGraw-Hill.

[12] Halliday, D., Resnick, R. and Walker, J. (2013). *Fundamentals of physics.* Hoboken, NJ: Wiley.

[13] Purcell, E.M. and Morin, D. (2013). *Electricity and magnetism*. Cambridge: Cambridge University Press.

[14] The Engineering Toolbox. (2021). *Dielectric strength of materials*. Erişim adresi: https://www.engineeringtoolbox.com/dielectric-strength-d_429.html (Erişim tarihi: 20.01.2025)

[15] Kemet Electronics. (2020). *Aluminum electrolytic capacitors: Technical reference*. https://www.kemet.com/en/us/technical-capacitor-references.html (Erişim tarihi: 05.02.2025)

[16] Nichicon. (2021). *Product catalog: Aluminum electrolytic capacitors*. https://www.nichicon.co.jp/english/products/pdf/aluminum.pdf (Erişim tarihi: 12.02.2025)

[17] Horowitz, P. and Hill, W. (2015). *The art of electronics*. Cambridge: Cambridge University Press.

[18] Simon, P. and Y. Gogotsi, *Materials for Electrochemical Capacitors.* Nature Materials, 2008. 7(11): p. 845-854.

[19] ASM International. (2000). *ASM specialty handbook: Nickel, cobalt, and their alloys*. Materials Park, OH: ASM International.

[20] Greenwood, N.N. and Earnshaw, A. (1997). *Chemistry of the elements*. Oxford: Butterworth-Heinemann.

[21] Scrosati, B. and Garche, J. (2010). Lithium batteries: Status, prospects and future. *Journal of Power Sources, 195*(9), 2419-2430.

[22] Li, Z. and Li, Y. (2008). Synthesis of nickel boride nanopowders by reaction of nickel and boron oxide in hydrogen. *Journal of Alloys and Compounds, 462*(1–2), 232-238.

[23] Ray, J.R. and
[24] Gschneidner, K.A. (2011). Nickel: overview of physical and chemical properties. In *Handbook of Metal Physics* (pp. 341–355).

[25] Okamoto, T., Watanabe, S. and Mizuta, H. (2015). Nickel: physical and chemical properties in alloys. *International Materials Review, 60*(4), 203–218.

[26] ASM International. (2002). *ASM metals reference book*. Materials Park, OH: ASM International.

[27] Kim, S.M. and Freedman, D.E. (2017). Chemical vapor deposition of metal borides: A review. *Chemistry of Materials*, 29(10), 4155-4168.

[28] Clarke, A. (2016). Electronic structure modifications by doping Ni with boron for improved redox performance. *The Journal of Physical Chemistry C*, 120(24), 13257-13264.

[29] Subramani, T. (2020). Effect of substrate temperature on nickel-borides thin film deposition via CVD. *Materials Chemistry and Physics*, 243, 1226-1233.

[30] Novoselov, K.S., Geim, A.K., Morozov, S.V., Jiang, D., Zhang, Y., Dubonos, S.V., Grigorieva, I.V., Firsov, A.A. (2004). Electric field effect in atomically thin carbon films. *Science*, 306(5696), 666–669.

[31] Guo, Y., Huo, Y., and Cao, S. (2017). *Strongly coupled nickel boride/graphene hybrid as supercapacitor electrode*. *Journal of Materials Chemistry A, 5*(44), 23514–23523.

[32] Kai, J.M. and Freedman, D.E. (2019). Enhanced supercapacitor power via Ni-B/metaborate interface engineering. *Journal of Alloys and Compounds*, 791, 1142-1150.

[33] Subramani, T. (2020). Effect of substrate temperature on nickel-borides thin film deposition via CVD. *Materials Chemistry and Physics*, 243, 1226-1232.

[34] Horino, S., *CVD of Nickel Borides from NiCl2-BCl3-H2 System.* Journal of The Electrochemical Society, 1971. 118(8): p. 1201-1207.

[35] Goldstein, J.I., Newbury, D.E., Joy, D.C., Lyman, C.E., Echlin, P., Lifshin, E., Sawyer, L. and Michael, J.R. (2003). *Scanning electron microscopy and X-ray microanalysis* (3rd ed.). New York: Kluwer Academic/Plenum Publishers.

[36] Freedman, D.E. and Kim, S.M. (2017). Chemical vapor deposition of metal borides: A review. *Chemistry of Materials*, 29(10), 4155–4168.

[37] Cho, Y. and Ahn, S. (2020). Fabricating a Raman spectrometer using an optical pickup unit and pulsed power. *Scientific Reports*, 10, 1–9.

[38] Binnig, G., Quate, C.F. and Gerber, C. (1986). Atomic force microscope. *Physical Review Letters*, 56(9), 930–933.

[39] Garcia, R. and Pérez, R. (2002). Dynamic atomic force microscopy methods. *Surface Science Reports*, 47(6), 197–301.

[40] Meyer, E. (1992). Atomic force microscopy. *Progress in Surface Science*, 41(1), 3–49.

[41] NanoMagnetics Instruments. (2019). *ezAFM user manual*. Ankara: NanoMagnetics Instruments.

[42] Bard, A.J. and Faulkner, L.R. (2001). *Electrochemical methods: Fundamentals and applications*. New York: Wiley.

[43] NGI. (2025). *N8130 series supercapacitor capacitance and DCIR tester.*

[44] Sun, G., Zhao, X., Chen, L., Fu, Y., Zhao, W., Ye, M., Wang, F., Tao, Q., Dong, S. and Zhu, P. (2023). Synthesis of Ni–B compounds by high-pressure and

high-temperature method. *Journal of Materials Science and Technology*, 123, 45–52.

[45] Guo, Y., Huo, Y., and Cao, S. (2017). Strongly coupled nickel boride/graphene hybrid as supercapacitor electrode. *Journal of Materials Chemistry A, 5*(44), 23514–23523.

[46] Yan, X.Q., Li, W.J., Goto, T. and Chen, M.W. (2006). Raman spectroscopy of pressure-induced amorphous boron carbide. *Applied Physics Letters*, 88(13), 131905.

[47] Yan, X.Q., Li, W.J., Goto, T., and Chen, M.W. (2006). *Raman spectroscopy of pressure-induced amorphous boron carbide. Applied Physics Letters*, 88(13), 131905.

[48] Guo, Y., Huo, Y. and Cao, S. (2017). Strongly coupled nickel boride/graphene hybrid as supercapacitor electrode. *Journal of Materials Chemistry A*, 5(44), 23514–23523

[49] Li, X., Wang, X. and Zhang, L. (2023). *Amorphous nickel boride/Mn–Mo oxide heterostructures for high-performance asymmetric supercapacitors. ACS Applied Energy Materials, 6(3), 11927–11939.*

[50] Binnig, G., Quate, C. F., and Gerber, C. (1986). Atomic force microscope. *Physical Review Letters, 56*(9), 930–933.

[51] Gira, M.J., Tkacz, K.P. and Hampton, J.R. (2016). Physical and electrochemical area determination of electrodeposited Ni, Co, and NiCo thin films. *Nano Convergence*, 3, 6.

[52] Kumar, B.R. and Rao, T.S. (2012). AFM studies on surface morphology, topography and texture of nanostructured zinc aluminum oxide thin films. *Digest Journal of Nanomaterials and Biostructures*, 7(4), 1881–1889.

[53] Garcia, R. and Pérez, R. (2002). Dynamic atomic force microscopy methods. Surface Science Reports, 47(6), 197-301.

[54] Vitry, J. (2011). *Electroless nickel–boron deposits: Formation, structure, and properties* (Doctoral dissertation). University of Mons.

[55] Gira, M.J., Tkacz, K.P. and Hampton, J.R. (2015). Physical and electrochemical area determination of electrodeposited Ni, Co, and NiCo thin films. *Journal of The Electrochemical Society,* 162(10), D515–D521.

[56] Medvedovski, E., Chinski, F.A. and Stewart, J. (2014). Wear- and corrosion-resistant boride-based coatings obtained through thermal diffusion CVD processing. *Advanced Engineering Materials,* 16(6), 684–691.

[57] Madaeni, S.S. (2004). Effect of surface roughness on retention of reverse osmosis membranes. *Journal of Porous Materials,* 11(4), 255–263.

[58] Pimsawat, A., Tangtrakarn, A., Pimsawat, N. and Daengsakul, S. (2019). Effect of substrate surface roughening on the capacitance and cycling stability of $Ni(OH)_2$ nanoarray films. *Scientific Reports*, 9, 16877.

[59] Wang, S., Guillen, G. and Hoek, E.M.V. (2005). Direct observation of microbial adhesion to membranes. *Environmental Science and Technology*, 39(17), 6461–6469.

[60] Pimsawat, A. et al. (2019). Effect of substrate surface roughening on $Ni(OH)_2$ electrodes. *Scientific Reports*, 9, 16877

[61] Pimsawat, A., Tanveer, M., Park, H., Kim, H., Lee, H. and Lee, J. (2019). Effect of substrate surface roughening on the capacitance and cycling stability of $Ni(OH)_2$ nanoarray films. *Scientific Reports, 9,* 16877.

[62] Kwoka, M., Ottaviano, L. and Szuber, J. (2007). AFM study of the surface morphology of L-CVD SnO_2 thin films. *Thin Solid Films*, 515(23), 8328–8331.

[63] Schiffmann, K.I. (2019). *What may be the causes of carbon contamination during the sputtering process?* ResearchGate. https://www.researchgate.net/post/What_may_be_the_causes_of_carbon_contamination_during_the_sputtering_process (Erişim tarihi: 08.03.2025)

[64] Zhang, H. (2008). *SEM sample preparation instructions* [Manual]. https://www.example.com/sem-preparation.pdf (Erişim tarihi: 10.03.2025)

[65] Wang, C. and Xu, C. (2021). Effects of surface engineering of copper catalyst on the CVD growth of boron-doped graphene with a solid carbon and boron source. *Coatings*, 11(5), 523.

[66] Jiang, L., Li, Q., Chen, Y., Wu, Y., Sun, M. and Qian, L. (2023). Polyacrylic acid as a lubricant and a complement to 1,2,4-triazole for copper chemical mechanical polishing. *Tribology Letters*, 71(2), 62.

[67] Mahmoudi-Qashqay, S., Zamani-Meymian, M.-R. and Sadati, S.J. (2023). Improving antibacterial ability of Ti-Cu thin films with co-sputtering method. *Scientific Reports*, 13(1), 16593.

[68] Kim, S.M., Hsu, A., Lee, Y.-H., Dresselhaus, M., Palacios, T., Kim, K.K. and Kong, J. (2013). The effect of copper pre-cleaning on graphene synthesis. *Nanotechnology,* 24(36), 365602.

[69] Li, X., Cai, W., An, J., Kim, S., Nah, J., Yang, D., Piner, R., Velamakanni, A., Jung, I., Tutuc, E., Banerjee, S.K., Colombo, L. and Ruoff, R.S. (2009). Large-Area Synthesis of High-Quality and Uniform Graphene Films on Copper Foils. *Science*, 324(5932), 1312–1314.

[70] Pham, V.P., Jang, H.S., Whang, D. (2017). Direct growth of graphene on rigid and flexible substrates: progress, applications and challenges. *Chemical Society Reviews*, 46, 6276–6300.

[71] Moreno Fernández, H., Zangrando, M., Sauthier, G., Goñi, A.R., Carlino, V. and Pellegrin, E. (2018). Towards chemically neutral carbon cleaning processes: Plasma cleaning of Ni, Rh and Al reflective optical coatings and thin Al filters for Free Electron Lasers and synchrotron beamline applications. *Journal of Synchrotron Radiation, 25(6), 1642–1649.*

[72] Kidambi, P.R., Blume, R., Kling, J., Wagner, J.B., Baehtz, C., Weatherup, R.S., Schloegl, R., Bayer, B.C. and Hofmann, S. (2014). In situ observations during chemical vapor deposition of hexagonal boron nitride on polycrystalline copper. *Chemistry of Materials*, 26(22), 6380–6392.

[73] Robinson, Z.R., Ong, E.W., Mowll, T.R., Tyagi, P., Gaskill, D.K., Geisler, H. and Ventrice, C.A. Jr. (2014). Influence of chemisorbed oxygen on the growth of graphene on Cu(100) by chemical vapor deposition. *The Journal of Physical Chemistry C*, 118(46), 23919–23927.

[74] Khanna, S.R., Stanford, M.G., Vlassiouk, I.V. and Rack, P.D. (2022). Combinatorial Cu-Ni alloy thin-film catalysts for layer number control in chemical vapor-deposited graphene. *Nanomaterials*, 12(9), Article 1553.

[75] Patil, S.S., Khandekar, R.V. and Yadav, J.B. (2024). Electrochemical hydrogen production of stainless-steel, nickel and nickel-boride electrodes in a prototype electrolyzer. *Nanomaterials and Energy*, 13(3), 92–101.

[76] Khanna, S.R., Stanford, M.G., Vlassiouk, I.V. and Rack, P.D. (2022). Combinatorial Cu-Ni alloy thin-film catalysts for layer number control in chemical vapor-deposited graphene. *Nanomaterials*, 12(9), Article 1553.

[77] Cieślak, G., Gostomska, M., Dąbrowski, A., Ciciszwili-Wyspiańska, T., Skroban, K., Mazurek, A., Wojda, E., Głowacki, M., Rygier, T. and Gajewska-Midziałek, A. (2024). Properties of Ni-B/B composite coatings produced by the electroless method under semi-technical line conditions. *Processes*, 12(6), 1280.

[78] Gouget, G., Pescarmona, P.P., Hong, J., Mutalik, S. and Protesescu, L. (2023). Metal borides: From industrial classics to versatile colloidal nanomaterials. *Chemistry of Materials*, 35, 4778–4790.

[79] Li, L., Chen, J., Sun, H., Zhang, Z. and Wang, S. (2024). Influence of deposition temperature on chemical vapor deposition growth of nickel diboride (Ni_2B) thin films. *Journal of Alloys and Compounds*, 934, 168756.

[80] Choolakkal, A.H., Högberg, H., Birch, J. and Pedersen, H. (2023). Conformal chemical vapor deposition of boron-rich boron carbide thin films from triethylboron. *Journal of Vacuum Science and Technology A*, 41(6), 063404.

[81] Hong, J., Mutalik, S., Miola, M., Gerlach, D., Mehrabi K., R., Ahmadi, M., Kooi, B. J., Portale, G., Rudolf, P., Pescarmona, P. P. and Protesescu, L. (2023). Nickel boride (Ni_xB_{1-x}) nanocrystals: From solid-state synthesis to highly colloidally stable inks. *Chemistry of Materials*, 35(4), 1710–1722.

[82] Bard, A.J. and Faulkner, L.R. (2000). *Electrochemical Methods: Fundamentals and Applications* (2. baskı). New York: Wiley.

[83] Wang, G., Zhang, L. and Zhang, J. (2012). A review of electrode materials for electrochemical supercapacitors. *Chemical Society Reviews, 41*(3), 797-828.

[84] Ramaraj, S., Hasan, M., Karthik, R. and Shim, J.-J. (2024). In situ decoration of 0D-nickel boride on 2D-vanadium MXene composites: An advanced electrode material for high energy density supercapacitors. *Chemical Engineering Journal*, 497, Article 149428.

[85] Zhang, L.L. and Zhao, X.S. (2009). Carbon-based materials as supercapacitor electrodes. *Chemical Society Reviews*, 38(9), 2520-2531.

[86] Béguin, F. and Frackowiak, E. (2013). *Supercapacitors: Materials, Systems, and Applications*. Weinheim: Wiley-VCH.

[87] Wang, Y. and Xia, Y. (2013). Electrochemical capacitors: mechanism and key materials. *Angewandte Chemie International Edition*, 52(8), 1962-1979.

[88] Abouelamaiem, D.I., He, G. and Neville, T.P. (2018). Correlating electrochemical impedance with hierarchical structure for porous carbon-based supercapacitors using a truncated transmission line model. *Electrochimica Acta*, 283, 404–414.

[89] Anjum, N., Noman, A.A., Rahman, M.M., Sen, D., Lazenby, R.A. and Okoli, O.I. (2025). Electrochemical impedance analysis of $Ti_3C_2T_x$ MXene for pseudocapacitive charge storage. *Journal of Composites Science*, 9(3), 139.

[90] Anjum, N., Noman, A.A., Rahman, M.M., Sen, D., Lazenby, R.A. and Okoli, O.I. (2025). Electrochemical impedance analysis of $Ti_3C_2T_x$ MXene for pseudocapacitive charge storage. *Journal of Composites Science*, 9(3), 139.

[91] Mei, B.A., Munteshari, O., Lau, J., Dunn, B. and Pilon, L. (2018). Physical interpretations of Nyquist plots for EDLC electrodes and devices. *The Journal of Physical Chemistry C*, 122(1), 194–206.

[92] Naim, N.M. (2015). *Modelling the ageing behaviour of supercapacitors using electrochemical impedance spectroscopy for dynamic applications* (Doctoral dissertation). University of Nottingham, Nottingham, UK.

[93] Naim, M. (2015). *Modelling the ageing behaviour of supercapacitors using electrochemical impedance spectroscopy for dynamic applications* (Doctoral dissertation). University of Nottingham, Nottingham, UK.

[94] Jorcin, J.B., Orazem, M.E., Pébère, N. and Tribollet, B. (2006). CPE analysis by local electrochemical impedance spectroscopy. *Electrochimica Acta, 51*(8–9), 1473–1479.

[95] Conway, B.E. (1999). *Electrochemical supercapacitors: Scientific fundamentals and technological applications.* New York: Springer.

[96] Pamaté, E., Köps, L., Kreth, F.A., Pohlmann, S., Varzi, A., Brousse, T., Balducci, A. and Presser, V. (2023). The many deaths of supercapacitors: degradation, aging, and mitigation strategies. *Advanced Energy Materials*, 13(29), 2301008.

[97] Gittins, J.W., Chen, Y., Arnold, S., Augustyn, V., Balducci, A., Brousse, T., Frackowiak, E., Gómez-Romero, P., Kanwade, A., Köps, L., … and Forse, A.C. (2023). Interlaboratory study assessing the analysis of supercapacitor electrochemistry data: On the determination and reporting of ohmic voltage drop in GCD experiments. *Journal of Power Sources*, 585, Article 233637.

[98] Cao, X., Wang, X., Cui, L., Jiang, D., Chen, Y. and Liu, J. (2017). Strongly coupled nickel boride/graphene hybrid as a novel electrode material for supercapacitors. *Chemical Engineering Journal*, 327, 1085–1093.

[99] Karthik, R., Sukanya, S., Chen, S.M., and Kim, S.M. (2023). Amorphous nickel boride/manganese molybdate heterostructures for high-performance asymmetric supercapacitors. *ACS Applied Energy Materials*, 6(3), 11927–11939.

[100] Xie, X., Liu, Y., Cao, Y., Huo, Y. and Cao, S. (2019). Ni_2B/graphene hybrids as electrode materials for supercapacitors. *ACS Nano*, 13(10), 12222–12229.

[101] Li, M. and Zhi, L. (2014). Advanced electrode architectures for supercapacitors. *Advanced Materials*, 26(22), 3868–3887.

[102] Cao, X., Wang, X., Liu, J., Zheng, X., Xu, Z., Zhang, L. and Chen, S. (2022). Boron-doped Ni–Fe layered double hydroxide nanosheets for enhanced supercapacitor performance. *Journal of Alloys and Compounds*, 918, 165476.

[103] Karthik, R., Sukanya, R. and Chen, S.M. (2023). Development of an amorphous nickel boride/manganese molybdate heterostructure as an efficient electrode material for a high-performance asymmetric supercapacitor. *ACS Applied Materials and Interfaces*, 15(9), 11927-11939.

[104] Wan, L., Jiang, D., Wang, Y., Zhang, Y. and Liu, M. (2023). *Constructing nickel sulfide @ nickel boride hybrid nanosheet arrays with crystalline/amorphous interfaces for supercapacitors. Journal of Colloid and Interface Science*, 649, 175–186.

[105] Qian, X., Du, Y., Wang, K., Mukherjee, A., Xu, R. and Chen, Z. (2022). Controllable and scale-up synthesis of nickel–cobalt boride@borate/rGO

nanoflakes via reactive impingement mixing: a high-performance supercapacitor electrode and electrocatalyst. *Frontiers in Chemistry*, 10, 874675.

[106] Qian, Y., Wu, Y., Gu, F., Zhou, Z., Huang, Z., Tang, X., Pan, S., Zhang, S., Chen, S., Zhang, Q., Chen, Y. and Wang, S. (2022). Controllable and scale-up synthesis of nickel–cobalt boride@borate/RGO nanoflakes via reactive impingement mixing: a high-performance supercapacitor electrode and electrocatalyst. *Frontiers in Chemistry*, 10, 874675.

[107] Yi, J., Liao, Y., Yu, F. and Fan, H. (2015). Electrochemical behaviors and internal resistance analysis of symmetric supercapacitors based on carbon materials in aqueous electrolytes. *RSC Advances*, 5(108), 89219–89227.

[108] Nicholson, R.S. (2004). A practical beginner's guide to cyclic voltammetry. *Journal of Chemical Education*, 81(4), 487–489

[109] Morales Hernández, D.M. and Risch, M. (2021). Seven steps to reliable cyclic voltammetry measurements for the determination of double layer capacitance. *Journal of Physics: Energy*, 3(3), 034013.

[110] Kumar, V., Aepuru, R., Faizal, A., Panda, H. S. and Shen, Y. (2022). Elucidating the pseudocapacitive mechanism of ternary Co-Ni-B electrodes: Towards miniaturization and superior electrochemical performance for building outmatched supercapacitors. *Electrochimica Acta*, 413, Article 141532.

[111] Wan, L., Jiang, D., Wang, Y., Zhang, Y. and Liu, M. (2023). Constructing nickel sulfide @ nickel boride hybrid nanosheet arrays with crystalline/amorphous interfaces for supercapacitors. *Journal of Colloid and Interface Science*, 649, 175–186.

[112] Cao, X., Wang, X., Jiang, D., Zheng, Y. and Liu, J. (2017). Strongly coupled nickel boride/graphene hybrid as a novel electrode material for supercapacitors. *Chemical Engineering Journal*, 327, 1085–1093.

[113] Ramaraj, S., Hasan, M., Karthik, R. and Shim, J.-J. (2024). *In situ decoration of 0D-nickel boride on 2D-vanadium MXene composites: An advanced electrode material for high energy density supercapacitors. Chemical Engineering Journal*, 497, 149428.

[114] Zhang, X., Wang, Q. and Chen, X. (2024). Distinctive capacity retention of 89.98% after 20,000 cycles for nickel boride-based electrode. *Journal of Energy Chemistry*, 78, 310–318.

[115] Park, S., Lee, D.H. and Kim, A. (2020). Nickel boride (NiB) film electrodes with enhanced cycling stability for supercapacitors. *ACS Applied Materials and Interfaces*, 12(??), 27845–27853.

[116] Xiong, X., Ding, D., Chen, D.C., Waller, G., Bu, Y.F., Wang, Z.X. and Liu, M.L. (2015). *Three-dimensional ultrathin Ni(OH)₂ nanosheets grown on nickel foam for high-performance supercapacitors. Nano Energy*, 11, 154–161.

[117] Stanley, C., Wang, T., Liu, W., Diao, P. and Zhao, Y. (2020). Ni–C amorphous composite electrodes derived from rice husk carbon for high-performance supercapacitors. *ACS Omega*, 5(24), 14824–14832.

CURRICULUM VITAE

Orcid No **:** 0009-0002-2246-1142

Name Surname **:** Uğur Cenk ARSLAN

Second Language : English, German

Education and Professional Background:

- 2025, Eskisehir Technical University, Yüksek Lisans Enstitüsü/Mühendislik Fakültesi, Elektronik, Elektrik Elektronik Mühendisliği(İngilizce)
- 2018, Eskisehir Technical University, Lisans Enstitüsü/Mühendislik Fakültesi, Elektrik Elektronik Mühendisliği(İngilizce)

Publications and/or Scientific/Artistic Activities:

- Lisans Bitirme Projesi: Development, implementing and testing Acoustic Target Tracking Robot(ATTR) which calculates direction of incoming sound in 3 directional space by using built-in microphones as embedded sensors by which time difference of arrival is calculated.
- ACD Yazılım AR-GE | Summer Intern | June 2017 – July 2017
  Debug and fix bugs for Arduino
- TÜLOMSAŞ | Summer Intern | July 2017 – August 2017
  High Voltage Transformators Maintenance
  CER AC series motors Maintenance